Modelling Over- and Compound Tides of the Irish and Celtic Seas Using Variational Data Assimilation Methods

Dissertation
zur Erlangung des Doktorgrades
der Naturwissenschaften
im Department Geowissenschaftten
der Universität Hamburg

vorgelegt von
Agus Setiawan
aus Kebasen, Indonesien

Hamburg
2007

Als Dissertation angenommen von Department Geowissenschaften der Universität Hamburg

Auf Grund der Gutachten von Prof. Dr. Wilfried Zahel
und Dr. Peter Damm

Hamburg, den 4. Juli 2007

Prof. Dr. Kay-Christian Emeis
Leiter des Department Geowissenschaften

Contents

List of Figures

List of Tables

Abstract

A data assimilation procedure is developed and applied to a 5 minutes resolution non-linear tidal model of the Irish and Celtic Seas making use of an efficient iterative method for the solution of the minimization problem. M_2 and S_2 tidal constituents are used for defining the external forcing at the open boundary nodes. As a rule periodicity does not apply to tidal signals due to two or more astronomical partial tides because of the incommensurability of tidal frequencies. So M_2 and S_2 have a beat period of 14.7 days, but according to incommensurability their superposition is not periodic. Therefore a certain time interval must be used for data assimilation purposes, where initial conditions (continuation conditions) must be introduced.

Firstly, the method is applied to a canal model scenario with a dynamic model yielding results defined as real and a dynamical model made deficient and producing results that are to be corrected making use of values taken from the field regarded as real. The canal with constant depth has a closed end and an open end, at which the tidal wave being determined by two astronomical constituents enters the canal. The experiments show that by applying the assimilation procedure, the deviation of the "to be corrected" solution from the "reference" solution can be reduced significantly, from 35.68% to less than 5%. The first and second order differences of the dynamical residuals are also introduced in the minimization functional. From the investigation of the dynamical residuals it follows that using this method of data assimilation, information on the deficiencies of the classical model can be taken from the resulting dynamic residuals.

After successfully applying this method to a fictive data assimilation scenario, a non-linear depth averaged assimilation model is developed and applied to the Irish and Celtic Seas. Observations from 24 positions are assimilated, and the solution is then compared with that one of the classical model, with those of other available models as well as with data from independent stations. The evaluations suggest that the data assimilation procedure is working well and yields a very significant improvement of the solution. Results for M_2, S_2, $2SM_2$, M_2, MS_4, M_6, $2MS_6$, and $2SM_6$ are obtained which agree well with observations as well as with reliable results of high resolution models and other data assimilation models. First order differences of the dynamical residuals are introduced into the minimization functional and by it evidently an adequate spatial smoothing of the residuals is reached. The length scale of the residuals then corresponds to the decorrelation lengths assumed for the dynamical errors and hopefully to the scale of the compensated deficiencies, as applying to the fictive data assimilation scenario.

The data assimilation procedure, thus having successfully been tried out for a specific adjacent sea area comprising marked shallow water areas, is ready for directly being applied to arbitrary adjacent sea and shelf regions, taking into account as many astronomical tidal constituents as regarded necessary. The incorporation of this type of model into global ocean models guarantees proper consideration of shallow water effects, at the same time effectively assimilating data also from near coastal areas.

Chapter 1
Introduction

1.1. Introduction

Data assimilation is an analysis technique in which the observed information is accumulated into the model state by taking advantage of consistency constraints with laws of time evolution and physical properties (Bouttier and Courtier, 2002). Data assimilation techniques, to optimally combine observations and models, are mostly derived from meteorology. These techniques are geared towards determining a great number of variables from a relatively sparse and irregular set of observations (Fukumori, 2001). The assimilation of observation data into the ocean models have become most popular in the last decade, particularly after the availability of data records from ships, moorings, and the satellite missions. The availability of impressively accurate data from altimetry satellites, such as TOPEX/POSEIDON and JASON, is known to considerably improve the results of numerical ocean models using assimilation techniques.

Many assimilation techniques have been developed for meteorology and oceanography such as variational methods in three and four dimensions (3D-Var and 4D-Var), Kalman filtering, optimal interpolation, and successive correction (Thacker, 1988; Anderson et al., 1996; Courtier, 1997; Kalnay, 2003; Bennett, 2002). They differ in their numerical cost, their optimality, and in their suitability for real-time data assimilation. In oceanography, data assimilation, with different techniques and for different purposes, has been applied for global and regional scale.

The data assimilation problem consists in using the available observations together with the model to provide an accurate description of the state variables. There are mainly two different forms of performing data assimilation, sequential and variational assimilations (Anderson et al., 1996; Talagrand, 1997; Robinson and Lermusiaux, 2000). In sequential assimilation, the observations are used in small batches in time as they become available, whereas in variational assimilation, all of the observations are used together over a time window. Variational assimilation solves the analysis problem through the optimisation of a given criterion. An objective of the variational method is to minimize a cost function (or objective function), which is determined by data and dynamics, by varying control variables. The control variables are often defined by initial conditions, boundary conditions, external forcing or model parameters. A global minimum is iteratively searched for the cost function until the data-model misfit is reduced below a certain threshold. This method is equivalent to the minimization of the likelihood function.

In oceanography, the first assimilation technique was imported from solid earth geophysics by introducing a formal least squares inverse methodology (Malanotte-Rizzoli and Tziperman, 1996; Wunsch, 1996). According to Malanotte-Rizzoli and Tziperman (1996), generally there are three main categories of efforts combining ocean numerical model and oceanographic data: model improvement, study of dynamical processes through state estimation, and ocean/climate forecast. With the availability of tidal data in the open ocean, Bennett and McIntosh (1982) and McIntosh and Bennett (1984) (mentioned in Egbert et al., 1994 and Egbert and Bennett, 1996), pursued a more formal approach which used inverse methods to construct a regional scale solution for the tides in Bass Strait.

Zahel (1991) applied the inverse method to a 4° Atlantic Ocean tide model, introducing harmonic constants from 16 pelagic and island positions and solving the minimisation problem iteratively by using the conjugate gradient least squares (CGLS) method (Paige and Saunders, 1982). This method is an extremely effective and flexible assimilation procedure and requires comparatively small computer memory to solve the problem. Combining data and model information is performed by searching for the least squares solution to the discretized model and data equations, where the weighting of the equations is determined by the knowledge about data and model errors. Due to the lack of more information, the data errors are assumed to be uncorrelated.

1.2. Motivation

Zahel (1991) applied the assimilation procedure, utilizing tidal elevation and tidal current data and being based on the minimization of a least squares functional defined by the residuals of dynamics and data, to different open ocean tide scenarios. By applying the assimilation procedure to a 4° Atlantic Ocean model and introducing harmonic constants from 16 pelagic and island positions, the overestimation of tidal amplitudes appearing in the free tidal model is reduced, and the rms deviation of tidal elevation at positions of assimilated data is reduced from 41.5% to 3%. The rms deviation relative to those harmonic constants which were solely selected for comparison is simultaneously reduced from 49.8% to 27.4%. The application of the assimilation procedure to a 4° global tide model, including the North Polar Sea, with data from 35 positions selected for assimilation, yielded significant changes, where the overestimation of tidal amplitude disappears in the whole ocean area in the mean. At the data positions the relative rms deviation from measured tidal elevations amounts to 0.9%, while at the 49 positions of data solely used for comparison, the corresponding deviation is reduced by a factor of more than 2.5 in magnitude. Later this model was generalized by the consideration of tidal loading gravity data in the data assimilation procedure and has applied successfully to a 1° global tide model (Zahel, 1995).

Gekeler (1995) applied the method of Zahel (1991, 1995) to the shelf sea area of the Irish and Celtic Seas by assimilating 14 offshore tidal elevation data of M_2 tide. This model uses a grid resolution of 5 minutes in latitude and longitude. Along the open boundary, tidal elevations from a global ½° model of Grawunder (1995) are used, and a successive correction procedure based on the method of Optimal Interpolation (OI) by Miller (1986) is applied to correcting the open boundary values also. Comparing the results to independent observation data, a relative error of 28.9% is obtained.

Ray (2001) applied a method similar to that of Zahel (1991) to a global tidal model with 0.5° spatial resolution limiting the model domain to between the latitudes 66°S and 66°N (the TOPEX/POSEIDON orbital inclination) and adopting a full sea surface elevation grid as constraint. Barotropic tidal currents are deduced from an altimetric tide solution by solving the two-dimensional momentum equations and the continuity equation in a least squares fashion. Good agreement is obtained with measurements, suggesting that the method will prove as a useful tool for investigating various aspects of tidal dynamics.

Due to the non-linearity taking effect on the continental shelves, the over- and the compound tides play an important role there, other than in the open ocean. Now, the altimetry applications are being developed over the coastal regions and precise tidal assessments are now needed. It is a well known fact that obtaining tidal elevation from barotropic tidal model is rather adequately possible if sufficient resolution is provided and tuning of the bottom friction coefficient (r) is allowed. Sinha and Pingree (1997) simulated the frictional dissipation of the M_2 constituent replacing the quadratic friction term by a linearised form using a friction tensor derived from the M_2 currents, and they obtained M_4 and M_6 overtides to high grade of accuracy. Lefevre et al. (2000) used a finite element method with 5 km resolution at the coast and chose r=0.0015 to assess 9 constituents, 1 overtide (M_4) and 1 compound tide (MS_4). The accuracy of the latter 2 tidal components is however not satisfactory.

Andersen (1999) showed that non-linear shallow water tides (M_4, M_6, MS_4, MN_4, $2SM_2$, M_8) can be empirically derived from TOPEX/POSEIDON altimetry. The altimetric observations are analyzed using the "response method" (Munk and Cartwright, 1966), and the tidal estimates are interpolated onto regular points. This empirical model has problems, however, within the nearest kilometre of the coast (M_4) and in the most complex parts of the shelf (M_6).

Taguchi (2002) made direct use of the full non-linear shallow water equations without introducing any linearization and applied data assimilation models to the M_2 constituent and relevant overtides M_4 and M_6 for the same area as used by Gekeler (1995). The cost function was defined by the dynamical equation, the data equations and by the first and second order differences of the dynamical residuals. Minimizing this cost function globally yields among others things a field of dynamical residuals the smoothness of which corresponds to that of the

assumed dynamical error covariances. The direct method of Zahel (1991, 1995, and 2000) and moreover the adjoint method (Sirkes et al., 1996) were applied. By assimilating elevation data from 69 stations, the results are in very good agreement with independent data from observations.

Andersen et al. (2006) obtained the overtide M_4 over the north-west European shelf by hybrid altimetry data assimilation, first using the non-linear model to generate the prior solution, and then using the linearised shallow-water equations to define the data assimilation functional penalty for the representer method (Egbert et al. 1994; Bennett, 2002). By this method the equation of continuity is not fulfilled.

In ocean tide dynamics, non-linearity appears due to interaction between partial tides and proves important in shallow waters areas (Sinha and Pingree, 1997). So far, works in data assimilation models having been done and mentioned above are limited only to one partial tide. It gives motivation to treat the case of more than one partial tide, where as a rule periodicity no more exists due to incommensurability of tidal frequencies.

1.3. Objectives and outline of this study

Based on the successful works of Taguchi (2002) for M_2 and its overtides M_4 and M_6, the assimilation procedure developed by Zahel (1991, 1995, and 2000) is to be generalized in this present study to the Irish and Celtic Seas for M_2 and S_2 tidal constituents and their over- and compound tides. The model area has been selected in view of the availability of advanced classical solutions on the one hand, and of data assimilation experiments related to the present one on the other hand, but having been restricted either on linear tides or on non-linear single constituent astronomical tides.

In the case of one partial tide, the model field is strictly periodic while in the case of more than one partial tide, as a rule periodicity no more exists due to incommensurability of tidal frequencies. It means that the assimilation procedure which has been applied by Taguchi (2002) can not be applied in this case. The M_2 and S_2 have a beat period of 14.7 days, but their superposition because of the incommensurability is not periodic. Therefore a certain time interval must be used for data assimilation purposes, where initial conditions (continuation conditions) must be introduced. Due to limitations by computer memory and CPU time, this time period has to be chosen amounting to even considerably less than the beat period. With successfully applying the data assimilation to the restricted time interval and producing the continuation conditions for the next interval, at least a total time period of 14.7 days in the case of M_2 and S_2 should be reached. Using the technique for more than two astronomical tidal constituents is straightforward, of course. Dependent upon the constituents used, a longer total time interval must be reached by the continuation procedure.

The discussions in this thesis are divided into 5 chapters. Chapter 1 as an introduction gives a brief description of data assimilation in ocean numerical models and also the motivation and objectives of this study. Chapter 2 describes variational data assimilation and the algorithm of conjugate gradient least squares (CGLS) method. An experiment with applying the assimilation procedure on a hydrodynamic model of a canal then is discussed in detail in Chapter 3. Chapter 4 describes the implementation of the assimilation procedure into a 2D non-linear tidal model of the Irish and Celtic Seas. The evaluation of both models and their results is performed in detail in Chapter 5. The presentation of models and results is closed in Chapter 6 by conclusions drawn from the findings.

Chapter 2
Variational Data Assimilation

2.1. Background

According to Robinson and Lermusiaux (2000), a data assimilation system consists of three components: (1) a set of observations; (2) a dynamical model; and (3) a data assimilation scheme or melding scheme. As has already been mentioned in the previous chapter, there are mainly two different forms of performing data assimilation, sequential and variational assimilations. Regarding to the variational assimilations, in the recent years much effort has been made developing variational data assimilation systems to replace previously used schemes e.g. the Cressman, Newtonian nudging, optimum interpolation (OI) and analysis correction algorithms (Barker et al., 2004). Variational data assimilation was firstly proposed in principle by Sasaki (1970) and was given a large practical boost by the works of Lewis and Derber (1985), Le Dimet and Talagrand (1986) and Thacker and Long (1987) (mentioned in Anderson et al., 1996).

Sasaki (1970) has classified variational assimilation into three formalisms: (1) "timewise localized" formalism; (2) formalism with strong constraint; and (3) formalism with weak constraint. In the first two formalisms, exact satisfaction of selected prognostic equations is formulated as constraint in the functional. However, only the second formalism contains explicitly the time variation terms in the Euler equations. The third formalism is characterized by the subsidiary condition which requires that the prognostic or diagnostic equations must be approximately satisfied. In other words, Robinson and Lermusiaux (2000) wrote that in strong constraint the model dynamics and boundary conditions are assumed to be free of error while in the weak constraint, the model dynamics, boundary conditions and initial conditions need to be corrected.

A number of authors have studied the variational assimilation of meteorological and oceanographical observations and, according to Courtier and Talagrand (1990), the various numerical experiments which have been performed show that variational assimilation does numerically converge to a solution and the results are physically quite reasonable.

2.2. General description of variational data assimilation

The variational data assimilation method provides an analysis $\boldsymbol{x}$ via the minimization of a prescribed cost function $J(\boldsymbol{x})$. This technique allows to solve the global problem in one go, and it is now widely used in the meteorological and

oceanographic community (Rabier and Liu, 2004).

The set of observations can be written in the general standard form,

$$\boldsymbol{d} = \boldsymbol{D}\boldsymbol{x} + \boldsymbol{\varepsilon}_d$$

and the dynamic model

$$\boldsymbol{b} = \boldsymbol{A}\boldsymbol{x} + \boldsymbol{\varepsilon}_b$$

with appropriate initial and/or boundary conditions.

The least squares method for obtaining the estimation consists in minimizing the cost function:

$$\boldsymbol{J}(\boldsymbol{x}) = (\boldsymbol{A}\boldsymbol{x} - \boldsymbol{b})^T \boldsymbol{C}^{-1} (\boldsymbol{A}\boldsymbol{x} - \boldsymbol{b}) + (\boldsymbol{D}\boldsymbol{x} - \boldsymbol{d})^T \boldsymbol{S}^{-1} (\boldsymbol{D}\boldsymbol{x} - \boldsymbol{d}) \qquad (2.1.1)$$

where $\boldsymbol{C}$ and $\boldsymbol{S}$ denote dynamical and data error covariance matrices, respectively. $\boldsymbol{A}$ is a matrix containing coefficients used in the dynamic equations and $\boldsymbol{D}$ is called the data operator. Usually assuming the data errors as uncorrelated, $\boldsymbol{S}$ takes diagonal form. With the lower triangular matrix $\boldsymbol{R}$ resulting from the Cholesky decomposition $\boldsymbol{C}=\boldsymbol{R}\boldsymbol{R}^T$, the least squares solution to the system of equations made up by

$$\boldsymbol{R}^{-1}\boldsymbol{A}\boldsymbol{x} = \boldsymbol{R}^{-1}\boldsymbol{b} \qquad (2.1.2)$$

$$\boldsymbol{S}^{-1/2}\boldsymbol{D}\boldsymbol{x} = \boldsymbol{S}^{-1/2}\boldsymbol{d} \qquad (2.1.3)$$

is searched for. Applying the method of conjugate gradient least squares (CGLS) for obtaining this solution only requires performing matrix multiplications and solving linear algebraic equations with square lower and upper triangular matrices, respectively.

Instead of performing a Cholesky decomposition of $\boldsymbol{C}$ and solving triangular systems of non-linear equations at each CGLS-iteration step, as described above and achieved in Zahel (1997), here a principally equivalent, but computationally advantageous procedure has been applied. This procedure is defined by a least squares minimization functional which is made up by the squares of the dynamical residuals, those of their first, second and possibly higher order differences and of the data residuals. The relationship to explicitly introducing an error covariance matrix $\boldsymbol{C}$ be illustrated in the following briefly.

As is obvious a tridiagonal inverse with bandwidth one corresponds in one space dimension to an error covariance matrix $\boldsymbol{C}_1(\alpha)$ being determined by a simple exponential dependence of errors $\overline{\boldsymbol{\varepsilon}_i' \boldsymbol{\varepsilon}_j'} = \tilde{\sigma}^2 \, exp\left(-\alpha |i-j| \Delta x\right)$. The inverse of this

covariance matrix periodically continues in the first and in the last row when a periodic interval is considered. The non-zero entries $a=\tilde{\sigma}^{-2}(1+exp(-2\alpha))/(1-exp(-2\alpha))$ in the main diagonal and $b=-\tilde{\sigma}^{-2}exp(-\alpha)/(1-exp(-2\alpha))$ in the first super diagonal lead to the model determined constituent of the functional $r^H C^{-1} r$ merging into $\sum_i \mu_0 \boldsymbol{r}_i^* \boldsymbol{r}_i + \sum_i \mu_i (\boldsymbol{r}_{i+1}^* - \boldsymbol{r}_i^*)(\boldsymbol{r}_{i+1} - \boldsymbol{r}_i)$ with $\mu_0 = a + 2b, \mu_1 = -b$ and $\mu_0 = a + b$ at a closed boundary. More general covariance matrices can readily be obtained by multiplying basic matrices $\boldsymbol{C}_1(\alpha^{(k)})$ with each other. To such a matrix product with n factors does belong an inverse based matrix with width n and a minimization functional including squares of residual differences up to order n. The coefficients of these contributions depend on those belonging to the basic matrices $(\mu_0^{(k)}, \mu_1^{(k)})$ and can be obtained by evaluating the power series $\prod_k (\mu_0^{(k)} + \mu_1^{(k)} dx)$ in terms of the x-differences and collecting the contributions to the differences of equal order.

Generalization to two space dimensions is straightforward, where the basic matrix $\boldsymbol{C}_2(\alpha)$ now results from the multiplication of two exponential matrices of the above type, one referring to the x-direction, the other to the y-direction, together yielding factors $\mu_0^2, \mu_0\mu_1, \mu_0\mu_1,$ and μ_1^2 for the squares of the residuals, of their x-, y-, and xy-differences, respectively. Again more general dependencies expressed by exponential functions can be obtained by multiplying matrices $\boldsymbol{C}_2(\alpha)$ with each other, where the differences and the accompanying coefficients appearing can be taken from the evaluation of the respective two dimensional power series in terms of the x- and y-differences dx, dy.

Actually, first and second order differences of the dynamical residuals have been considered in the minimization functional with choosing weighting coefficients such that the assigned covariance between the dynamical errors shows a spatial dependence close to that of the normal curve with a specific decorrelation length scale.

2.3. The conjugate gradient method

The conjugate gradient (CG) method was developed in the early fifties by Hestenes and Stiefel. This method came into wide use first in the mid-seventies when it was realized that it should be regarded as an iterative method. It has now become a standard tool for solving large sparse linear systems and linear least square problems (Shewchuk, 1994; Björck, 1996).

The CG method is a special case of Krylov space methods. Given a matrix $\boldsymbol{B} \in \mathbf{R}^{nxn}$ and a vector $\boldsymbol{c} \in \mathbf{R}^n$ the Krylov subspace $\mathcal{K}_k(\boldsymbol{B},\boldsymbol{c})$ is

$$\mathcal{K}_k(\boldsymbol{B},\boldsymbol{c})=\text{span}\{\boldsymbol{c},\boldsymbol{Bc},\ldots,\boldsymbol{B}^{k-1}\boldsymbol{c}\}$$

The k^{th} iterate in the CG method is uniquely determined by the following property. Let $\hat{\boldsymbol{x}}=\boldsymbol{A}^{\dagger}\boldsymbol{b}$ be the pseudo inverse solution and $\hat{\boldsymbol{r}}=\boldsymbol{b}-\boldsymbol{A}\hat{\boldsymbol{x}}$ the corresponding residual. Then $\boldsymbol{x}^{(k)}$ minimize the error functional

$$\boldsymbol{E}_{\mu}\left(\boldsymbol{x}^{(k)}\right)=\left(\hat{\boldsymbol{x}}-\boldsymbol{x}^{(k)}\right)^{T}\left(\boldsymbol{A}^{T}\boldsymbol{A}\right)^{\mu}\left(\hat{\boldsymbol{x}}-\boldsymbol{x}^{(k)}\right)$$

over all vectors $\boldsymbol{x}^{(k)}$ in the affine subspace

$$\boldsymbol{x}^{(k)}\in\boldsymbol{x}^{(0)}+K_k\left(\boldsymbol{A}^{T}\boldsymbol{A},\boldsymbol{s}^{(0)}\right),\quad \boldsymbol{s}^{(0)}=\boldsymbol{A}^{T}\left(\boldsymbol{b}-\boldsymbol{A}\boldsymbol{x}^{(0)}\right)$$

Only the values $\mu = 0, 1, 2$ are practical interest, and they correspond to the cases

$$\mu=0 \text{ minimizes } \left\|\hat{\boldsymbol{x}}-\boldsymbol{x}^{(k)}\right\|_2,$$
$$\mu=1 \text{ minimizes } \left\|\hat{\boldsymbol{r}}-\boldsymbol{r}^{(k)}\right\|_2^2=\left\|\boldsymbol{r}^{(k)}\right\|_2^2-\left\|\hat{\boldsymbol{r}}\right\|_2^2,$$
$$\mu=2 \text{ minimizes } \left\|\boldsymbol{A}^{T}\left(\hat{\boldsymbol{r}}-\boldsymbol{r}^{(k)}\right)\right\|_2^2=\left\|\boldsymbol{s}^{(k)}\right\|_2^2$$

and for $\mu = 1$ the method is denoted CGLS in Paige and Saunders (1982).

Algorithm CGLS: Let $\boldsymbol{x}^{(0)}$ be an initial approximation, set:

$$\boldsymbol{r}^{(0)}=\boldsymbol{b}-\boldsymbol{A}\boldsymbol{x}^{(0)},\quad \boldsymbol{s}^{(0)}=\boldsymbol{p}^{(0)}=\boldsymbol{A}^{T}\boldsymbol{r}^{(0)},\quad \gamma^{(0)}=\left\|\boldsymbol{s}^{(0)}\right\|_2^2$$

for k = 1,2,… while $\gamma^{(k)} > \text{tol}$ compute

$$\boldsymbol{q}^{(k)}=\boldsymbol{A}\boldsymbol{p}^{(k)}$$
$$\alpha^{(k)}=\frac{\gamma^{(k)}}{\left\|\boldsymbol{q}^{(k)}\right\|_2^2}$$
$$\boldsymbol{x}^{(k+1)}=\boldsymbol{x}^{(k)}+\alpha^{(k)}\boldsymbol{p}^{(k)}$$
$$\boldsymbol{r}^{(k+1)}=\boldsymbol{r}^{(k)}-\alpha^{(k)}\boldsymbol{q}^{(k)}$$
$$\boldsymbol{s}^{(k+1)}=\boldsymbol{A}^{T}\boldsymbol{r}^{(k+1)}$$
$$\gamma^{(k+1)}=\left\|\boldsymbol{s}^{(k+1)}\right\|_2^2$$
$$\beta^{(k)}=\frac{\gamma^{(k+1)}}{\gamma^{(k)}}$$
$$\boldsymbol{p}^{(k+1)}=\boldsymbol{s}^{(k+1)}+\beta^{(k)}\boldsymbol{p}^{(k)}$$

Chapter 3
Schematic Canal Model

3.1. The governing equations

In the first step, the application of assimilation procedure for two or possibly more partial tides is done in a one dimensional canal model, based on the system of equations shown below:

$$\frac{\partial^2 u}{\partial t^2} + R\frac{\partial u}{\partial t} + r*|u|\frac{\partial u}{\partial t} + cu - r - gh\frac{\partial^2 u}{\partial x^2} = 0 \qquad (3.1.1)$$

$$\frac{\partial u}{\partial t} = w \qquad (3.1.2)$$

Substituting (3.1.2) into (3.1.1) yields:

$$\frac{\partial w}{\partial t} + Rw + r*|u|w + cu - r - gh\frac{\partial^2 u}{\partial x^2} = 0 \qquad (3.1.3)$$

where:

R and r*: friction coefficients
c: damping coefficient
r: external force
h: water depth
g: acceleration due to gravity
u: velocity in x-direction

Equations (3.1.2) and (3.1.3) are solved numerically by applying the explicit scheme:

$$w^n = \frac{\left(1 - 0.5\Delta t\left(R + r*|u^n|\right)w^{n-1} - cu^n\Delta t + r^n\Delta t + ghu_{xx}\Delta t\right)}{1 + 0.5\Delta t\left(R + r*|u|\right)} \qquad (3.1.4)$$

$$u^n = u^{n-1} + w^n\Delta t \qquad (3.1.5)$$

To perform the assimilation procedure, equation (3.1.1) is discretized as:

$$\frac{u_i^{n+1}-2u_i^n+u_i^{n-1}}{\Delta t^2}+R\left(\frac{u_i^{n+1}-u_i^{n-1}}{2\Delta t}\right)+r*\left|u_i^n\right|\left(\frac{u_i^{n+1}-u_i^{n-1}}{2\Delta t}\right)$$
$$+cu_i^n-r_i^n-gh\left(\frac{u_{i+1}^n-2u_i^n+u_{i-1}^n}{\Delta x^2}\right)=0$$

After regrouping the terms, the equation above can be written as:

$$\left(\frac{1}{\Delta t^2}+\frac{R}{2\Delta t}+\frac{r*\left|u_i^n\right|}{2\Delta t}\right)u_i^{n+1}+\left(-\frac{2}{\Delta t^2}+c+\frac{2gh}{\Delta x^2}\right)u_i^n-\frac{gh}{\Delta x^2}u_{i+1}^n-\frac{gh}{\Delta x^2}u_{i-1}^n$$
$$+\left(\frac{1}{\Delta t^2}-\frac{R}{2\Delta t}-\frac{r*\left|u_i^n\right|}{2\Delta t}\right)u_i^{n-1}=r_i^n \qquad (3.1.6)$$

3.2. Data assimilation procedure

Equation (3.1.6) can be written, in the form of linear algebraic system, as:

$$\boldsymbol{Ax}=\boldsymbol{b} \qquad (3.2.1)$$

The vector $\boldsymbol{x}$ of unknown is made up by the u_i^k, while vector $\boldsymbol{b}$ is made up by external force (and initial values at the very beginning first and second time steps):

$$-b_{i\,I}=\left(-\frac{2}{\Delta t^2}+c+\frac{2gh}{\Delta x^2}\right)u_i^{(0)}+\left(\frac{1}{\Delta t^2}-\frac{R}{2\Delta t}-\frac{r*\left|u_i^{(0)}\right|}{2\Delta t}\right)u_i^{(-1)}$$
$$-r_i^{(0)}-\frac{gh}{\Delta x^2}u_{i+1}^{(0)}-\frac{gh}{\Delta x^2}u_{i-1}^{(0)} \qquad (3.2.2)$$

$$-b_{i\,II}=\left(\frac{1}{\Delta t^2}-\frac{R}{2\Delta t}-\frac{r*\left|u_i^{(1)}\right|}{2\Delta t}\right)u_i^{(0)}-r_i^{(1)} \qquad (3.2.3)$$

$$-b_{i\,III}=-r_i^{(n)} \qquad (3.2.4)$$

where $u^{(-1)}$ and $u^{(0)}$ are the initial values obtained from the forward model at the very beginning of assimilation process and from two last time steps within a time block at the continuation.

Matrix $\boldsymbol{A}$ is sparse and made up by dynamic equations and consists of linear and

non-linear parts. In the matrix form, equation (3.1.6) by using linear algebraic system in equation (3.2.1) can be written in the following general form

$$\begin{pmatrix} \boldsymbol{A}_{L1} & \boldsymbol{A}_{L2} & \boldsymbol{A}_{L3} & 0 & \dots & 0 & 0 & 0 \\ 0 & \boldsymbol{A}_{L1} & \boldsymbol{A}_{L2} & \boldsymbol{A}_{L3} & \dots & 0 & 0 & 0 \\ 0 & 0 & \boldsymbol{A}_{L1} & \boldsymbol{A}_{L2} & \dots & 0 & 0 & 0 \\ 0 & 0 & 0 & \boldsymbol{A}_{L1} & \dots & 0 & 0 & 0 \\ & & & & \dots & & & \\ 0 & 0 & 0 & 0 & \dots & \boldsymbol{A}_{L1} & \boldsymbol{A}_{L2} & \boldsymbol{A}_{L3} \\ 0 & 0 & 0 & 0 & \dots & 0 & \boldsymbol{A}_{L1} & \boldsymbol{A}_{L2} \\ 0 & 0 & 0 & 0 & \dots & 0 & 0 & \boldsymbol{A}_{L1} \end{pmatrix} \begin{pmatrix} \boldsymbol{x}^{n} \\ \boldsymbol{x}^{n-1} \\ \boldsymbol{x}^{n-2} \\ \boldsymbol{x}^{n-3} \\ \dots \\ \boldsymbol{x}^{3} \\ \boldsymbol{x}^{2} \\ \boldsymbol{x}^{1} \end{pmatrix} +$$

$$\begin{pmatrix} \boldsymbol{A}_{NL1}^{(n)} & 0 & \boldsymbol{A}_{NL2}^{(n)} & 0 & \dots & 0 & 0 & 0 \\ 0 & \boldsymbol{A}_{NL1}^{(n-1)} & 0 & \boldsymbol{A}_{NL2}^{(n-1)} & \dots & 0 & 0 & 0 \\ 0 & 0 & \boldsymbol{A}_{NL1}^{(n-2)} & 0 & \dots & 0 & 0 & 0 \\ 0 & 0 & 0 & \boldsymbol{A}_{NL1}^{(n-3)} & \dots & 0 & 0 & 0 \\ & & & & \dots & & & \\ 0 & 0 & 0 & 0 & \dots & \boldsymbol{A}_{NL1}^{(3)} & 0 & \boldsymbol{A}_{NL2}^{(3)} \\ 0 & 0 & 0 & 0 & \dots & 0 & \boldsymbol{A}_{NL1}^{(2)} & 0 \\ 0 & 0 & 0 & 0 & \dots & 0 & 0 & \boldsymbol{A}_{NL1}^{(1)} \end{pmatrix} \begin{pmatrix} \boldsymbol{x}^{n} \\ \boldsymbol{x}^{n-1} \\ \boldsymbol{x}^{n-2} \\ \boldsymbol{x}^{n-3} \\ \dots \\ \boldsymbol{x}^{3} \\ \boldsymbol{x}^{2} \\ \boldsymbol{x}^{1} \end{pmatrix} = \begin{pmatrix} \boldsymbol{r}^{n} \\ \boldsymbol{r}^{n-1} \\ \boldsymbol{r}^{n-2} \\ \boldsymbol{r}^{n-3} \\ \dots \\ \boldsymbol{b}_{III} \\ \boldsymbol{b}_{II} \\ \boldsymbol{b}_{I} \end{pmatrix} \qquad (3.2.5)$$

In this connection $\boldsymbol{A}_{L1}$ and $\boldsymbol{A}_{L3}$ obviously denote diagonal matrices, while $\boldsymbol{A}_{L2}$ is a tridiagonal matrix. The matrices $\boldsymbol{A}_{NL1}^{(n)}$ and $\boldsymbol{A}_{NL2}^{(n)}$ are diagonal and depend on $\boldsymbol{x}^n$.

The vectors $\boldsymbol{x}^k$ and $\boldsymbol{r}^k$ are composed of the corresponding values $\boldsymbol{u}_i^k$ and $\boldsymbol{r}_i^k$ at the positions i=1,...,L. The boundary condition at the closed end is realized by prescribing $\boldsymbol{x}_0^k = 0$; in the actual application $\boldsymbol{r}_i^k = 0$ with the exception of $\boldsymbol{r}_L^k$ which is defined by the condition $\dfrac{h\left(\boldsymbol{u}_{L+1}^k - \boldsymbol{u}_L^k\right)}{\Delta x} = \boldsymbol{f}^k$, $\boldsymbol{f}^k$ being determined by tidal elevations at the open boundary.

The data equation is given by:

$$\boldsymbol{D}\boldsymbol{x} = \boldsymbol{d} \qquad (3.2.6)$$

With observations taken from m positions, only $m*n$ rows of the matrix $\boldsymbol{D}$ and the corresponding component of the vector $\boldsymbol{d}$ contain non-zero entries, where n here is the total number of time steps within a time block. Only m rows of the $\boldsymbol{D}^k$ have

non-zero entries, if $\boldsymbol{u}_i^k$ is directly prescribed at position i. For example, if m=1 at cells number i, the matrix form of equation (3.2.6) can be written as:

$$\begin{pmatrix} D^n & 0 & 0 & 0 & ... & 0 & 0 & 0 \\ 0 & D^{n-1} & 0 & 0 & ... & 0 & 0 & 0 \\ 0 & 0 & D^{n-2} & 0 & ... & 0 & 0 & 0 \\ 0 & 0 & 0 & D^{n-3} & ... & 0 & 0 & 0 \\ & & & & ... & & & \\ 0 & 0 & 0 & 0 & ... & D^3 & 0 & 0 \\ 0 & 0 & 0 & 0 & ... & 0 & D^2 & 0 \\ 0 & 0 & 0 & 0 & ... & 0 & 0 & D^1 \end{pmatrix} \begin{pmatrix} \boldsymbol{x}^n \\ \boldsymbol{x}^{n-1} \\ \boldsymbol{x}^{n-2} \\ \boldsymbol{x}^{n-3} \\ ... \\ \boldsymbol{x}^3 \\ \boldsymbol{x}^2 \\ \boldsymbol{x}^1 \end{pmatrix} = \begin{pmatrix} d^n \\ d^{n-1} \\ d^{n-2} \\ d^{n-3} \\ ... \\ d^3 \\ d^2 \\ d^1 \end{pmatrix} \qquad (3.2.7)$$

The minimization functional used is defined by equation (2.1.1) as has already mentioned in the previous chapter.

The dynamic equation (2.1.2) with the lower triangular matrix $\boldsymbol{R}$, together with the data equation (2.1.3) can then be replaced by the following system:

$$\begin{aligned} &\boldsymbol{WAx} = \boldsymbol{Wb} \\ &w_1(z_i - z_j) = 0 \\ &w_2(z_i + z_j - 2z_k) = 0 \\ &\boldsymbol{S}^{-1/2}\boldsymbol{Dx} = \boldsymbol{S}^{-1/2}\boldsymbol{d} \end{aligned}$$

where $\boldsymbol{W}$ is a diagonal matrix, w_1 and w_2 are weighting factors and $\boldsymbol{z}$ is row vector of $\boldsymbol{A}$. The subscripts i, j, k in z variable indicate neighbouring space positions in x-direction.

3.3. Model setup

The model domain for testing the assimilation procedure is defined by 24 grid-points and assumed open at one end and closed at the other one. The total simulation time interval (LAE) of 420 steps is divided into several time blocks (KAE) and a continuation procedure is used until convergence for each block is obtained (see Figure 3.3.1). The total time interval necessary for this purpose has a length of approximately 3*LAE time steps. Firstly, equations (3.1.4) and (3.1.5) are used to calculate the "reference" solution and then by reducing the values of g (acceleration due to gravity) to 0.95g, solution to the "deficient" system ("to be corrected") is calculated and used as first guess in the assimilation procedure.

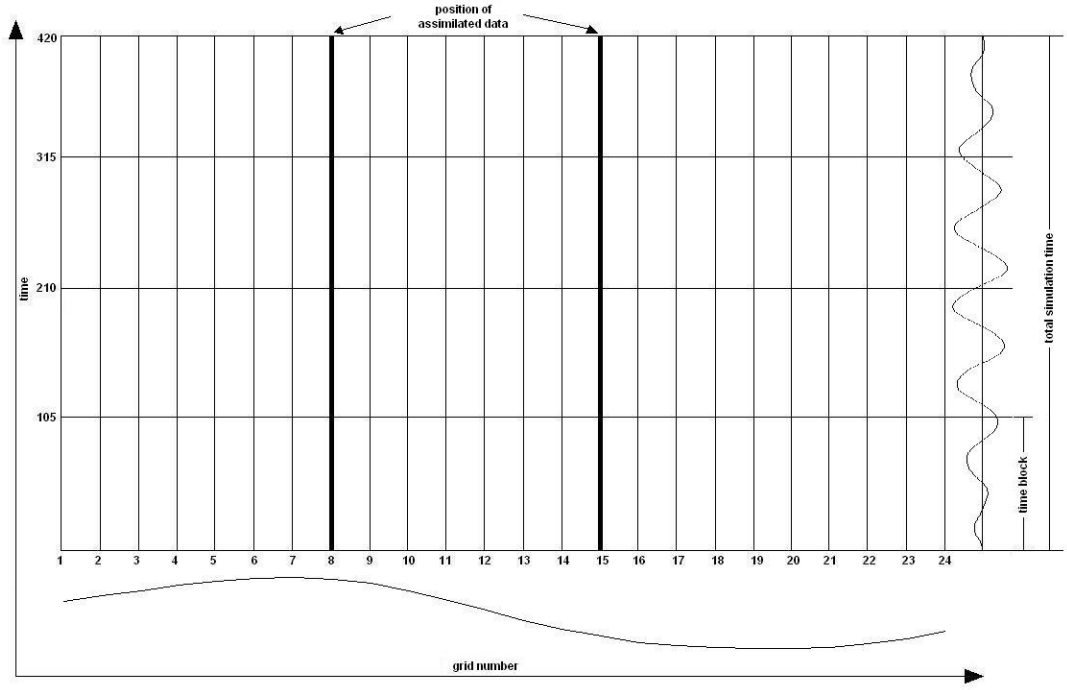

Figure 3.3.1 One dimensional canal model domain and setup.

With this setting, the relative rms deviation between "reference" and "to be corrected" solutions is 35.68%. Data (obtained from "reference" solution) are assimilated at grid number 8 and 15. Two partial tides with angular frequencies σ_1=1.2x10^{-5} rad/s and σ_2=1.4x10^{-5} rad/s and amplitudes A_1=0.1 and A_2=0.075 meters, respectively, are used for defining external forcing (r) in the model domain. The depth of the canal (h) is 200 meter, time step (Δt) is set equal to $2\pi/(\sigma_2 - \sigma_1)$ divided by total number of time steps, and space step (Δx) is set equal to $2\Delta t\sqrt{gh}$. The damping coefficient (c) is set equal to 3.0 x 10^{-12} s^{-2}, while R is set equal to 1.5 x 10^{-7} s^{-1} and r* to 5.0 x 10^{-6} m^{-1}. Weighting for data equation is set to 1 x 10^{-4} and weighting w_1 for first difference of the residuals is set to 0.5 and w_2 for second difference to 1.0. For this numerical canal experiment, with two astronomical constituents determining the open boundary forcing, a beat period corresponding to 420 time steps is used. Computations have been performed using time block lengths of 84, 105, 140, 210, and 420 time steps. Additionally, further computations with time block length 105+20, 105+40, and 210+50 have been performed. Here, continuation to the following time block does not start at the end of the previous block, but 20, 40 or 50 steps earlier, by this way introducing an overlapping interval of 20, 40 or 50 time steps.

In this canal experiment the total tidal signal, defined by σ_1 and σ_2, has been chosen without loss of generality as strictly periodic in order to more easily studying the performance of the method. The restriction to two instead of more astronomical tidal constituents is motivated by a greater clearness when analyzing the numerical results.

Chapter 4
Two Dimensional Non-Linear Model of Irish and Celtic Seas

4.1. The shallow water equations

After success application of this method into a schematic canal model experiment, the non-linear 2-D depth averaged model is developed. The system of equations from Mihardja (1991) is used as the basis in this study:

$$\frac{\partial U}{\partial t}+\frac{U}{HR\cos\phi}\frac{\partial U}{\partial \lambda}+\frac{V}{HR}\frac{\partial U}{\partial \phi}-fV+\frac{gH}{R\cos\phi}\frac{\partial \zeta}{\partial \lambda}$$
$$-A_h\left(\frac{1}{R^2\cos^2\phi}\frac{\partial^2 U}{\partial \lambda^2}+\frac{1}{R^2}\frac{\partial^2 U}{\partial \phi^2}\right)+\frac{rU}{H^2}\sqrt{\left(U^2+V^2\right)}=0 \qquad (4.1.1)$$

$$\frac{\partial V}{\partial t}+\frac{U}{HR\cos\phi}\frac{\partial V}{\partial \lambda}+\frac{V}{HR}\frac{\partial V}{\partial \phi}+fU+\frac{gH}{R}\frac{\partial \zeta}{\partial \phi}$$
$$-A_h\left(\frac{1}{R^2\cos^2\phi}\frac{\partial^2 V}{\partial \lambda^2}+\frac{1}{R^2}\frac{\partial^2 V}{\partial \phi^2}\right)+\frac{rV}{H^2}\sqrt{\left(U^2+V^2\right)}=0 \qquad (4.1.2)$$

$$\frac{\partial \zeta}{\partial t}+\frac{1}{R\cos\phi}\frac{\partial (V\cos\phi)}{\partial \phi}+\frac{1}{R\cos\phi}\frac{\partial U}{\partial \lambda}=0 \qquad (4.1.3)$$

where $U=\int_{-h}^{\zeta} u\,dz$, and $V=\int_{-h}^{\zeta} v\,dz$ denote the volume transport in *x*- and *y*-directions, respectively, while ζ denotes the water elevation, λ and ϕ denote the geographic longitude and latitude, $H = h + \zeta$ is the actual water depth (where *h* is the undisturbed depth), *R* is the Earth radius (6378200.0 meters), $f = 2\omega\sin\phi$ is Coriolis parameter with $\omega = 7.2911 \times 10^{-5}$ rad/sec denoting the mean angular velocity of the Earth, $g = 9.806$ m/s^2 is acceleration due to gravity, A_h is horizontal turbulent exchange coefficient, and *r* is the bottom friction coefficient. The choosing of A_h and *r* values will be discussed separately in Section 4.5.

4.2. Discretization of the equations

The system of equations above is solved numerically by an explicit scheme with central difference for diffusive and convective terms and forward difference for the rest of the terms:

$$U_{i,j}^{n+1} = r_{um}U_{i,j}^{n} - q_{conux}U_{i,j}^{n}\left(U_{i+1,j}^{n} + U_{i-1,j}^{n}\right) - q_{conuy}\overline{V}\left(U_{i,j-1}^{n} + U_{i,j+1}^{n}\right)$$
$$+ q_{ahux}\left(U_{i-1,j}^{n} + U_{i+1,j}^{n} - 2U_{i,j}^{n}\right) + q_{ahuy}\left(U_{i,j-1}^{n} + U_{i,j+1}^{n} - 2U_{i,j}^{n}\right) \qquad (4.2.1)$$
$$+ q_{fx}\overline{V} - 2q_{gu}\left(\zeta_{i+1,j}^{n} - \zeta_{i,j}^{n}\right)$$

$$V_{i,j}^{n+1} = r_{vm}V_{i,j}^{n} - q_{convx}\overline{U}\left(V_{i+1,j}^{n} + V_{i-1,j}^{n}\right) - q_{convy}V_{i,j}^{n}\left(V_{i,j-1}^{n} + V_{i,j+1}^{n}\right)$$
$$+ q_{ahvx}\left(V_{i-1,j}^{n} + V_{i+1,j}^{n} - 2V_{i,j}^{n}\right) + q_{ahvy}\left(V_{i,j-1}^{n} + V_{i,j+1}^{n} - 2V_{i,j}^{n}\right) \qquad (4.2.2)$$
$$- q_{fy}\overline{U} - 2q_{gv}\left(\zeta_{i,j}^{n} - \zeta_{i,j+1}^{n}\right)$$

$$\zeta_{i,j}^{n+1} = \zeta_{i,j}^{n} - \frac{\Delta t}{\Delta y \cos\phi_{u,j}}\left(V_{i,j-1}^{n+1}\cos\phi_{v,j-1} - V_{i,j}^{n+1}\cos\phi_{v,j}\right) - \frac{\Delta t}{\Delta x}\left(U_{i,j}^{n+1} - U_{i-1,j}^{n+1}\right) \qquad (4.2.3)$$

where:

$$r_{um} = \frac{1}{1 + \frac{r\Delta t}{0.5\left(H_{i,j} + H_{i+1,j}\right)^2}\sqrt{U^2 + \overline{V}^2}}\ ,\ r_{vm} = \frac{1}{1 + \frac{r\Delta t}{0.5\left(H_{i,j} + H_{i,j+1}\right)^2}\sqrt{\overline{U}^2 + V^2}}$$

$$q_{conux} = r_{um}\frac{\Delta t}{\Delta x\left(H_{i,j} + H_{i+1,j}\right)},\ q_{conuy} = r_{um}\frac{\Delta t}{\Delta y\left(H_{i,j} + H_{i+1,j}\right)}$$

$$q_{convx} = r_{vm}\frac{\Delta t}{\Delta x\left(H_{i,j} + H_{i,j+1}\right)},\ q_{convy} = r_{vm}\frac{\Delta t}{\Delta y\left(H_{i,j} + H_{i,j+1}\right)}$$

$$\overline{U} = 0.25\left(U_{i,j} + U_{i-1,j} + U_{i,j+1} + U_{i-1,j+1}\right),\ \overline{V} = 0.25\left(V_{i,j} + V_{i,j-1} + V_{i+1,j} + V_{i+1,j-1}\right)$$

$$q_{ahux} = A_h r_{um}\frac{\Delta t}{\Delta x^2},\ q_{ahuy} = A_h r_{um}\frac{\Delta t}{\Delta y^2},\ q_{ahvx} = A_h r_{vm}\frac{\Delta t}{\Delta x^2},\ q_{ahvy} = A_h r_{vm}\frac{\Delta t}{\Delta y^2}$$

$$q_{fx} = \Delta t\, f_u\, r_{um},\ q_{fy} = \Delta t\, f_v\, r_{vm},\ f_u = 2\omega\sin\phi_u,\ f_v = 2\omega\sin\phi_v$$

$$\Delta x = \Delta\lambda R\cos\phi,\ \Delta y = \Delta\phi R$$

An Arakawa C-grid is used for all dynamical calculations (Kantha and Clayson (2000; see Figure 4.2.1 for the convention). The model domain is divided into *n* columns and *m* rows, for a total of *nm* grid cells. The longitude and latitude limits correspond to the edges of the model domain, not the centres of the edge grid cells. Elevations ζ are taken to be averages over each cell. Similarly, grid bathymetry is given for each cell, and should correspond to average water depth in each cell. Volume transports *U* and *V* are specified on grid cell edges, and are

interpreted to be the average volume transport over the cell edge. Boundary conditions at the coast are specified on the U and V nodes. Open boundary conditions are given by specifying the elevation ζ for open boundary edge cells. Along closed land boundaries the normal component of volume transport is set to zero.

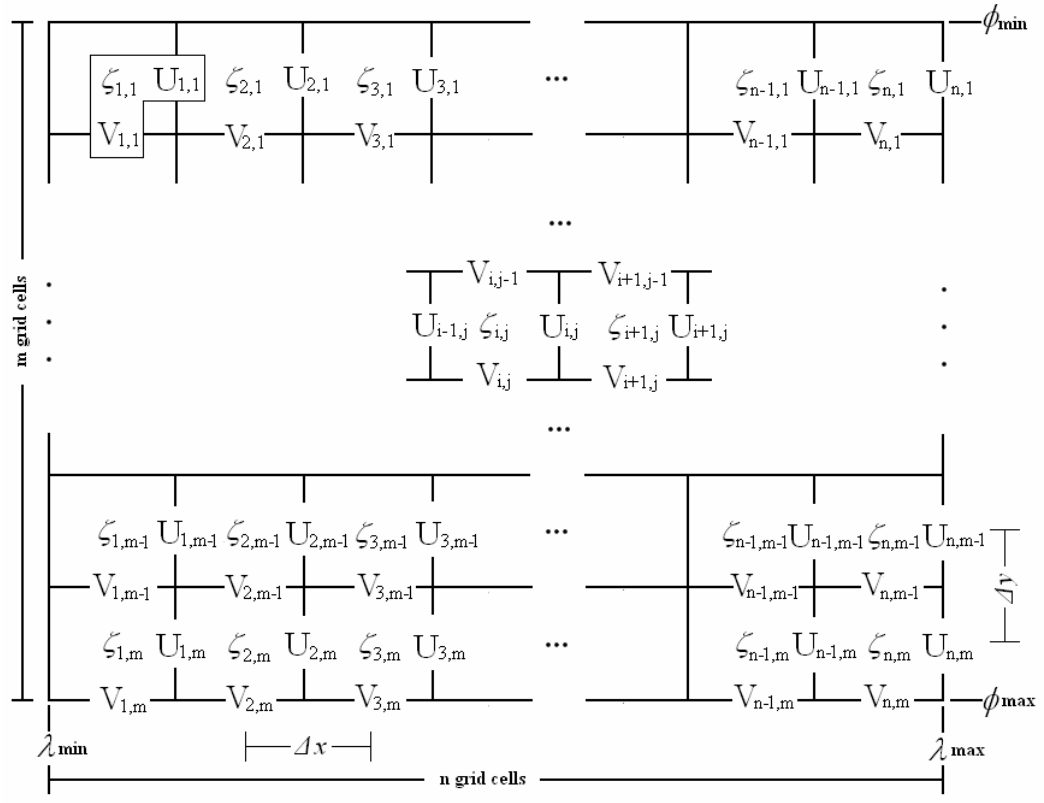

Figure 4.2.1 Grid convention used in 2D model.

4.3. Data assimilation procedure

An inverse direct method of the global ocean model applied by Zahel (1991) is used in this work and extended to the 2D non-linear shallow water equations on the basis of the schematic canal model. The method minimizes the dynamics and data residues in the sense of the least squares problem and at the same time looks for the most likely residuals, which are assumed statistically as normally distributed.

The system of equations (4.2.1), (4.2.2), and (4.2.3) can be written in the form of a linear algebraic system as has already mentioned in equation (3.2.1). The unknowns $\boldsymbol{x}$ are made up by elevation ζ and horizontal volume transport components U and V. The vector $\boldsymbol{b}$ consists of b_ζ, b_U, and b_V. In the interior, at the first time step, vector $\boldsymbol{b}$ is defined by:

$$b_{U,p} = r_{um,p}U_{i,j}^{(0)} - q_{conux,p}U_{i,j}^{(0)}\left(U_{i+1,j}^{(0)} + U_{i-1,j}^{(0)}\right) - q_{conuy,p}\overline{V}^{(0)}\left(U_{i,j-1}^{(0)} + U_{i,j+1}^{(0)}\right) + q_{ahux,p}\left(U_{i-1,j}^{(0)} + U_{i+1,j}^{(0)} - 2U_{i,j}^{(0)}\right) + q_{ahuy,p}\left(U_{i,j-1}^{(0)} + U_{i,j+1}^{(0)} - 2U_{i,j}^{(0)}\right) + q_{fx,p}\overline{V}^{(0)} - 2q_{gu,p}\left(\zeta_{i+1,j}^{(0)} - \zeta_{i,j}^{(0)}\right) \quad (4.3.2)$$

$$b_{V,p} = r_{vm,p}V_{i,j}^{(0)} - q_{convx,p}\overline{U}^{(0)}\left(V_{i+1,j}^{(0)} + V_{i-1,j}^{(0)}\right) - q_{convy,p}V_{i,j}^{(0)}\left(V_{i,j-1}^{(0)} + V_{i,j+1}^{(0)}\right) + q_{ahvx}\left(V_{i-1,j}^{(0)} + V_{i+1,j}^{(0)} - 2V_{i,j}^{(0)}\right) + q_{ahvy}\left(V_{i,j-1}^{(0)} + V_{i,j+1}^{(0)} - 2V_{i,j}^{(0)}\right) - q_{fy}\overline{U}^{(0)} - 2q_{gv}\left(\zeta_{i,j}^{(0)} - \zeta_{i,j+1}^{(0)}\right) \quad (4.3.3)$$

$$b_{\zeta,p} = \zeta_{i,j}^{0} \quad (4.3.4)$$

Superscript *(0)* in *U, V,* $\overline{U}$, $\overline{V}$, and ζ indicating that the values of these variables are taken from the first guess. In the equations above, a subscript *p* has also introduced as a vector row index, converted from the space and time indexes (*i*,*j*,*n*).

The values of vector ***b*** on the next time steps within a time block are zero except for b_U and b_V close to the open boundaries where the pressure gradient term needs prescribed elevation values from the open boundaries:

$$b_{U,p} = 2q_{gu,p}\zeta_{OB\,i,j} \quad (4.3.5)$$

$$b_{V,p} = 2q_{gv,p}\zeta_{OB\,i,j} \quad (4.3.6)$$

And at the open boundaries, b_ζ are defined by the tidal elevation ζ_{OB}:

$$b_{\zeta,p} = \zeta_{OB\,i,j} \quad (4.3.7)$$

The matrix ***A*** consists of coefficients appearing in dynamics equations. ***A*** is a sparse matrix due to the fact that loading and self-attraction effects, as far as it is generated in adjacent sea areas, can be neglected (Gekeler, 1995). A special treatment is needed to manage the large sparse matrix generated within a time block to reduce the need of computer memory and also to speed up the matrix-vector multiplication (see Section 4.5 for detail description).

The data equation is given by equation (3.2.6) with ***x*** defined by sea surface elevation and the right hand side of equation (3.2.6) being generated by:

$$d_{\varsigma,p} = \sum_{l=1}^{NC} a_l \cos\left(\sigma_l\, k\, \Delta t - \varphi_l\right) \quad (4.3.8)$$

where *NC* is the number of tidal constituents (in this case *NC*=8: M_2, S_2, $2SM_2$, M_4, M_6, MS_4, $2MS_6$, and $2SM_6$); A_l, σ_l, and φ_l are amplitude, angular frequency,

and phase of the *l-th* tidal constituent, respectively, Δt denotes the time step, and k indicates the number of time level.

Observations used in data equation are taken from m positions, and only $m*n$ rows of the matrix $\boldsymbol{D}$ and the vector $\boldsymbol{d}$ contain non-zero entries (n indicates the total number of time level within a time block). The cost function is given by (2.1.1).

Two cases of assimilation procedure are applied in this study, with and without residual smoothing processes. In the case of applying the residual smoothing process, the dynamic equation (2.1.2) with the lower triangular matrix $\boldsymbol{R}$, together with the data equation (2.1.3) can then be replaced by the following system:

$$\begin{aligned} &\boldsymbol{WAx} = \boldsymbol{Wb} \\ &w_1\left(z_i - z_j\right) = 0 \\ &\boldsymbol{S}^{-1/2}\boldsymbol{Dx} = \boldsymbol{S}^{-1/2}\boldsymbol{d} \end{aligned}$$

Where $\boldsymbol{W}$ is a diagonal matrix, w_1 is weighting factor and $\boldsymbol{z}$ is row vector of $\boldsymbol{A}$. The subscripts i, j in $\boldsymbol{z}$ variable indicate neighbouring space positions in x- and y-directions.

4.4. Model domain

The area of this study is the region of the Irish and Celtic Seas, 50°N-57°N and 2°W-8°W (Figure 4.4.1). The Irish Sea separates the islands of Ireland and Great Britain. It is connected to the Atlantic Ocean by the North Channel and Saint George's Channel. The Celtic Sea is the area of the Atlantic Ocean off the south coast of Ireland. It is bounded to the east by Saint George's Channel and the Bristol Channel. The northern portion of this sea had previously been considered part of Saint George's Channel and the southern part had no common name.

This study uses bathymetry data from ETOPO5 (National Geophysical Data Centre, 1988) with spatial resolution ($\Delta\phi$ and $\Delta\lambda$) of 5 minutes or equal to 9 km. This adjacent sea area has varying water depths from more than 150 m in the vicinity of northern and southern boundary to a mean depth of 55 m in the eastern Irish Sea, where areas of very shallow water exist (Figure 4.4.1). The comparatively coarse spatial resolution used in this study is not suitable to produce a realistic solution in the small scale areas, such as the Bristol Channel and Severn estuary. Only by applying a high resolution classical model, including a complex adjustment of friction parameters and open boundary values, the specific effects in these small areas can be reproduced directly, i.e. without data assimilated.

The Celtic Sea has strong depth gradients at its west side towards the open sea. The tidal waves appearing on the European shelf, to which the area of investigations belongs to, are produced in the open Atlantic Ocean and are

deformed by the islands of Ireland, Scotland, and Great Britain. The waves arriving from the deep ocean essentially spread on the shelf as Kelvin waves. They propagate across the Celtic Sea to the Irish Sea and across the English Channel northward into the North Sea. In the shallow water areas, mainly in the west and south parts of the North Sea and the English and Saint George's Channels, the tidal energy is dissipated, where the semi-diurnal tidal flow rates are largest.

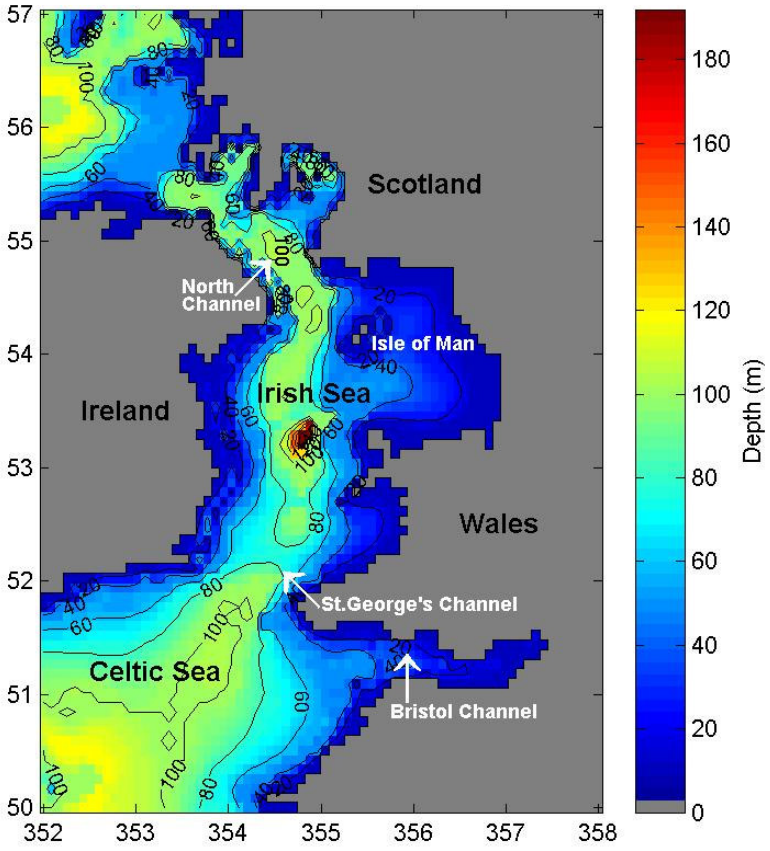

Figure 4.4.1 Bathymetric map of Irish and Celtic Seas.

The incoming Kelvin waves are grown due to their high flow rates by the constant effect of the bottom friction and reflected at the end of the basin with smaller amplitude. A consequence of it is the misalignment of the amphidromic for the side of the energy maximum of the reflected wave, as with the M_2-tide in the Irish Sea and in English Channel is observed (Simpson, 1998).

In the south part, part of the tidal energy flux from the Celtic Sea goes northward to the Irish Sea through the Saint George's Channel. In the north part of European continental shelf, part of tidal energy flux off the west coast of Scotland goes southward through the North Channel and into the Irish Sea (Davies and Kwong, 2000).

In the Irish Sea, the tidal currents are strong generally (in the order of 1.5 m/s) except in a small area to the west of the Isle of Man where the tidal currents are weak (in the order of 0.2 m/s) (Lee and Davies, 2001).

4.5. Model setup

Based on the Courant-Friedricks-Lewy (CFL) condition, the time step (Δt) equal to 120 seconds is used in the forward as well as data assimilation models. With that value, 1 day simulation time is equal to 720 time steps. The elevation of M_2 and S_2 tidal constituents used at the open boundaries defining the northern, western, and southern transition to the open ocean are taken from the regional tidal solution for the North Sea from Oregon State University Tidal Inversion Software (OTIS, Egbert and Erofeeva, 2002).

Davies and Jones (1992) have chosen two different values of bottom friction coefficient (r) in their 3D model, namely 0.0025 and 0.0050, respectively. By using $r = 0.0025$, the values of sea surface elevation were found to be in the order of 10 to 20% higher than the observed elevations, while using $r = 0.0050$ the values are in good agreement with observations. Further, they report that an analysis of computed and observed results showed that in general M_2 amplitudes and phases obtained by applying the 2D model ($r = 0.0025$) and the 3D model ($r = 0.0050$) differ little. Based on these finding, the value of $r = 0.0025$ is used in this study.

Some experiments have been done in this study to choose the value of coefficient of horizontal diffusion (A_h) appropriately, and it is found that $A_h = 5 \times 10^3$ m^2/s yields best results with respect to numerical stability and the agreement to the observation and other model results. Weis (2006) has done some experiments in tuning the values of A_h and mentioned that for 5 minutes resolution simulation, the range of values guaranteeing numerical stability lies between 5×10^3 and 45×10^3 m^2/s. Therefore, $A_h = 5 \times 10^3$ m^2/s is used in this study.

The first guess of U, V, and ζ fields used in beginning the assimilation procedure are taken from the forward model results. The tidal data for assimilation and data only used for comparison (at so called independent stations) are taken from Alcock and Howarth (1978), Alcock et al. (1980), Alcock (1982a, b), Alcock and Pugh (1982), Davies and Jones (1992), Davies and Hall (2000), and Taguchi (2002). These data are already given in amplitude and phase of elevation (harmonic constants).

The number of stations used in the assimilation procedure in this study are less than have been used by Taguchi (2002) because when including more than one partial tide and their over- and compound tides, corresponding data are not always available in the reports and papers mentioned above. The positions of available data from 24 stations used in assimilation are given in Table 4.5.1 and Figure

4.5.1, those of data only used for comparison are listed in Table 4.5.2 and depicted in Figure 4.5.2.

The assimilation model is run in 2 different ways, with and without applying residual smoothing process. The residual smoothing process, which has already been mentioned in Section 3.2, is applied to smooth the dynamical residuals. Assimilations with time block of 1 day and 4 days are performed where for each time block the minimization is iteratively achieved for taking into consideration the non-linear contributions. First guess fields for the solution dependent coefficients are taken from the forward solution. These fields are also used for defining the initial condition for the first time block. Subsequent time blocks are started making use of fields from the previous block.

In general, the assimilation procedure developed in this study is immediately suitable to include more than 2 partial tides as forcing at the open boundaries (as has been mentioned in Section 1.3). In this study the model calculations are limited to M_2 and S_2. The reason for this restriction is to make the interpretaion of results easier, also in view of the very different number of observation being available for the individual tidal constituents.

Table 4.5.1 Positions of data used in assimilation.

Station ID	Position		Location
	Lat	Long	
A01	53°46.000' N	3°43.000' W	Irish Sea
A02	53°46.000' N	4°08.000' W	Irish Sea
A03	52°04.000' N	5°47.000' W	Irish Sea
A04	54°09.000' N	3°40.000' W	Irish Sea
A05	54°39.000' N	3°55.000' W	Solway Firth
A06	53°30.000' N	3°11.900' W	Queens Channel
A07	51°45.200' N	6°35.700' W	Celtic Sea
A08	51°20.000' N	6°30.000' W	Celtic Sea
A09	50°35.000' N	6°10.000' W	Celtic Sea
A10	51°27.000' N	7°51.000' W	Celtic Sea
A11	50°33.000' N	7°32.000' W	Celtic Sea
A12	51°24.600' N	5°00.600' W	Bristol Channel
A13	50°55.100' N	4°59.900' W	Bristol Channel
A14	51°20.300' N	3°06.200' W	Severn Estuary
A15	51°12.900' N	3°28.300' W	Severn Estuary
A16	54°57.000' N	5°35.700' W	North Channel
A17	55°27.800' N	6°09.800' W	North Channel
A18	51°30.618' N	2°42.846' W	Avonmouth
A19	51°13.002' N	3°07.998' W	Hinkley Point
A20	51°34.002' N	3°58.002' W	Mumbles
A21	50°06.144' N	5°32.502' W	Newlyn
A22	53°18.822' N	4°37.158' W	Holyhead
A23	53°19.914' N	3°49.500' W	Llandudno
A24	54°39.900' N	5°40.140' W	Northern Ireland

In the positions where data are assimilated, both partial tides (M_2 and S_2) and their over- and compound tides (M_4, M_6, $2SM_2$, MS_4, $2MS_6$, and $2SM_6$) are used to generate elevation as has already been mentioned in equation (4.3.7). The angular frequencies of these tidal constituents are given in Table 4.5.3.

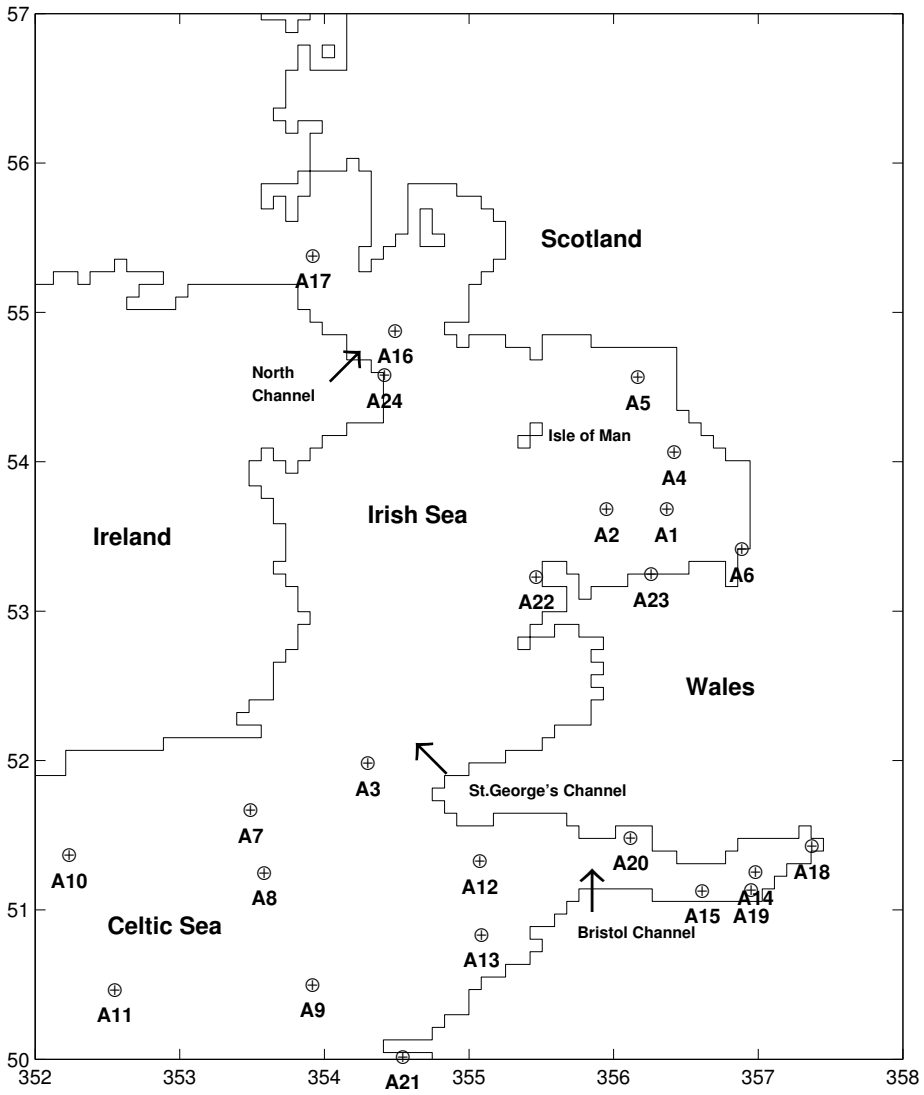

Figure 4.5.1 Positions of data used in assimilation.

The continuation is done after a sufficient number of CGLS and non-linear iteration steps are performed, and the computations are finished after the complete time period reached more than 14.7 days, the beat period of M_2 and S_2. With this length of time series, two predominant partial tides M_2 and S_2 can be distinguished unambiguously from the solution.

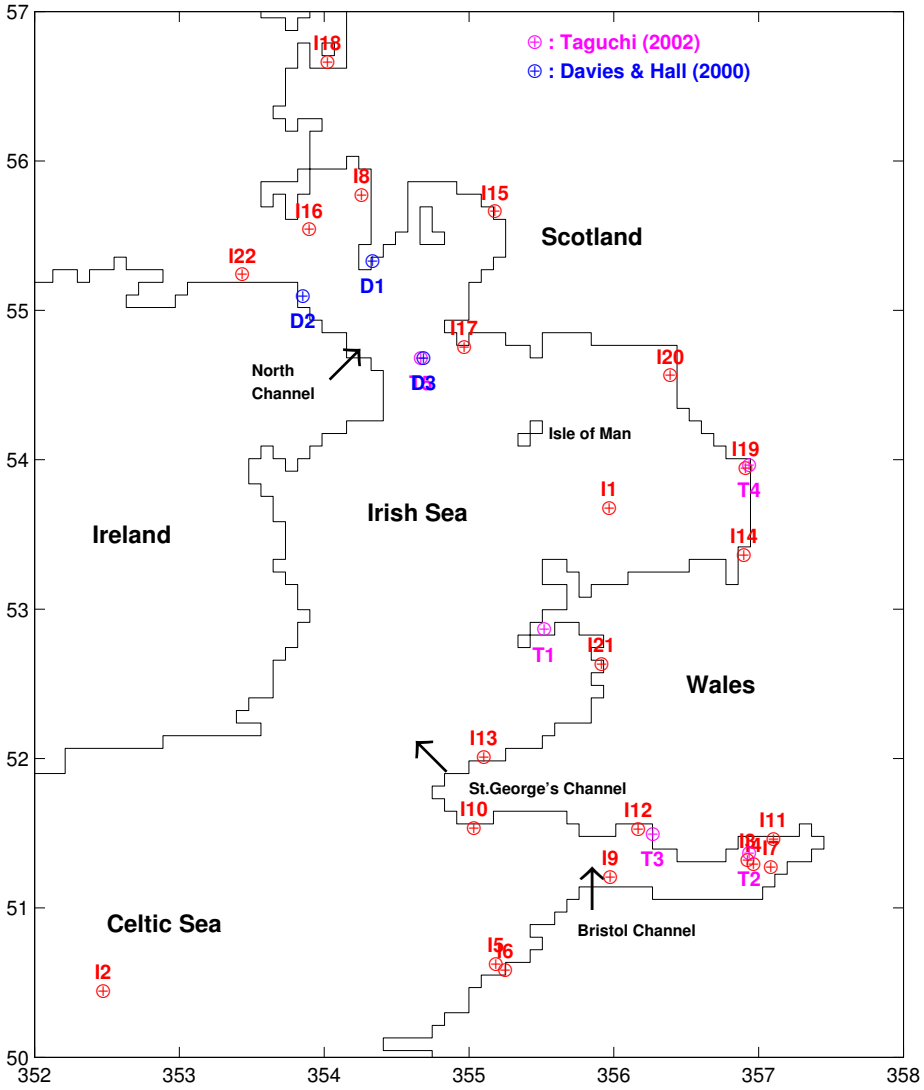

Figure 4.5.2 Positions of independent stations.

As has already been mentioned in Section 4.3, the matrix $\boldsymbol{A}$ which consists of coefficients appearing in dynamics equations is a sparse matrix. Based on the CGLS algorithm given in Section 2.2, there are two matrix-vector multiplications exist inside the CGLS loop. Beside that, the size of matrix $\boldsymbol{A}$ used in the calculation is rather large, therefore a special treatment is needed to manage the large sparse matrix created and used within a time block and matrix-vector multiplications to reduce the need of computer memory. To do this, a subroutine called APROD is created performing $(\boldsymbol{y}+\boldsymbol{A}\boldsymbol{x})$ in direct mode and $(\boldsymbol{x}+\boldsymbol{A}^T\boldsymbol{y})$ in transpose mode for a given n element vector $\boldsymbol{x}$ and m element vector $\boldsymbol{y}$ and $\boldsymbol{A}$ is not created explicitly (adopted from Paige and Saunders, 1982). An OpenMP parallelization (Chandra et al., 2001) is also applied to share the the matrix-vector multiplication processes into some processors to increase the calculation speed.

Table 4.5.2 Positions of independent stations.

Station ID	Position		Location
	Lat	Long	
I01	53°45.800' N	4°07.000' W	Irish Sea
I02	50°31.700' N	7°36.700' W	Celtic Sea
I03	51°24.400' N	3°09.700' W	Severn Estuary
I04	51°22.800' N	3°07.100' W	Severn Estuary
I05	50°37.500' N	4°54.000' W	Bristol Channel
I06	50°35.300' N	4°50.000' W	Bristol Channel
I07	51°21.500' N	3°00.000' W	Severn Estuary
I08	55°51.600' N	5°44.500' W	North Channel
I09	51°12.468' N	4°06.606' W	Ilfracombe
I10	51°42.354' N	5°03.030' W	Milford Haven
I11	51°33.000' N	2°58.998' W	Newport (Gwent)
I12	51°37.000' N	3°55.000' W	Swansea
I13	52°00.768' N	4°58.956' W	Fishguard
I14	53°27.000' N	3°01.002' W	Gladstone Dock
I15	55°44.970' N	4°54.294' W	Millport
I16	55°37.662' N	6°11.328' W	Port Ellen
I17	54°50.544' N	5°07.134' W	Portpatrick
I18	56°37.386' N	6°03.768' W	Tobermory
I19	54°01.884' N	2°55.236' W	Heysham
I20	54°39.000' N	3°34.086' W	Workington
I21	52°43.140' N	4°02.628' W	Barmouth
I22	55°12.000' N	6°39.000' W	Portrush
T01	52°57.000' N	4°34.000' W	Llanbedrog
T02	51°27.000' N	3°09.000' W	Fishguard
T03	51°35.000' N	3°49.000' W	Swansea
T04	54°03.000' N	3°09.000' W	Heysham
T05/D03	54°46.000' N	5°25.000' W	North Channel
D01	55°25.000' N	5°45.000' W	North Channel
D02	55°11.000' N	6°04.000' W	North Channel

Table 4.5.3 List of analysed tidal constituents.

Tidal Constituent	Frequency (σ, rad/s)	Origin
M_2	1.4053×10^{-4}	Lunar
S_2	1.4544×10^{-4}	Solar
M_4	2.8105×10^{-4}	$2 \times M_2$
M_6	4.2158×10^{-4}	$3 \times M_2$
$2SM_2$	1.5036×10^{-4}	$2 \times S_2 - M_2$
MS_4	2.8597×10^{-4}	$M_2 + S_2$
$2MS_6$	4.2650×10^{-4}	$2 \times M_2 + S_2$
$2SM_6$	4.3141×10^{-4}	$2 \times S_2 + M_2$

4.6. Harmonic analysis

In order to analyse the result from the assimilation model, an harmonic analysis is performed to obtain the amplitude and phase of both partial tides and their over- and compound tides. The harmonic constants obtained from this harmonic analysis then compare to the data from independent stations (see Table 4.5.2 and

Figure 4.5.2 for their detailed positions) to study the performance of the data assimilation procedure and the influence of the assimilated data.

Harmonic analysis is a method for determining the amplitude and phase of certain harmonic or wave components in a set of data. The time series of data set to be analysed can be regarded as having the form:

$$\zeta(t_n) = A_0 + \sum_{j=1}^{NC} \left(A_j \, cos(\sigma_j t_n) + B_j \, sin(\sigma_j t_n) \right) \qquad (4.6.1)$$

with j=1,...,NC is the number of tidal constituents to be analysed, A_0 is mean water level, σ_j is the angular frequency of j-th tidal constituent, and t_n indicates time. The values of amplitude (h_j) and phase (g_j) of respective tidal constituents searched for, then can be calculated by:

$$h_j = \sqrt{A_j^2 + B_j^2}$$

$$g_j = tan^{-1}\left(\frac{B_j}{A_j} \right)$$

A_j and B_j can be obtained by computing the least squares solution to the overdetermined linear algebraic system of equation $\boldsymbol{Ax} = \boldsymbol{b}$ with $\boldsymbol{A}$ as a matrix containing NC selected frequencies with size (N+1) x (NC+1), where N indicating the number of time levels. Vector $\boldsymbol{b}$ with size (N+1) is defined by the data set.

Chapter 5
Model Evaluation

5.1. Schematic canal model

In general, the experiment shows that by applying the assimilation procedure described the deviation of "to be corrected" solution from the "reference" solution can be reduced significantly. As already mentioned above, the original relative root mean square (rms) deviation between the "reference" and "to be corrected" solutions is 35.68%, and after applying the assimilation procedure, the relative rms deviations becomes less than 5% (see Table 5.1.1).

Table 5.1.1 Deviations of the "to be corrected" from the "reference" solution dependent upon time block characteristics of data assimilation.

Solution	Deviation (%)
"to be corrected" solution	35.68
KAE=84	4.30
KAE=105	4.05
KAE=140	3.94
KAE=210	3.24
KAE=420	1.38
KAE=105+20 overlap	2.79
KAE=105+40 overlap	1.49
KAE=210+50 overlap	1.19

The experiments with different time block lengths show that the deviation monotonously decreases with increasing block length. An interesting result is obtained when applying an overlapping interval of continuation in the assimilation procedure. In that case the deviation is significantly smaller as compared to the assimilation using the same time block length but without an overlapping interval.

When inspecting the amplitudes (Figure 5.1.1) of both partial tides (σ_1, σ_2) and some of their dominant over- and compound tides ($\sigma_3=2\sigma_1+\sigma_2$, $\sigma_4= 2\sigma_1- \sigma_2$, and $\sigma_7=3\sigma_1$), in general the "to be corrected" solution can be improved significantly except for σ_4 where the amplitude of the assimilation solution is overestimated for KAE=105 and even more for KAE=210. Only for KAE=420 one obtains satisfactory results. However the overestimation of the σ_4-amplitude is reduced significantly when the overlapping interval of continuation is applied, especially in the case of KAE=105+40 (see Table 5.1.2), showing a good agreement with σ_4-amplitude of the "reference" solution.

Table 5.1.2 gives the rms errors of the amplitudes and phases of the constituents

mentioned above. This table shows the rms errors of amplitudes and phases of the various assimilation results. In general the rms errors are significantly smaller than these of the "to be corrected" solution, except for σ_4 where the rms errors are even larger for time block lengths equal to 105 and 210 time steps than for the "to be corrected" solution.

The amplitude overestimation of σ_4 occurs perhaps because the σ_4-signal is very small as compared to the strong astronomical partial tides σ_1 with neighbouring frequency. This phenomenon is obviously sensitive to the length of the time block, because when choosing time block length equal to 420 time steps (complete beat period), the assimilation solution is sufficiently close to the "reference" solution, also with respect to σ_4.

Significant improvement of phases due to data assimilation can also be seen in the solutions (Figure 5.1.2), especially for σ_3 where the deviation between the "reference" and "to be corrected" solutions is very large. From this figure we can take that also for σ_4 the assimilation solutions for all time block selections are improved and are sufficiently close to the "reference" solution, except at cells number 15 up to 19 (for length of time block equal to 105 time steps) and at 16 up to 21 (for length time block equal to 210 time steps). On the other hand, the assimilation procedure with an overlapping interval of continuation can reduce the phases overestimation and underestimation, respectively, occurring in cells number 15 up to 19 (for length of time block equal to 105 time steps) and in 16 up to 21 (for length of time block equal to 210 time steps) decisively.

Table 5.1.2 The root mean square (rms) errors of amplitude and phase of the "to be corrected" and of assimilation solutions.

Amplitude (m)						
Constituents	To be corrected	KAE= 105	KAE= 210	KAE= 420	KAE= 105+20	KAE= 105+40
σ_1	0.04642	0.00217	0.00169	0.00119	0.00168	0.00101
σ_2	0.02498	0.00078	0.00080	0.00081	0.00098	0.00099
$\sigma_3=2\sigma_1+\sigma_2$	0.00236	0.00015	0.00010	0.00008	0.00010	0.00004
$\Sigma_4=2\sigma_1-\sigma_2$	0.00060	0.00096	0.00143	0.00023	0.00047	0.00009
$\sigma_7=3\sigma_1$	0.00096	0.00021	0.00009	0.00006	0.00004	0.00003
Phase (°)						
σ_1	10.02	2.74	1.88	1.05	1.90	1.07
σ_2	9.48	1.39	1.04	0.38	0.83	0.43
$\sigma_3=2\sigma_1+\sigma_2$	112.44	4.97	3.43	1.39	1.44	1.18
$\Sigma_4=2\sigma_1-\sigma_2$	23.30	46.94	40.44	10.64	25.65	2.93
$\sigma_7=3\sigma_1$	35.50	25.53	18.55	22.94	16.16	17.07

For σ_7, the phase at cell numbers 1 up to 5 is overestimated by the assimilation solutions with time block lengths equal to 105 and 210 time steps, while for time block length equal to 420 time steps, the phase is underestimated and close to the "to be corrected" solution. On the other hand, the assimilation procedure with an overlapping interval of continuation can reduce these phase overestimations by

about 50%. The same situation is found at cells number 7 up to 10, but as compared to the "to be corrected" solution, the results from the assimilation experiments yield better agreement with the "reference" solution at these cells. Again, the assimilation procedure with an overlapping interval of continuation can reduce this deviation significantly.

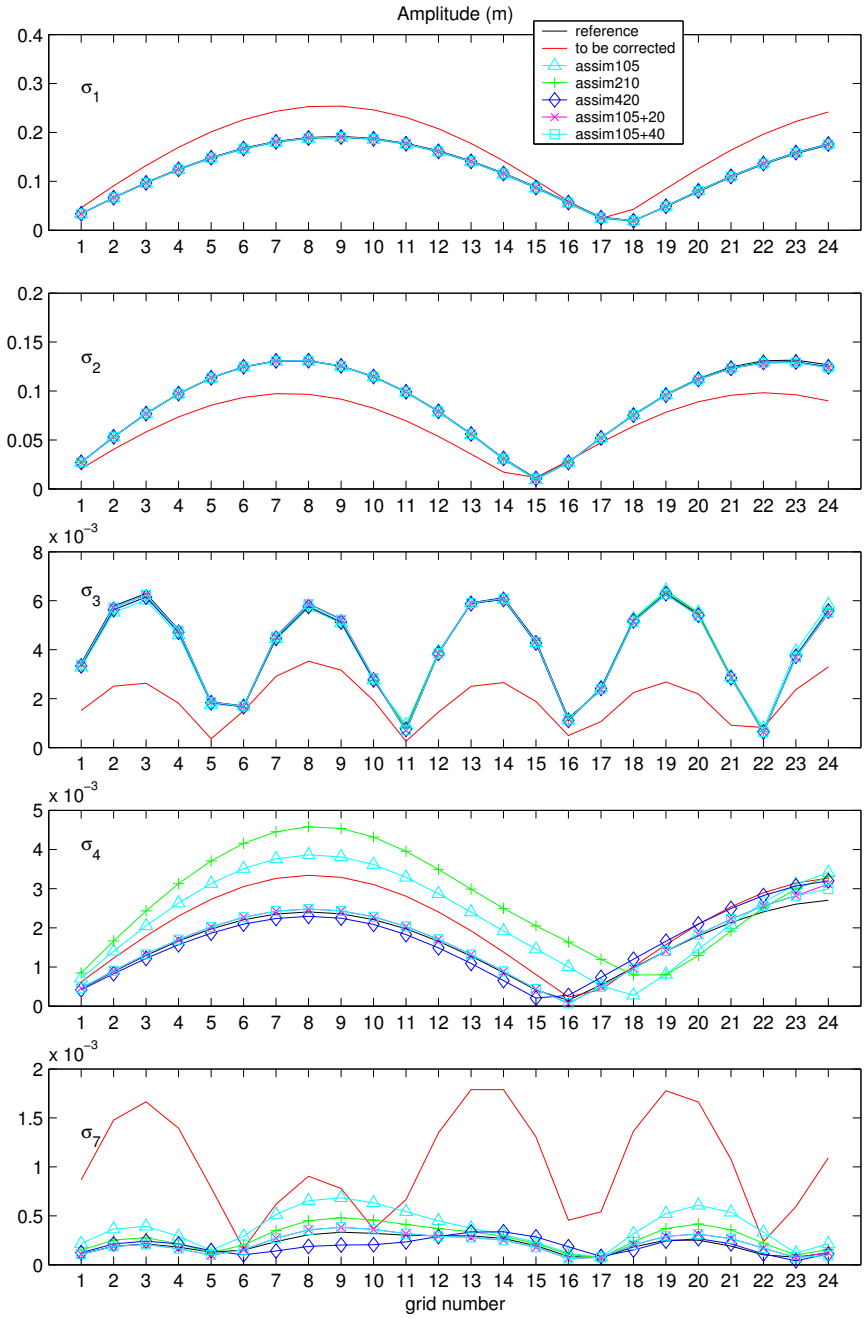

Figure 5.1.1 Comparison of amplitudes as given by the solutions "reference", "to be corrected", and "assimilation with time block equal to 105, 210, 420, 105+20, and 105+40 time steps" for σ_1, σ_2, σ_3, σ_4, and σ_7.

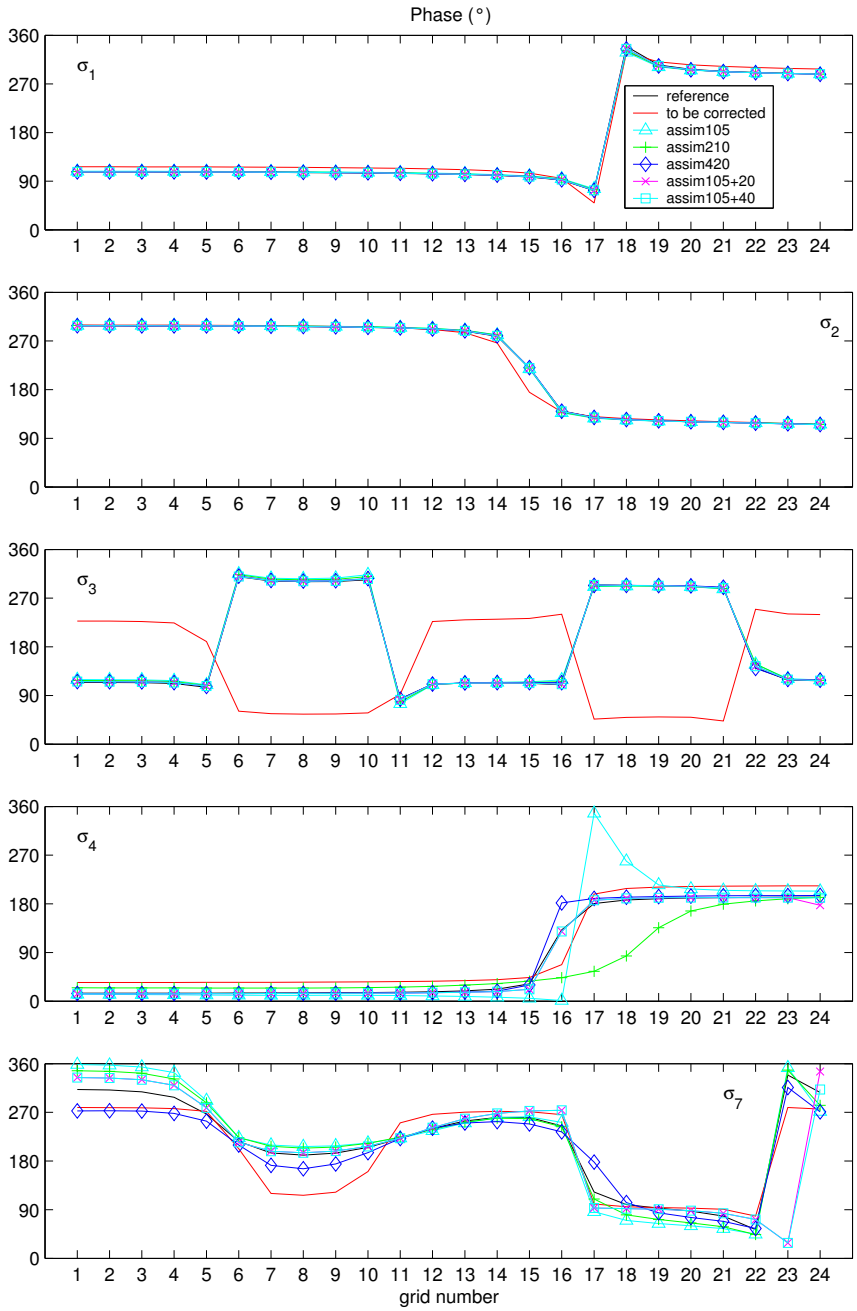

Figure 5.1.2 Comparison of phases as given by the solutions "reference", "to be corrected", and "assimilation with time block length equal to 105, 210, 420, 105+20, and 105+40 time steps" for σ_1, σ_2, σ_3, σ_4, and σ_7.

Apart from generating realistic results by making use of reliable data information, as mentioned above, it is aimed at also finding out what kind of model deficiency has been compensated by the data used for assimilation. As has been shown, instead of partial differential equation problem with unique solution a minimization problem is treated when assimilating data into a model. The

resulting data and dynamical residuals give information on the reliability of the magnitude of the corresponding assumed errors. The dynamical residuals, moreover, should allow drawing conclusions about the model deficiencies (Zahel et al., 2000). In this schematic model investigation the model deficiency is prescribed and fictive data have been produced by the reference model, having been defined as true. This procedure not only allows to compare the data induced improvement of the solution of the deficient model to the true solution, but also enables inspecting in how far the dynamical residual reflects important features of the true residual, i.e. the model defect.

From the equation system of the classical model and that of the data assimilation model, both in discretized form,

$$\boldsymbol{A}_w\boldsymbol{x}_w - \boldsymbol{b} = 0 \text{ and } \tilde{\boldsymbol{A}}_a\boldsymbol{x}_a - \boldsymbol{r} - \boldsymbol{b} = 0$$

is taken by some rewriting and comparison of individual terms

$$\boldsymbol{r} = \tilde{\boldsymbol{A}}_a(\boldsymbol{x}_a - \boldsymbol{x}_w) + (\tilde{\boldsymbol{A}}_a - \tilde{\boldsymbol{A}}_w)\boldsymbol{x}_w + (\tilde{\boldsymbol{A}}_w - \boldsymbol{A}_w)\boldsymbol{x}_w \qquad (5.1.1)$$

$\boldsymbol{A}_w$ denotes the matrix defining the true model, where the index indicates that the non-linear constituents are determined by the true solution $\boldsymbol{x}_w$. The matrix $\tilde{\boldsymbol{A}}_a$ defines the deficient model with the non-linear constituents determined the solution $\boldsymbol{x}_a$. The meaning of the matrix $\tilde{\boldsymbol{A}}_w$ is obvious. The third term on the right hand side represents the true residual, the other terms on the right hand side are correction terms tending to zero with $\boldsymbol{x}_a$ tending to $\boldsymbol{x}_w$. These terms have been evaluated for the experiment KAE=105+40 being regarded as feasible under the conditions of a realistic adjacent sea scenario. In brackets the corresponding values are given for the experiment KAE=210+50 yielding the smallest rms deviation of x_a from x_w of all experiments made (see Table 5.1.1), namely 1.19%.

The rms deviation of the dynamical residual from the true residual amounts to 28.7% (24.0%). The most important correction term is the first one, whereas the second one solely depends upon the non-linear constituents. As the non-linearity is weak in this model the second term is small. Considering the first term, the deviation from the true residual amounts to 1.7% (1.4%) in this experiment. Only grid points have been considered in the evaluation, for which the equation is not directly influenced by the initial condition and the open boundary condition.

Figures 5.1.3 and 5.1.4 show the residuals mentioned above at the beginning and at the end of each time block. The red line indicates the dynamical residual, while the blue one indicates the true residual. The black dashed line denotes the dynamical residual – correction term which comes close to the true residual, as the non-linearity is weak and the equation (5.1.1) must be fulfilled.

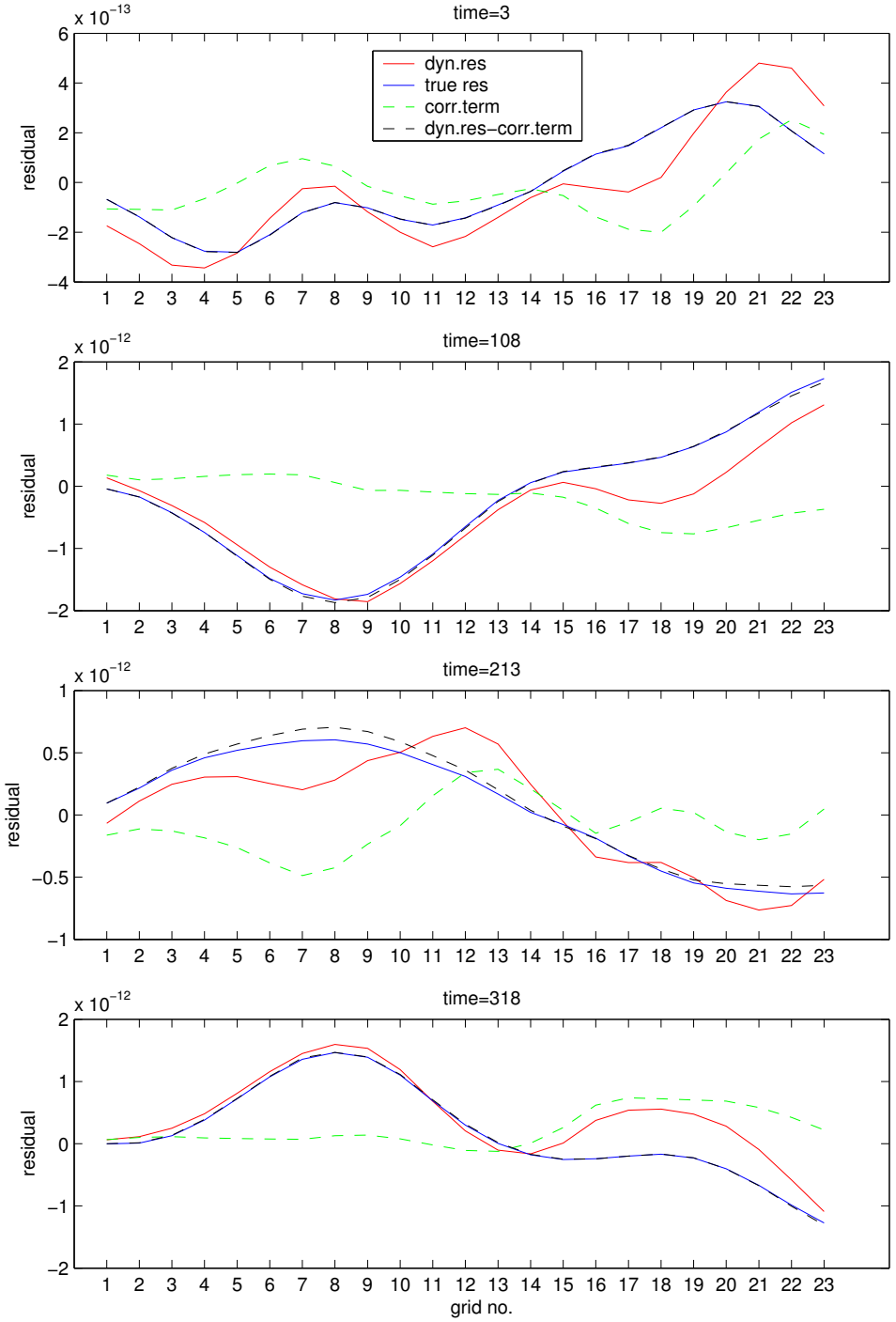

Figure 5.1.3 Plot of the residual for the experiment KAE=105+40 at the beginning of each time blocks. The rms deviation of the dynamical residual from the true residual amounts to 28.7% (dyn. res), and 1.7% when considering the correction term (dyn. res – corr. term).

It is important to note that the dynamical residual reflects the main features, e.g. maxima, minima, position of zero values of the true residual, although data are assimilated only from two positions (cell numbers 8 and 15). This result is also in

case of x_n tending to x_w in the mean not self-evident, because it is the first (and second) term which must become small everywhere. Hence, using this method of data assimilation suggests that in realistic scenario, information on the unknown deficiencies of the classical model can be taken from the resulting dynamic residual.

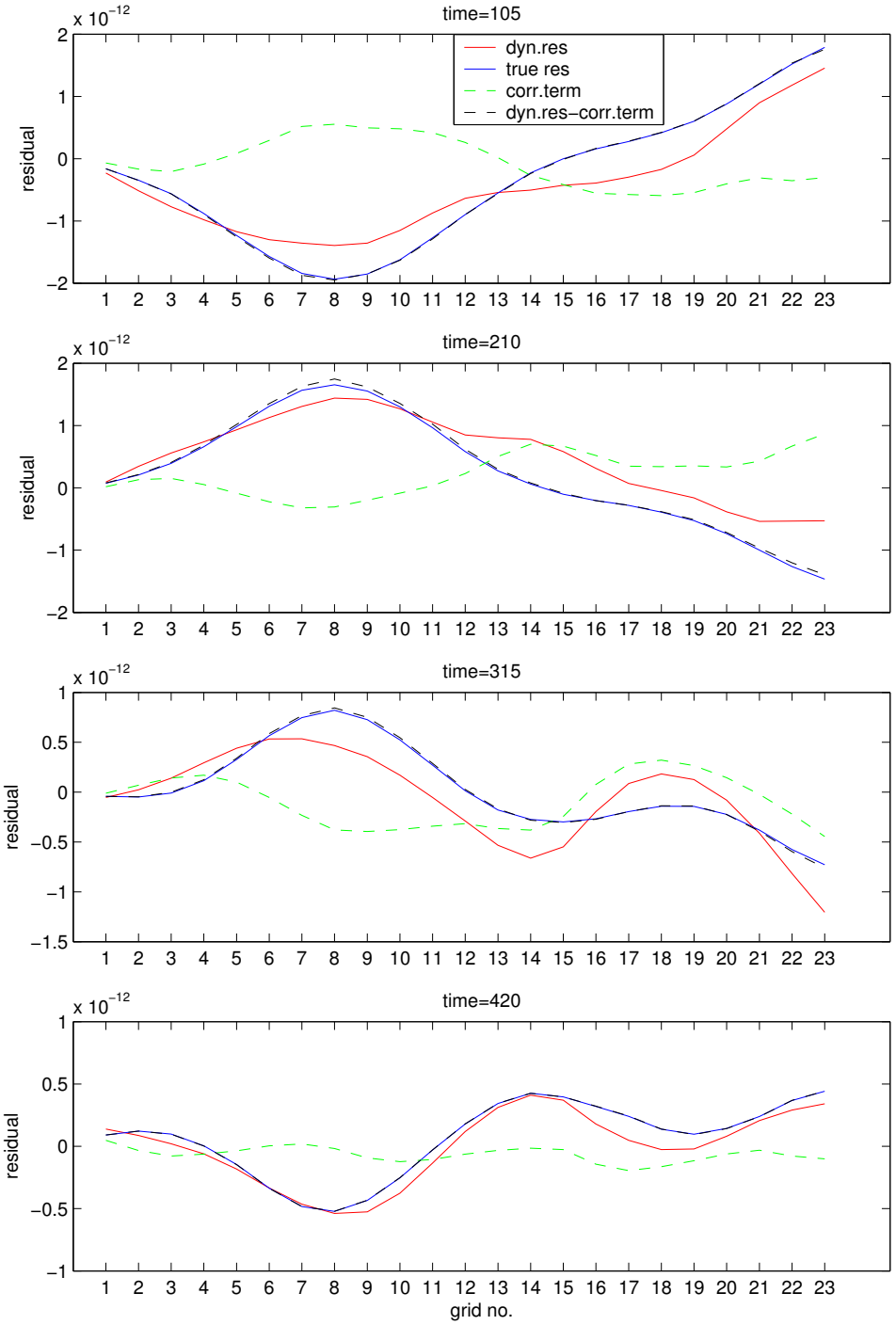

Figure 5.1.4 Plot of the residual for the experiment KAE=105+40 at the end of each time blocks.

5.2. Two dimensional non-linear model of Irish and Celtic Seas

5.2.1. The forward model

The forward model is run with the same parameter values as already mentioned in Section 4.5. The amplitudes and phases obtained from this model are used for generating first guess and initial value fields in the very beginning of performing the data assimilation procedure. At the next step of the assimilation process, the amplitudes and phases from the forward model results are used to determine the initial values, while the first guess fields needed in this step of the assimilation process are taken from the previous assimilation results.

The result of the forward model is compared to observations as listed in Tables 4.5.1 and 4.5.2 for M_2, S_2, $2SM_2$, M_4, MS_4, M_6, $2MS_6$, and $2SM_6$, to the model result of Davies and Jones (1992) for M_2 and S_2, and to the result of Andersen (1999) for M_4, M_6, and MS_4. This comparison is done in order to learn about the performance of the model and in particular to detect weaknesses. Furthermore, this comparison will also be used as the basis when deciding on the positions of data to be assimilated and when evaluating the data assimilation model result.

Figure 5.2.1 shows the scatter diagram of M_2 (top panel) and S_2 (bottom panel) comparing model results to observation. By using this diagram we can see easily how well the forward model result compares to the observations. For M_2, in general the amplitudes (left top panel) are fairly good, except in the area of Bristol Channel (square) and of the eastern Irish Sea (circle), where the amplitudes are underestimated. The phases (right top panel) are also satisfactorily reproduced except in the area of Bristol Channel (square), Sound of Jura (down triangle) and North Channel (diamond), where the phases are overestimated. For S_2, the underestimation of amplitudes (left bottom panel) are also found in the Bristol Channel (square), eastern Irish Sea (circle), Cardigan Bay (left triangle), and North Channel (diamond). Similar phase overestimations as for M_2 are also found for S_2 in the Bristol Channel (square), Sound of Jura (down triangle) and North Channel (diamond).

When comparing the results of the forward model to the observations in more detail, it is found that the amplitude of M_2 in the eastern Irish Sea (stations A01, A02, A04, A05, A06, A23, I01, I14, I19, I20, T4) and in the Bristol Channel (stations A14, A15, A18, A19, A20, I03, I04, I07, I11, I12, T02, T03) is underestimated by up to more than 30 cm (Figure 5.2.2 top panel). Underestimations of tidal amplitude by more than 20 cm are also found for S_2 in the eastern Irish Sea and Bristol Channel, and additionally also at station T01 in Cardigan Bay and at stations T05, D01, D02, and D03 in the North Channel (Figure 5.2.2 top panel). Overestimations of M_2- and S_2 phases reaching more than 45° are found in the Bristol Channel (stations A14, A18, A19, I03, I04, I07, I11, T02), North Channel (stations A17 and D01), and at stations I08 and I16 in the Sound of Jura (Figures 5.2.1 and 5.2.2 bottom panels).

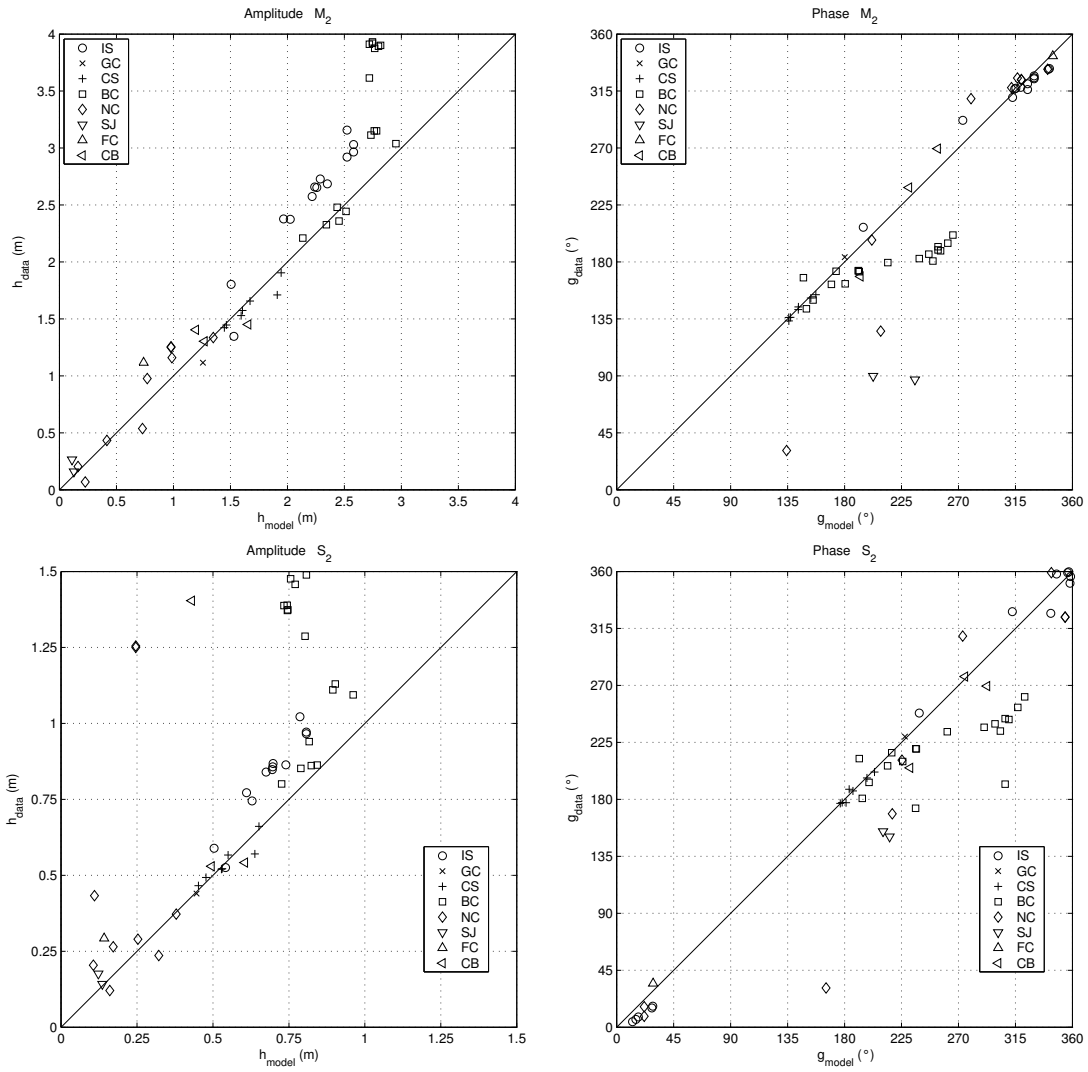

Figure 5.2.1 Scatter diagram of M_2 (top panel) and S_2 (bottom panel) amplitudes and phases obtained by the forward model results and observations.

These systematic amplitude underestimations and phase overestimations around the eastern Irish Sea and Bristol Channel are understandable. The forward model used in this study has a coarse grid resolution, and therefore the phenomena in the shallow water areas, where the non-linearity is rather strong, can not be reproduced sufficiently.

The cotidal charts of M_2 and S_2 from the forward model are compared to the model result of Davies and Jones (1992). For M_2 (Figure 5.2.3 left panel), the oscillation patterns in general are very similar, but the amplitudes at some places are lower than those obtained by them. Significant differences are found in the eastern Irish Sea (about 60 cm) and in the Bristol Channel (more than 100 cm). In general, the positions of amphidromic points are close to each other. Also for S_2 (Figure 5.2.3 right panel), the corange and cophase patterns of both solutions

appear being rather similar. The amplitudes, especially in the eastern Irish Sea and inwards in the Bristol Channel, differ only by 10 cm. The positions of amphidromic points are also generally close to each other.

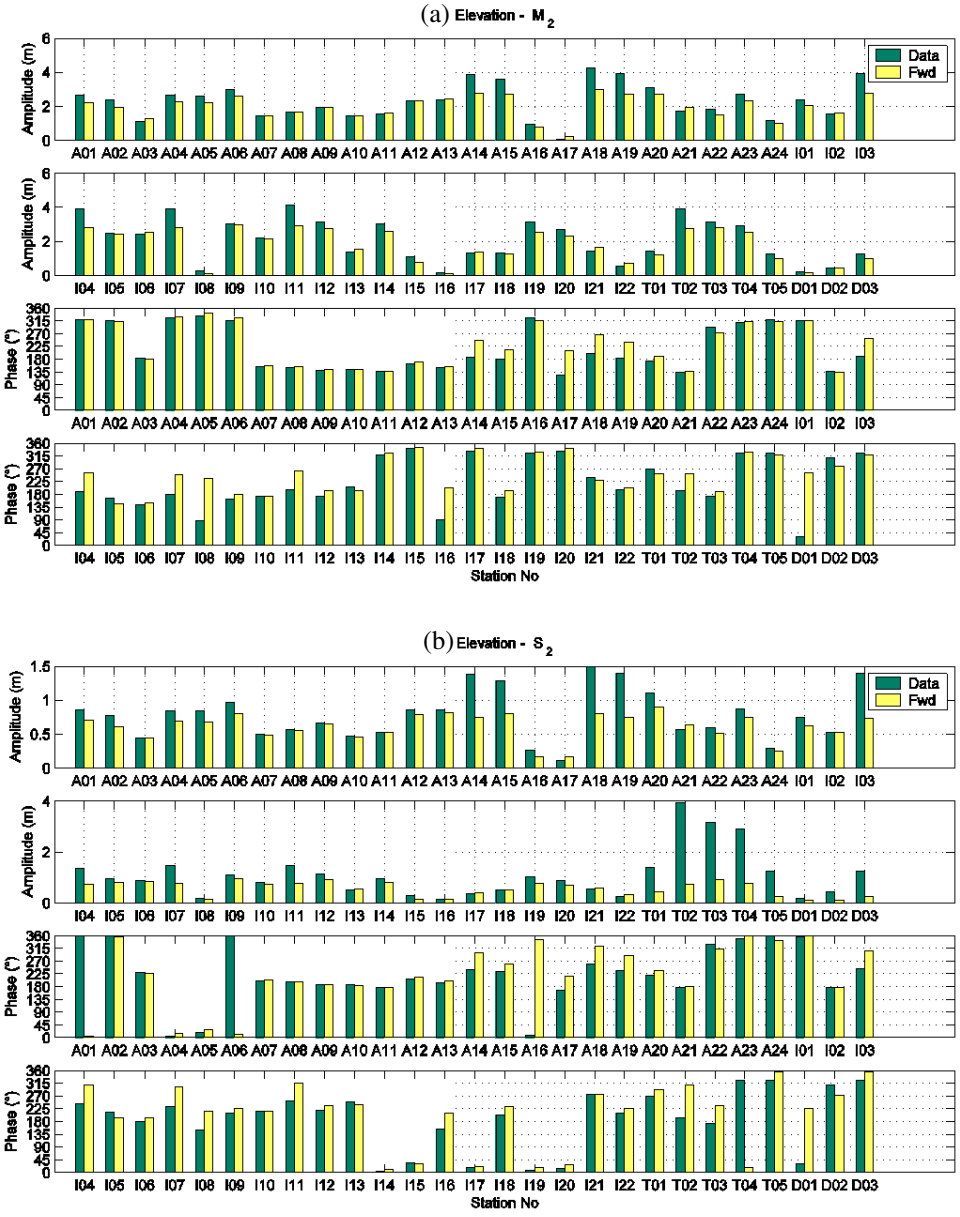

Figure 5.2.2 Comparison of (a) M_2 and (b) S_2 amplitudes and phases between forward model elevations and data.

The elevations of over- and compound tides obtained by the forward model are also tried to be evaluated. From Figure 5.2.4 it can be seen clearly that elevation underestimations as well as overestimations are found almost everywhere. Table 5.2.1 gives the rms errors of the forward model elevations compared to the observations. They suggest that the forward model can not produce tidal

elevations of shallow water tidal constituents adequately.

Sinha and Pingree (1997) have mentioned that accurate simulation of the higher tidal harmonics (the M_4 and M_6 constituents) poses a number of problems, which also have been addressed by others. Beside the model resolution, the simulation of higher harmonics is complicated due to the fact that they can be generated as well as be dissipated by friction. For M_4, advection and continuity effects are the important source terms, whereas M_6 is generated by bottom friction. Furthermore, any errors in the M_2 phase will be amplified twofold in the M_4, while increasing the diffusion coefficient, which can be chosen as a possibility to improve the M_4 result, will tend to reduce the M_2 tide.

Table 5.2.1 Amplitudes (h_f, cm) and phases (g_f, °) of rms errors of over- and compound tides obtained by the forward model.

	$2SM_2$		MS_4		$2MS_6$		$2SM_6$		M_4		M_6	
	h_f	g_f	h_f	g_f	h_f	g_f	h_f	g_f	h_f	g_f	h_f	g_f
rms error	3.1	66.3	4.4	73.8	2.7	111.1	0.7	86.1	8.3	61.1	2.4	111.6

5.2.2. The data assimilation model

Data assimilation experiments using the continuation procedure with time block lengths of 1 day and 4 days, respectively, are carried out until a total simulation time of more than 14.7 days is reached in each case. The weighting factors are chosen to take the values 1.0 $m^{-1}s$ for the dynamical U- and V equations, 1.0 m^{-1} for the dynamical ζ equation, and 1.0 m^{-1} for the data equation. Data from 24 positions are assimilated (see Figure 4.5.1). The assimilation experiment with 1 day time block is performed twice, firstly with and secondly without residual smoothing process. For the experiment with 4 days time block, the assimilation is performed without residual smoothing process only.

5.2.2.1. Data assimilation without smoothing of residual

5.2.2.1.1. One day time block length

In general, when comparing the results of the forward model with the solution obtained by the model with data assimilation, a significant improvement can be seen clearly (Figures 5.2.5 – 5.2.12). The model with data assimilation procedure yields results that are almost as realistic as those obtained by using a high resolution tidal model, which agree rather well with the observations.

By applying the model with assimilation procedure, the positions of amphidromic points of M_2 and S_2 are improved and agree very well with the observations and the high resolution tidal model results of Lee and Davies (2001) for M_2 in the Irish Sea, with those of Davies and Hall (2000) for M_2 and S_2 tides in the North

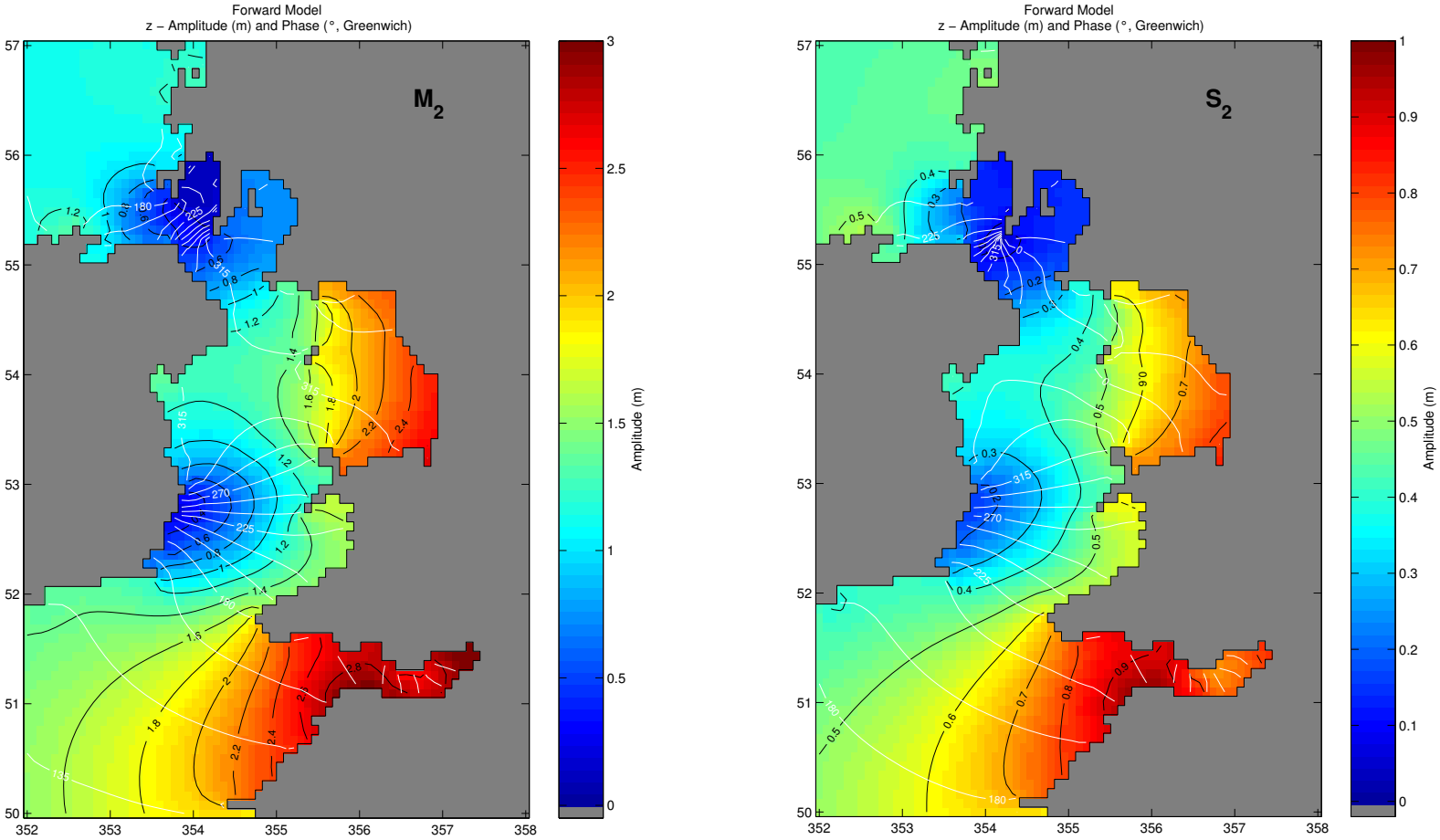

Figure 5.2.3 Tidal elevations of M_2 (left panel) and S_2 (right panel) from the forward model.

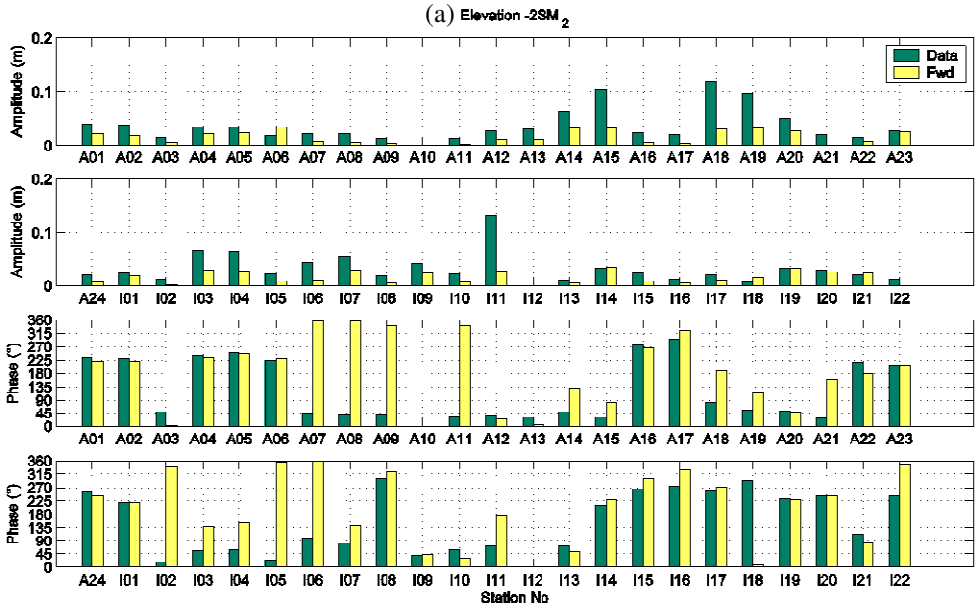

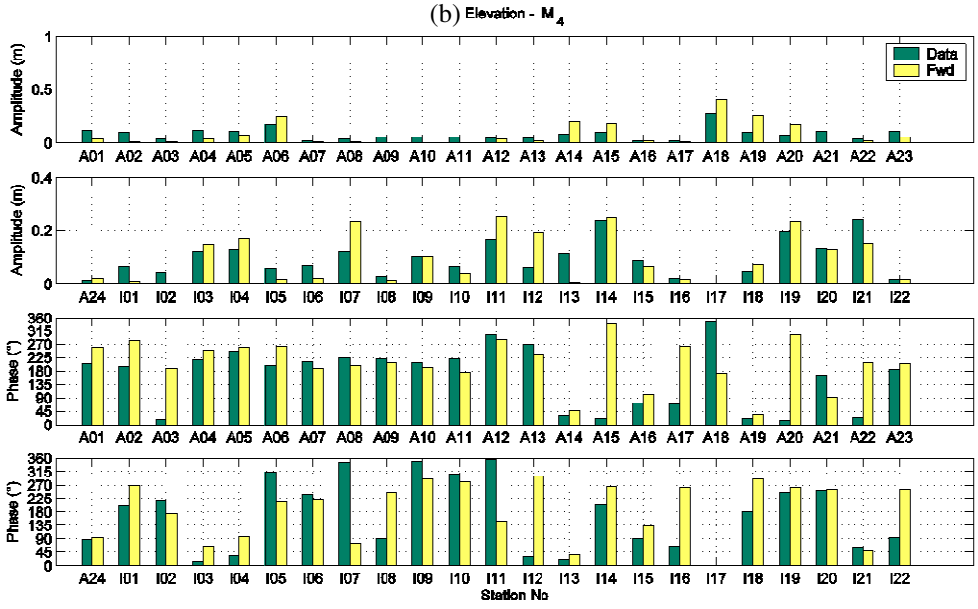

Figure 5.2.4 Comparison of (a) $2SM_2$, (b) M_4, (c) MS_4, (d) M_6, (e) $2MS_6$, and (f) $2SM_6$ amplitudes (top panel) and phases (bottom panel) between forward model elevations and data.

(c) Elevation - MS_4

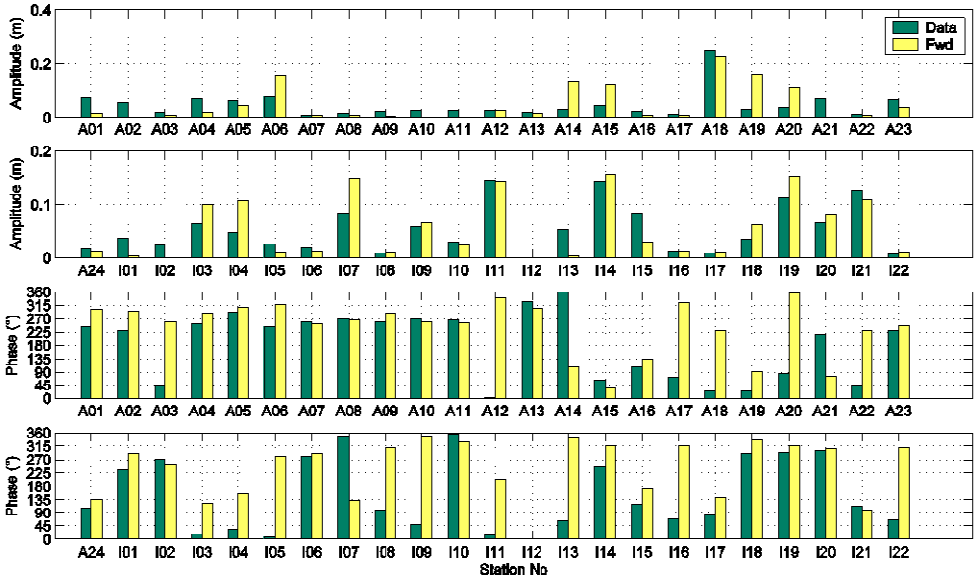

(d) Elevation - M_6

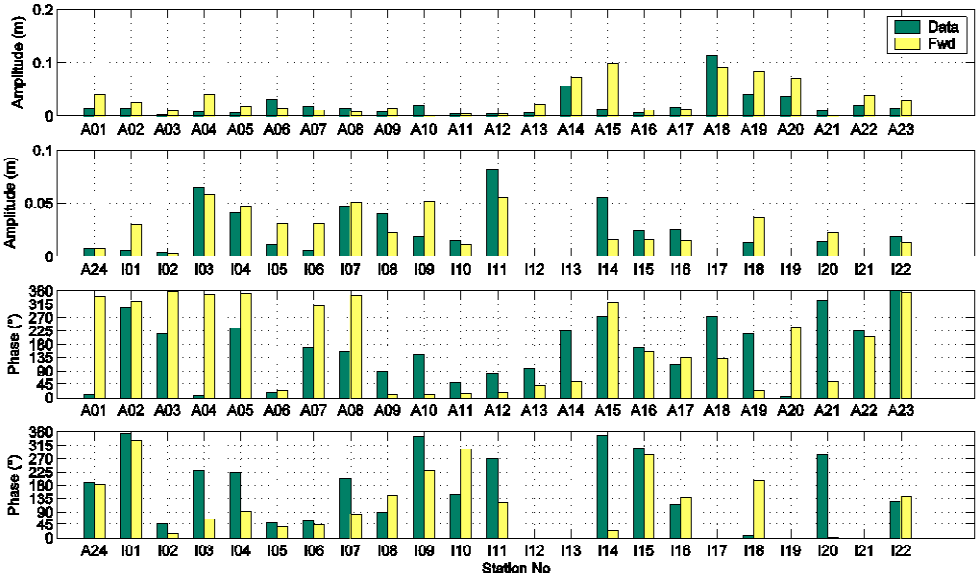

Figure 5.2.4 (continued).

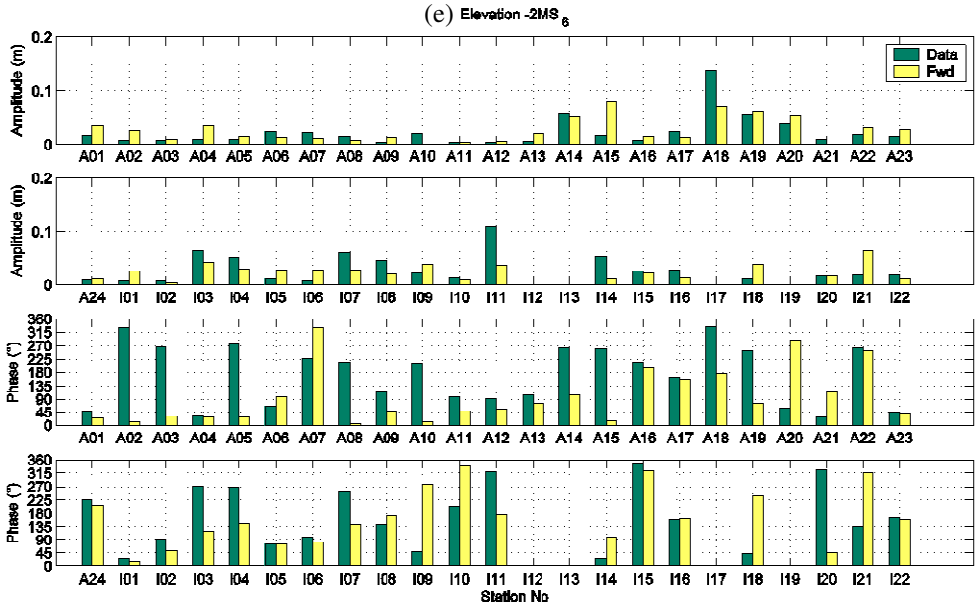

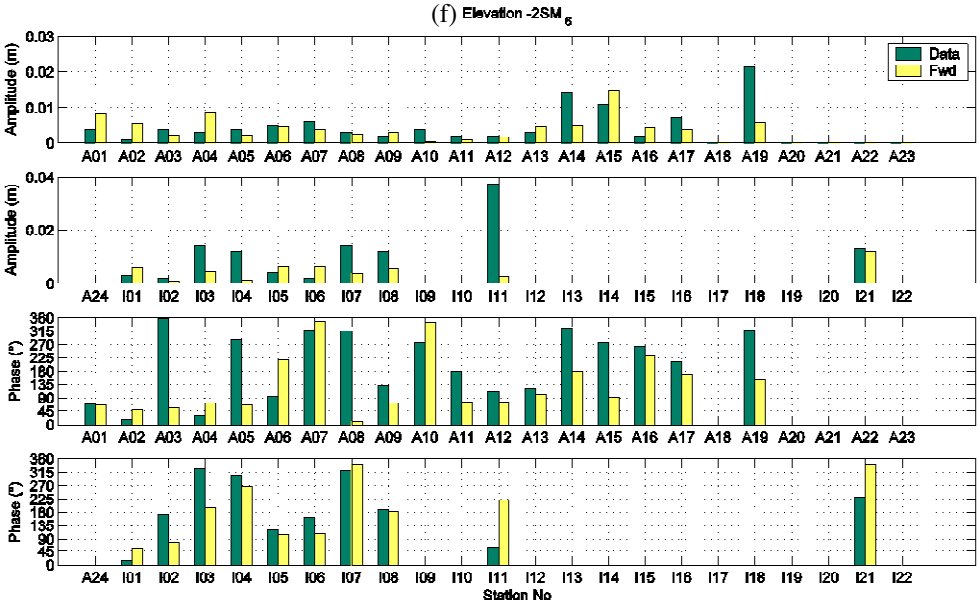

Figure 5.2.4 (continued).

Channel of the Irish Sea, with those of Jones and Davies (1996) for M_2, M_4, M_6 and S_2 tides in the eastern Irish Sea, as well as with the data assimilation results from Taguchi (2002) for M_2, M_4 and M_6. The patterns of M_4 and M_6 clearly resemble those given by Andersen (1999) who calculates shallow water tides on the European shelf based on the TOPEX/POSEIDON altimetry data. The pattern

of M_4 also clearly resembles that given by Andersen et al. (2006) who calculate shallow water tides on the European shelf based on hybrid altimetry data assimilation model. Unfortunately, the MS_4-tide obtained by Andersen (1999) is not as accurate as the hydrodynamic shelf model of Flather (1976, 1981), and therefore can not be used for comparison. There are also no corresponding fields for $2MS_6$, $2SM_6$ and $2SM_2$ which can be used for comparison. Hence the comparison can only be based on some data from independent stations inside the model domain.

The comparison of observed and computed (forward and assimilation models) M_2 and S_2 tidal elevation amplitudes and phases at independent stations (Figures 5.2.13.a and 5.2.13.b) shows that usually the amplitudes and phases, which are under- or overestimated by the forward model, can adequately be reproduced when applying the model with data assimilation.

From Figures 5.2.13.a and Table 5.2.2 we can take that larger absolute errors (the difference between assimilation results and data) of M_2 almost always appear at the stations located close to the coastline. The maximum difference of M_2 amplitude is found at station I17 in the eastern part of the North Channel where the amplitude of the assimilation result is 45.6 cm larger than the observed one amounting to 133.7 cm. At this station, the difference between the forward model and the observation is 17.3 cm (underestimated). At station I19 in the eastern Irish Sea the observed amplitude of 315.7 cm is underestimated by 20.4 cm, but compared to the forward model result a significant improvement is found at this station. The amplitude from the forward model at this station is underestimated by 100.8 cm. A similar case also can be found at station I05 in the Celtic Sea. Here, an original underestimation by the forward model of 103.0 cm is reduced by data assimilation to only 17.4 cm. Very significant improvements also can be found at stations I01, I03, I04, I07, I11, I12, I14, I20 where the underestimation appearing in the forward model can be minimized by assimilating data. When comparing the M_2 phase, usually it is found that the data assimilation model produces results which are close to the observations except at station I08 in the Sound of Jura where the phase is underestimated by more than 60°, and also at station I05 in the Celtic Sea close to the mouth of Bristol Channel, where the phase is underestimated by about 30°. Station I05 is located close to I06, but at station I06 it is found that the phase almost agrees with the observation. Phase overestimation is found at station I18 in the Sea of Hebrides, close to the northern open boundary.

Figure 5.2.13.b and Table 5.2.2 show the comparison between data, assimilation and forward model results for S_2 at the same independent stations mentioned above. It is found that the elevations obtained by the data assimilation model are also as a rule close to the observations. The underestimations obtained by the forward model can be reduced significantly when assimilating data from 24 positions. Although the result is satisfactory, some over- and underestimations worth mentioning are still found. At station I05, the amplitude and phase from the assimilation model are underestimated and almost agree with the forward model

result. At station I08 in the Sound of Jura the amplitude is also underestimated and smaller than the forward model result. Overestimations of amplitude are found at station I17 in the North Channel of the Irish Sea and at station I21 in the Cardigan Bay, while phase overestimation is found at station I18 in the Sea of Hebrides.

For $2SM_2$, as shown in Figure 5.2.13.c and Table 5.2.2, data assimilation can reduce the underestimation obtained by the forward model significantly. The rms error is reduced significantly, from 2.8 cm obtained by the forward model to 1.3 cm (amplitude) and from 72.2° to 31.9° (phase). Although data assimilation reduces the rms error significantly, the results from the data assimilation model are still overestimated as compared to the observations. This phenomenon is similar to that one having been obtained by the schematic canal model experiment where the overestimation arises for the σ_4 constituent, a corresponding compound tide.

For M_4, as shown in Figure 5.2.13.d and Table 5.2.2, some overestimations yielded by the forward model also can be reduced clearly. The rms error is reduced by more than 70% for the amplitude, from 8.6 cm to 2.3 cm, while for the phase the rms error is reduced from 69.0° to 47.4°. Inspecting the cotidal chart (Figure 5.2.8) and comparing the forward model (left panel) with the data assimilation model (right panel) results, an improvement of corange and cophase patterns can be seen clearly. The cotidal chart also agrees very well with Taguchi (2002). An amphidromic point in the St. George's Channel, which appears further southeast applying the forward model, can be significantly improved. The elevation pattern clearly resembles that given by Andersen et al. (2006) who calculates shallow water tide constituent M_4 on the European Shelf applying generalized inverse methods assimilating data from TOPEX/POSEIDON as well as from tide gauges. Jones and Davies (1996) have calculated also M_4 tide in the eastern Irish Sea using 3-D high resolution model (0.9 km by 1.0 km grid spacing). The pattern of elevation obtained by the data assimilation model in the eastern Irish Sea is also compared to their result, and it is found that essentially the pattern is rather similar, regarded to agree adequately with the pattern computed by Jones and Davies (1996). Improvements are also obtained for MS_4, M_6, $2MS_6$, $2SM_6$ tides (Figures 5.2.13.e – 5.2.13.h and Table 5.2.2). The cotidal chart of M_6 agrees very well with Taguchi (2002), and the elevation in the eastern Irish Sea compares well with Jones and Davies (1996). The large amplitude in the Morecambe Bay which can not be produced by the forward model, is generated by the data assimilation model however.

Table 5.2.3 gives the comparison of elevations obtained by the data assimilation model in this study with those from Taguchi (2002) at independent stations. For M_2, the rms error is nearly equal while for M_4, the rms error obtained in this study is larger than in Taguchi (2002). This significant difference is due to the fact that fewer data are assimilated in this study than in Taguchi (2002), as has already been mentioned in Section 4.5. Furthermore, only at two independent positions

inside the Bristol Channel the model results for M_4 have been compared. Although some improvements are obtained for this area applying the data assimilation model the computed elevation amplitudes still prove as underestimated for M_4.

A special comparison is done for the computed M_2- and S_2 elevations in the North Channel of the Irish Sea with high resolution (of order 1 km) classical model results of Davies and Hall (2000). This comparison is presented in Table 5.2.4. From this table it can be taken that the rms error of the M_2 amplitude resulting from the data assimilation model is by 5.5 cm smaller while the phase is by 10° larger than the corresponding values from Davies and Hall (2000). For the S_2 elevation the rms errors resulting from the data assimilation model are smaller than those yielded by the model of Davies and Hall (2000), i.e. they are smaller by 1.9 cm and by 41.6° smaller, respectively.

In this data assimilation model, tidal elevation and east-west and south-north volume transports are generated simultaneously. Besides examining the elevation fields, it is necessary to consider also the distribution of currents since changes in the gradient of elevation field produced by data assimilation can lead to disturbances in the current fields. The tidal current ellipses at every second grid point obtained by the data assimilation model are given in Figures 5.2.14 – 5.2.17. From those figures and other descriptions of the current field, it is evident that assimilating elevation data does not introduce physically unrealistic properties of this field, neither in the vicinity of positions from which data are assimilated. Although the current fields can scarcely be compared with reliable data, it is possible to realize that the computed patterns in general agree with those which are available from classical models (Davies and Jones, 1992; Lee and Davies, 2001) and from data assimilation model result of Gekeler (1995). Furthermore, the computed patterns are as smooth as is typical of real fields.

In the Celtic Sea region and in the area close to the northern open boundary the tidal current ellipses are well developed. Strong currents are found in the North Channel, St. George's Channel, eastern Irish Sea, and in the Bristol Channel. In the St. George's Channel the current ellipses of M_2 and S_2 are rectilinear, have south-north orientation and the speed exceeding 1.0 ms^{-1}. The $2SM_2$ and M_4 currents in this region are also strong (exceeding 0.2 ms^{-1}) and have a south-north orientation but with non-degenerated ellipses. In the Bristol Channel the current ellipses are also rectilinear and have an east-west orientation. In the northern and southern parts of eastern Irish Sea strong flow with current ellipses aligned in an east-west direction occurs being separated by near circular tidal ellipses to the east of Isle of Man. The $2SM_2$, M_4, and MS_4 currents in the southern part of eastern Irish Sea exceed 0.2 ms^{-1}.

5.2.2.1.2. Four days time block length

In the schematic canal model experiments, data assimilation experiments with different time block lengths are performed showing that the choice of time block length affects the rms deviation. However, already using moderate block length leads to good results. But some of the smaller over- and compound tides, which in these experiments are generally small as compared to the astronomical tides, prove as particularly sensitive to the block length.

In order to estimate precisely the effect of time block length on the results of two dimensional non-linear data assimilation model of Irish and Celtic Seas, apart from the experiment with one day time block length, an experiment with time block length of 4 days is performed in this work also. Results of this experiment are given in Figures 5.2.18 – 5.2.21.

In general, the cotidal charts of M_2 and S_2 are almost equal to those obtained by the assimilation with 1 day block length. The rms errors of amplitude and phase obtained by this experiment as compared with 1 day block length gives insignificant differences. For M_2, the amplitude and phase obtained by 4 days block length are larger by 0.9 cm and by 1.1°, respectively, while for S_2 the amplitude is by 0.1 cm smaller and the phase by 0.8° larger (see Table 5.2.5).

On the other hand, when comparing the results of 4 days time block assimilation model with those obtained by 1 day time block, a very different pattern of cotidal chart is found for $2SM_2$ elevation (Figure 5.2.19 left panel), while for other over- and compound tides the differences are not little significant. Table 5.2.6 gives the comparison of rms errors between the data assimilation model with 1 day and 4 days time blocks. This comparison suggests that the solution for $2SM_2$ constituent is clearly sensitive to the time block length as compared to observations at independent stations, the data assimilation model solution for $2SM_2$ with 1 day time block length gives better results than with 4 days time block length.

This phenomenon is quite similar to that obtained in the canal model experiments, as has already been mentioned in Section 5.1. In the canal model experiment, the elevation of $\sigma_4=2\sigma_1-\sigma_2$, which is corresponding to $2SM_2$ in the 2D assimilation model of Irish and Celtic Sea, is overestimated when the length of time block is increased to 105 and 210 instead of 84. In Section 5.1 it has already been mentioned that the amplitude overestimation of σ_4 occurs perhaps because the σ_4 signal is very small as compared to the strong astronomical partial tides σ_1 with neighbouring frequency. This phenomenon is obviously sensitive to the length of the time block, because when choosing time block length equal to 420 time steps (complete beat period), the assimilation solution is sufficiently close to the "reference" solution, also with respect to σ_4. In the case of $2SM_2$, the frequency is close to the S_2 and furthermore the amplitude is also very small compare to that of S_2.

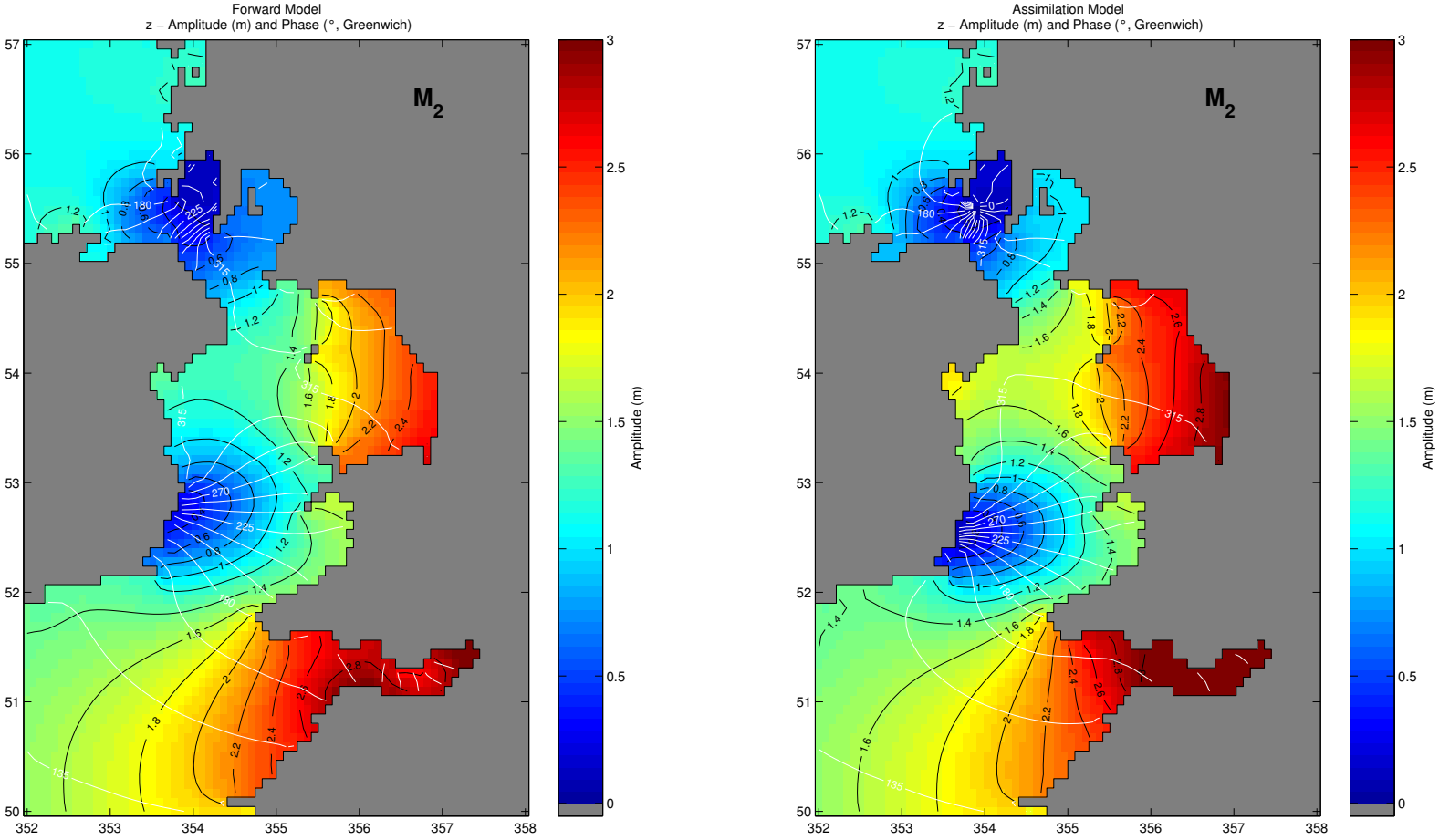

Figure 5.2.5 M_2 tidal elevation obtained by forward model (left) and data assimilation model with time block length of one day without smoothing of residual (right)

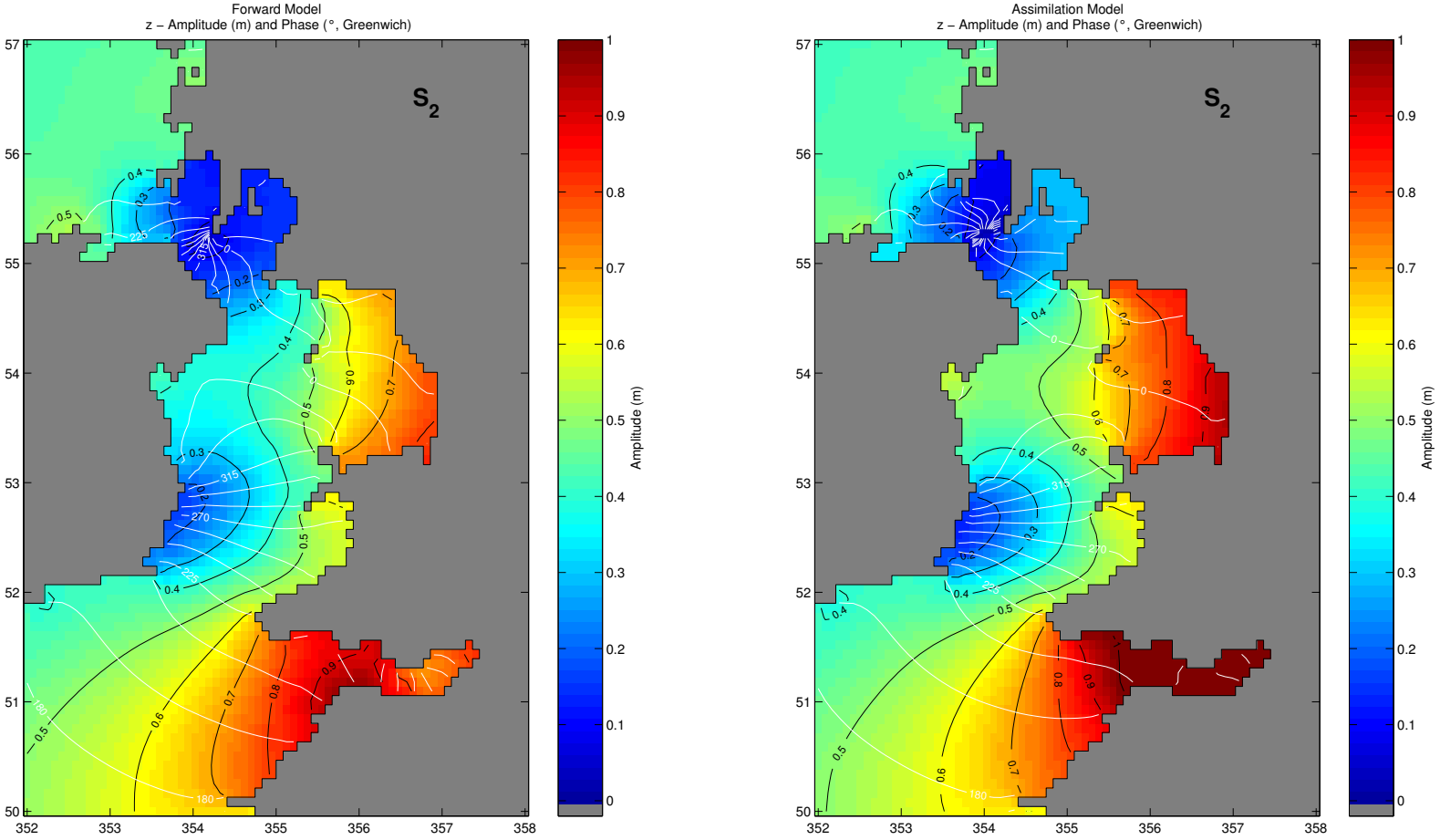

Figure 5.2.6 S_2 tidal elevation obtained by forward model (left) and data assimilation model with time block length of one day without smoothing of residual (right)

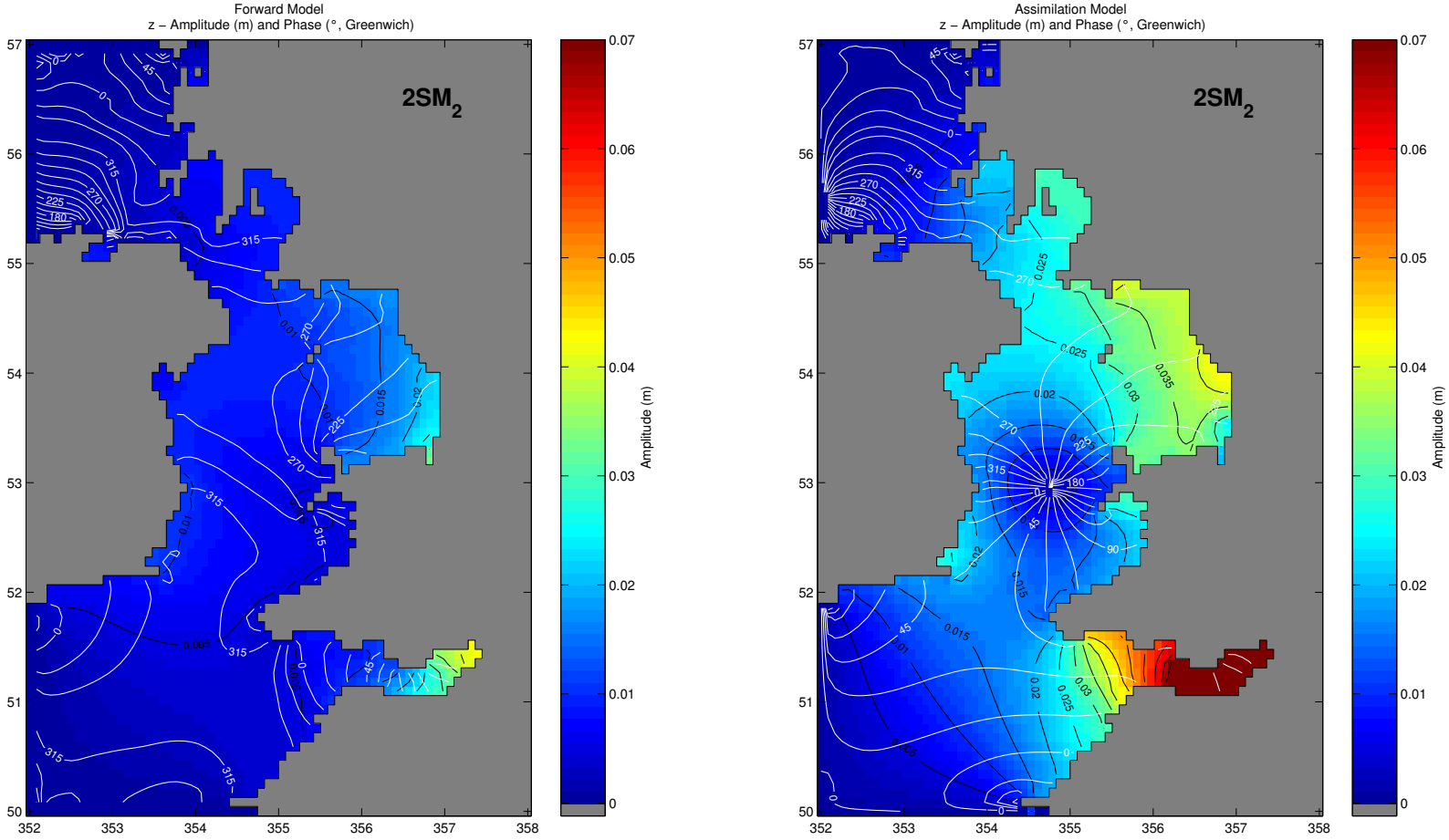

Figure 5.2.7 $2SM_2$ tidal elevation obtained by forward model (left) and data assimilation model with time block length of one day without smoothing of residual (right)

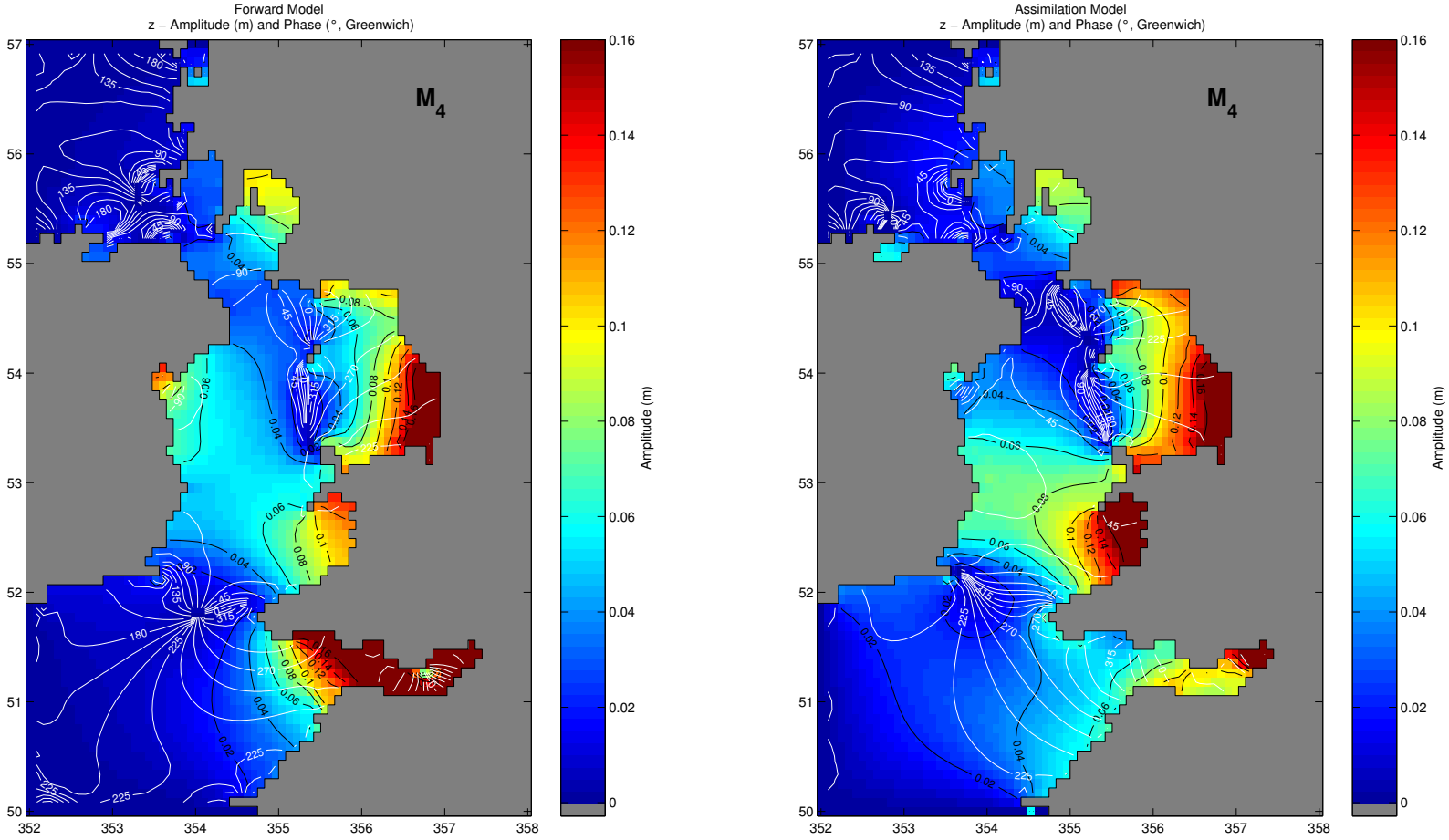

Figure 5.2.8 M_4 tidal elevation obtained by forward model (left) and data assimilation model with time block length of one day without smoothing of residual (right)

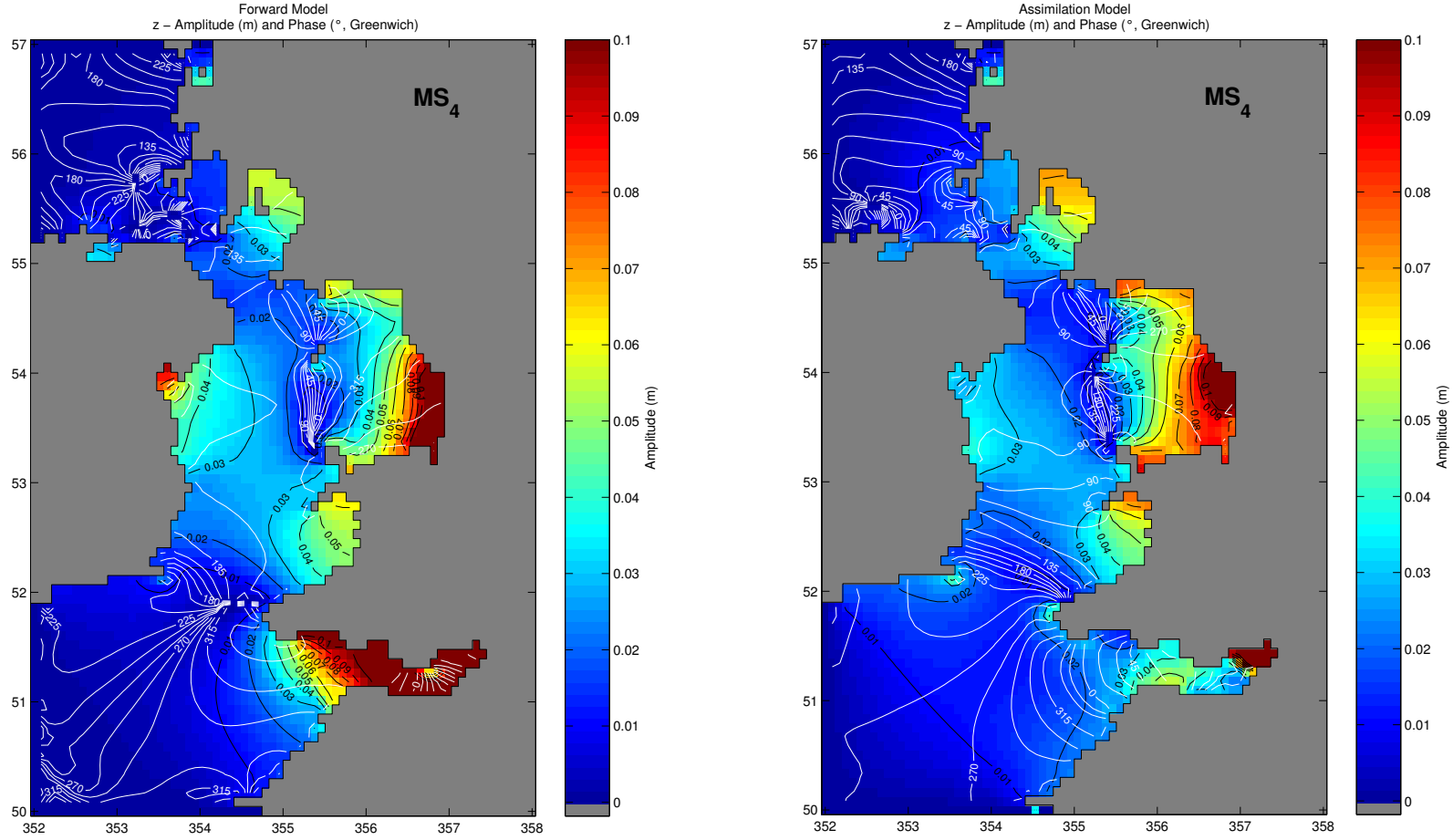

Figure 5.2.9 MS_4 tidal elevation obtained by forward model (left) and data assimilation model with time block length of one day without smoothing of residual (right)

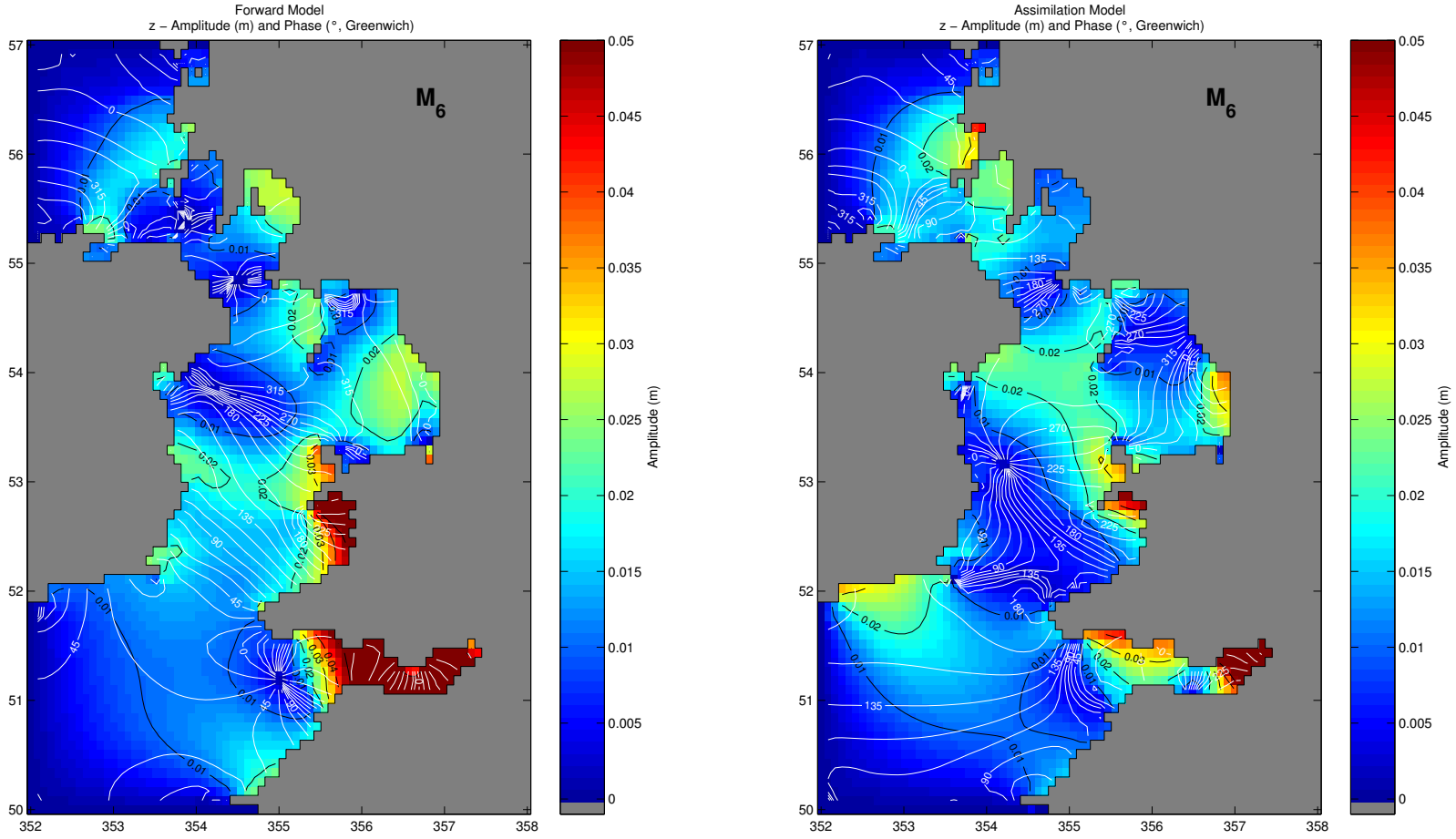

Figure 5.2.10 M_6 tidal elevation obtained by forward model (left) and data assimilation model with time block length of one day without smoothing of residual (right)

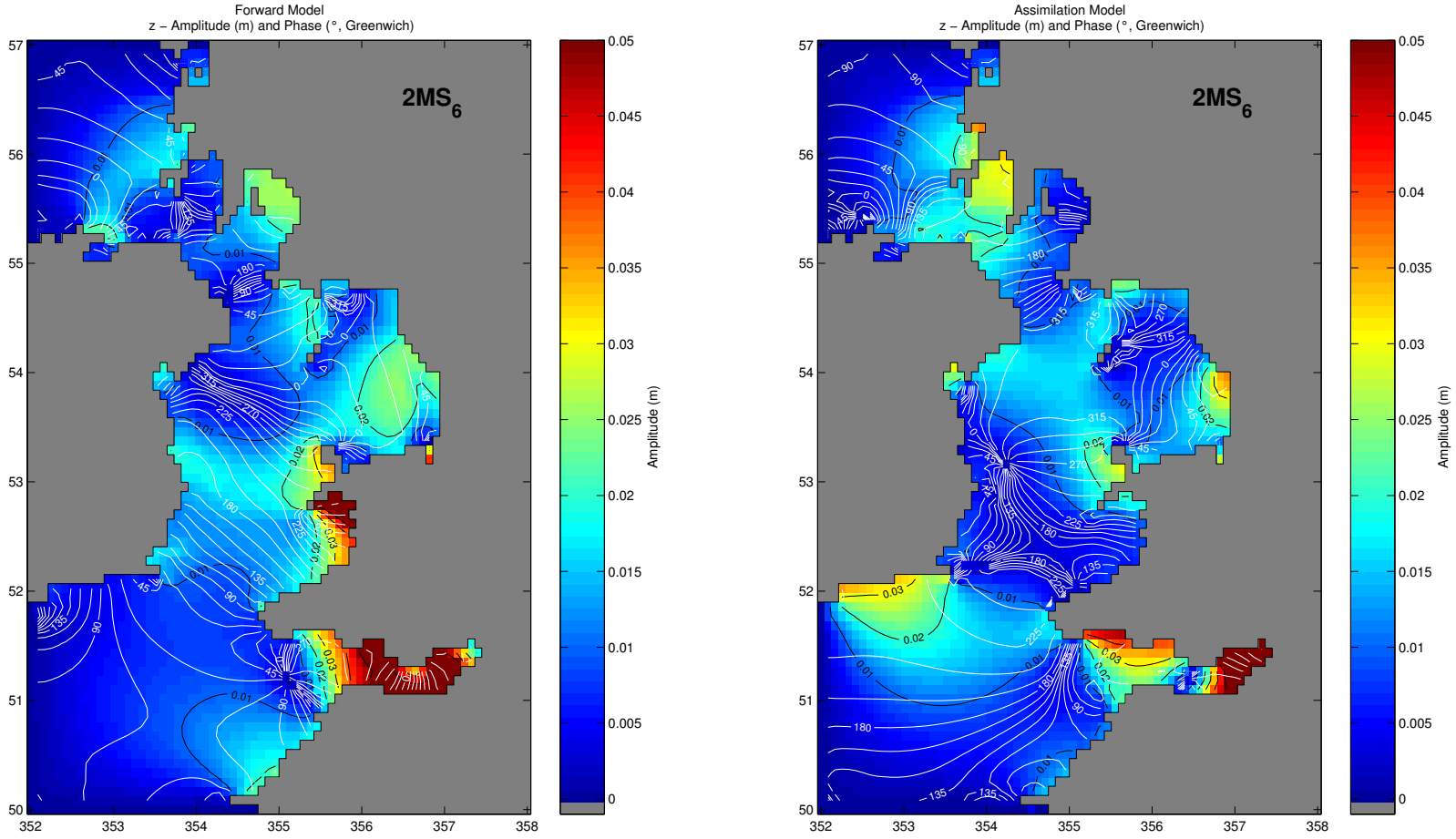

Figure 5.2.11 $2MS_6$ tidal elevation obtained by forward model (left) and data assimilation model with time block length of one day without smoothing of residual (right)

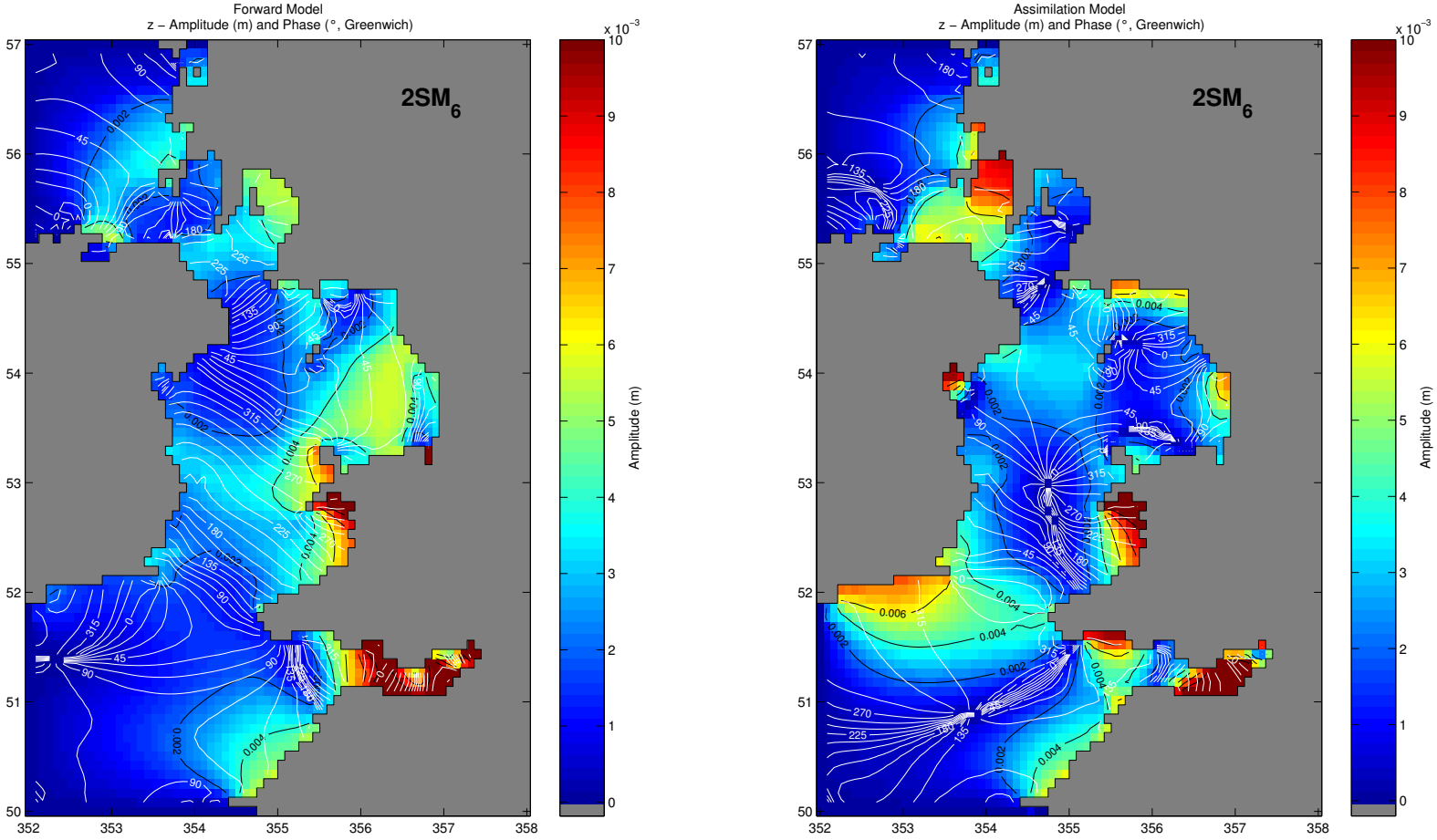

Figure 5.2.12 $2SM_6$ tidal elevation obtained by forward model (left) and data assimilation model with time block length of one day without smoothing of residual (right)

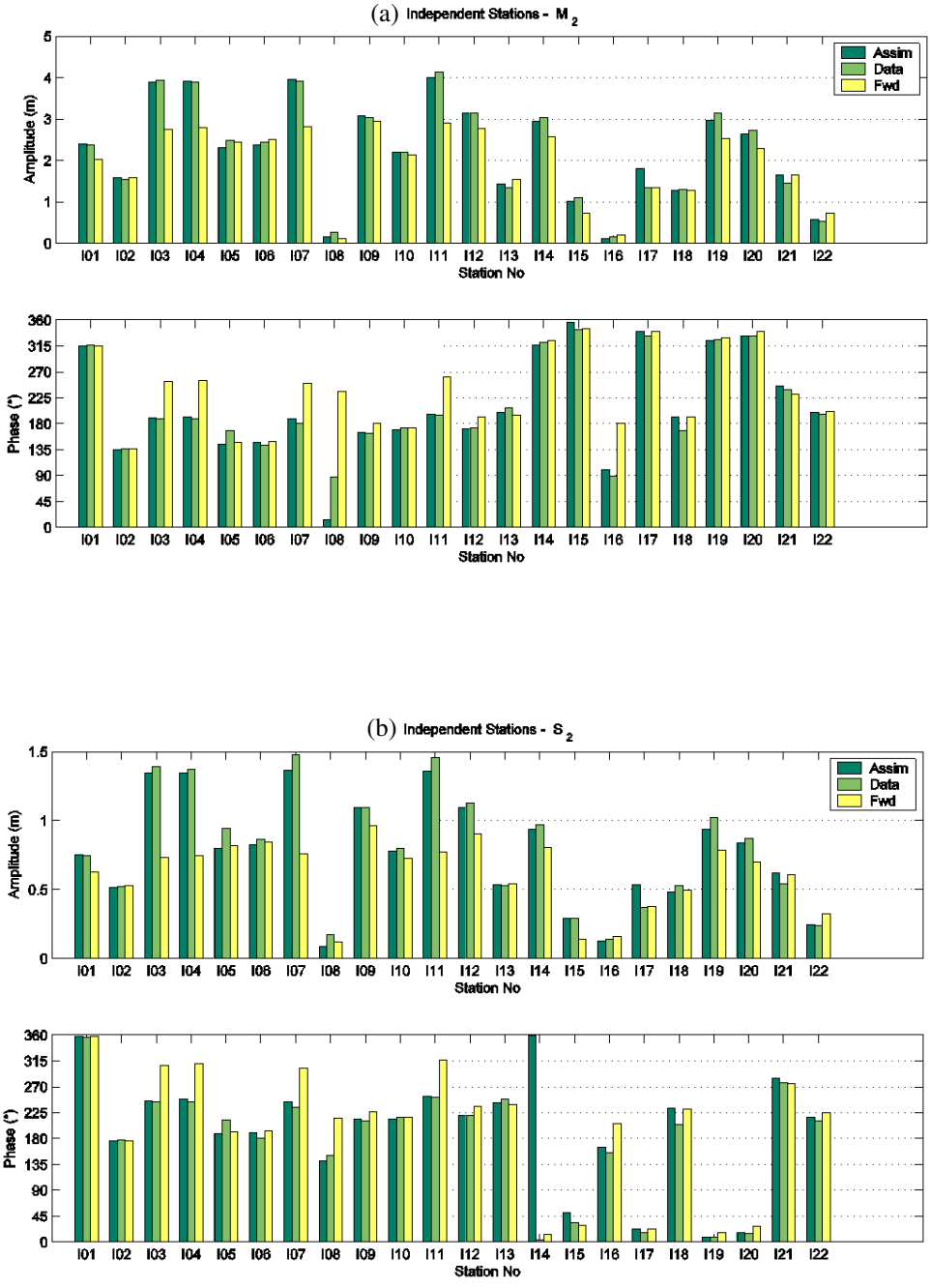

Figure 5.2.13 Comparison of (a) M_2, (b) S_2, (c) $2SM_2$, (d) M_4, (e) MS_4, (f) M_6, (g) $2MS_6$, and (h) $2SM_6$ amplitudes (top panel) and phases (bottom panel) between forward model and data.

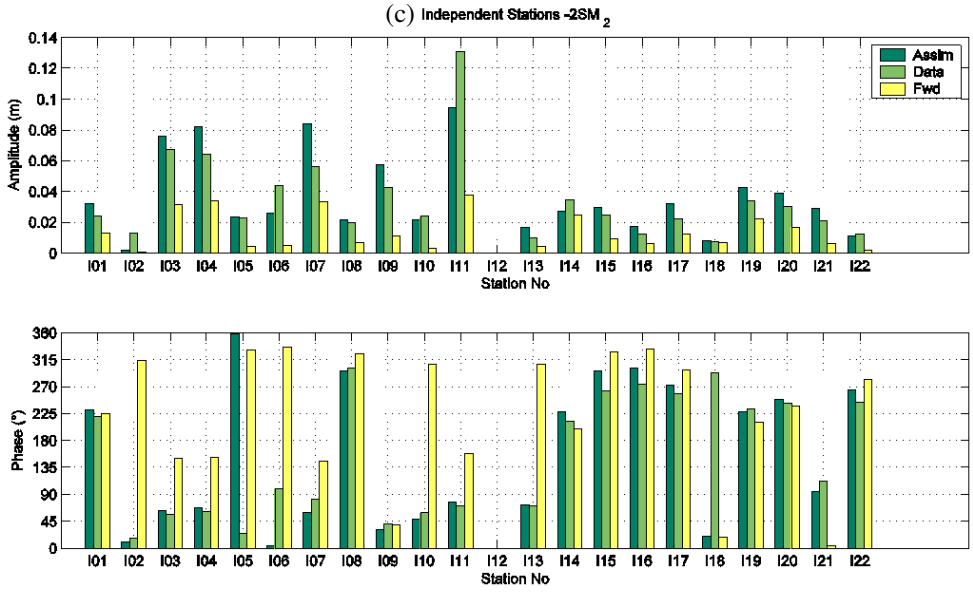

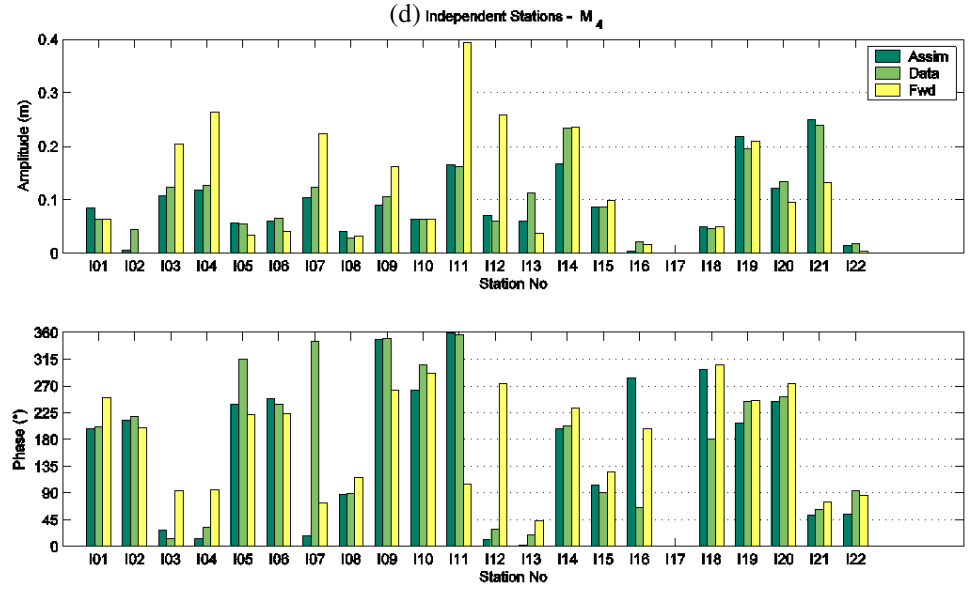

Figure 5.2.13 (continued)

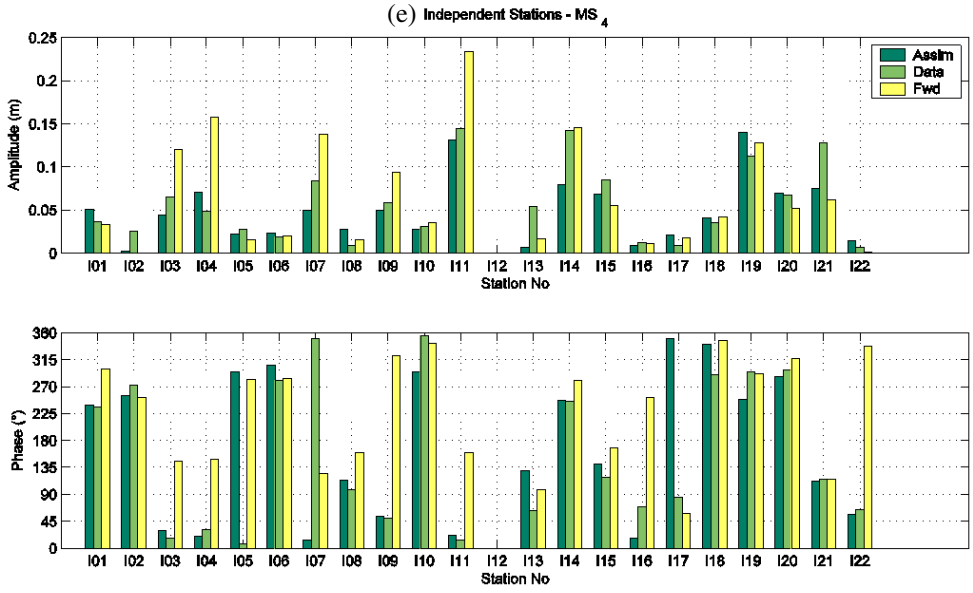

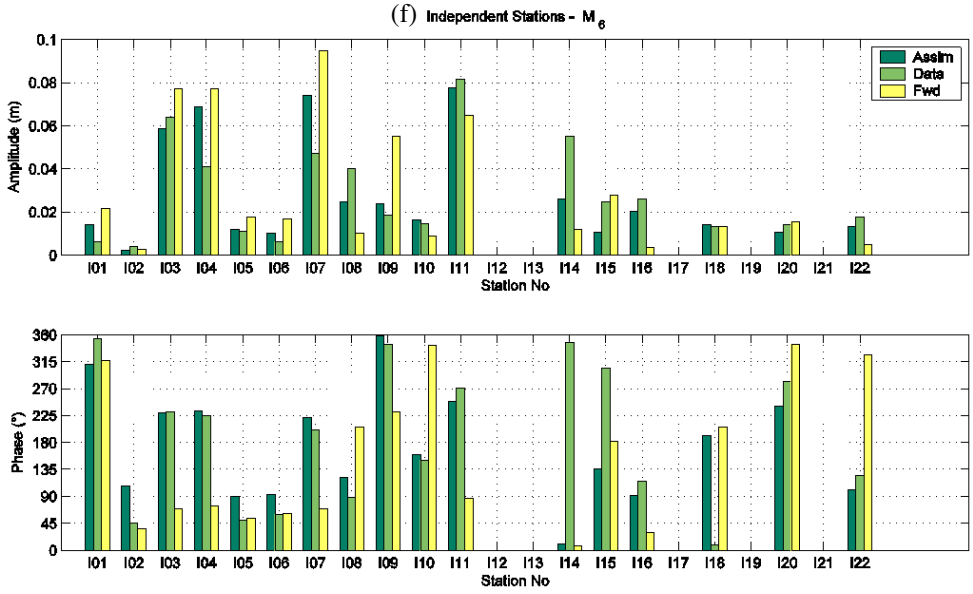

Figure 5.2.13 (continued)

(g) Independent Stations -2MS$_6$

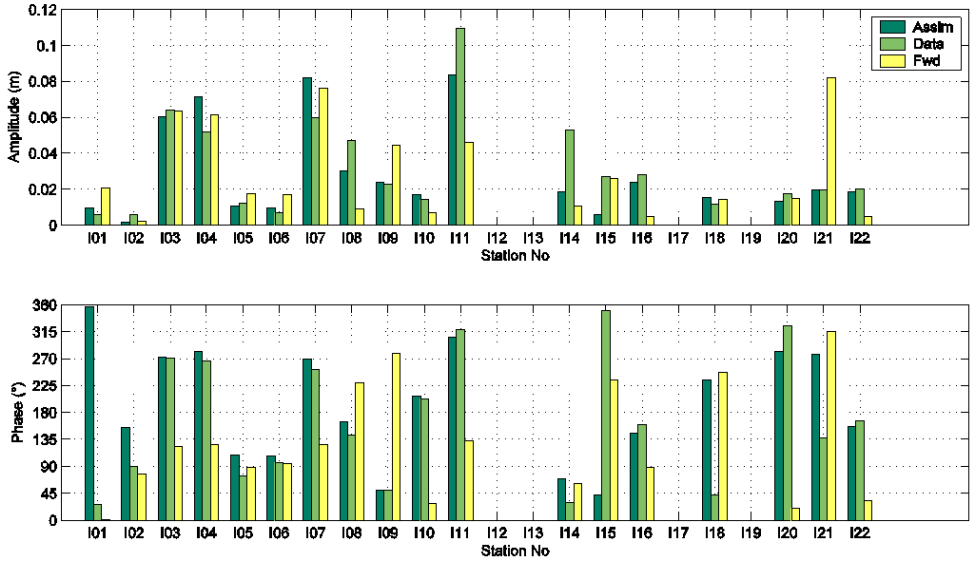

(h) Independent Stations -2SM$_6$

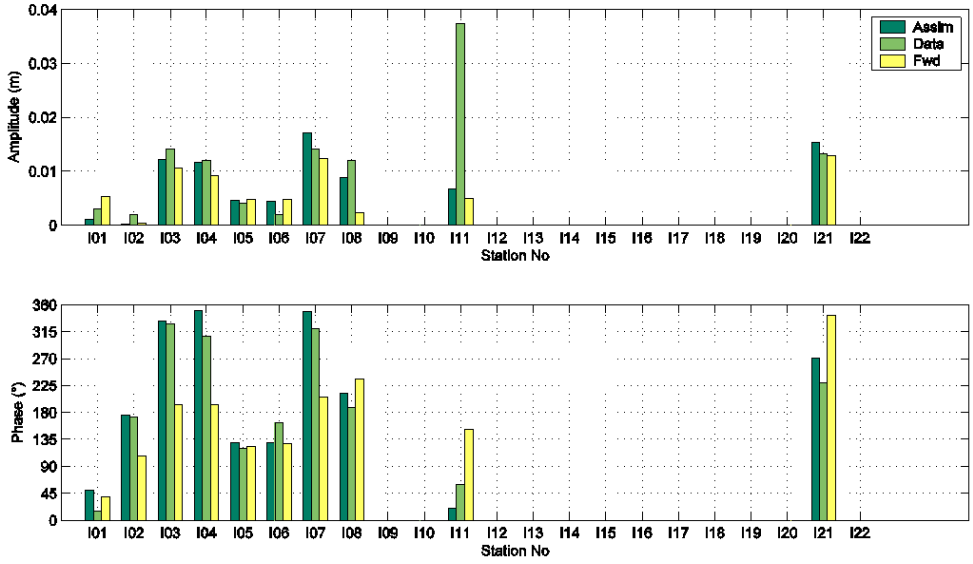

Figure 5.2.13 (continued)

Table 5.2.2 Comparison of observed (h_o,g_o), assimilation (h_a,g_a) and forward model (h_f,g_f) amplitudes (cm) and phases (°) at independent stations.

Station No.	M_2					
	h_o	g_o	h_a	g_a	h_f	g_f
I01	237.4	317.2	240.4	315.1	202.5	315.4
I02	152.9	136.1	158.7	135.3	159.4	135.9
I03	393.1	189.5	389.6	190.0	274.6	253.9
I04	389.3	188.8	392.3	191.3	279.9	255.9
I05	248.0	167.5	230.6	145.0	243.6	147.5
I06	244.4	143.0	236.8	146.6	251.4	149.8
I07	390.1	180.7	395.1	187.7	281.7	249.8
I08	26.5	87.0	15.9	13.1	11.1	235.6
I09	303.8	162.7	307.1	164.5	295.2	180.5
I10	221.0	172.7	220.9	170.0	213.5	173.3
I11	412.9	194.8	399.2	195.7	290.5	261.5
I12	315.0	173.2	313.3	171.8	276.2	191.0
I13	134.7	207.4	143.4	199.8	153.1	194.8
I14	303.1	320.7	294.7	316.4	258.1	324.6
I15	111.7	342.7	101.9	356.6	73.8	344.5
I16	16.0	89.8	11.3	99.9	19.6	180.7
I17	133.7	332.3	179.3	340.1	134.9	340.5
I18	130.4	168.5	127.2	192.6	127.2	192.5
I19	315.7	325.5	295.3	324.3	252.3	329.7
I20	272.9	332.1	264.1	332.7	228.8	341.0
I21	145.1	238.8	164.3	245.8	165.5	230.8
I22	53.7	197.3	58.1	200.2	72.9	201.6
rms error			13.5	18.0	55.0	47.8

Station No.	S_2					
	h_o	g_o	h_a	g_a	h_f	g_f
I01	74.5	356.0	80.1	354.6	62.9	358.5
I02	52.0	176.8	54.9	174.6	52.8	176.6
I03	138.8	243.8	140.7	243.3	73.4	306.9
I04	137.2	243.1	140.8	245.3	74.5	309.8
I05	94.0	212.2	84.6	185.9	81.7	191.6
I06	86.3	180.8	87.7	187.7	84.3	194.0
I07	147.6	234.0	142.9	241.0	75.6	303.1
I08	17.6	150.5	8.4	138.6	12.3	215.6
I09	109.4	209.9	115.5	210.7	96.2	225.9
I10	80.1	216.9	82.0	212.2	72.6	217.3
I11	145.8	252.7	142.3	251.2	77.1	316.8
I12	113.0	220.0	115.5	218.3	90.3	236.2
I13	52.6	248.2	56.4	239.9	54.1	239.0
I14	97.2	4.3	99.5	356.7	80.7	12.6
I15	29.3	34.6	30.6	48.5	14.2	28.8
I16	14.2	154.7	12.8	164.3	16.3	206.7
I17	37.3	16.2	56.8	20.7	37.9	21.8
I18	53.0	204.9	51.3	230.5	49.5	231.7
I19	102.2	8.1	99.8	5.7	78.6	17.1
I20	86.8	15.2	89.2	14.7	69.8	27.8
I21	54.2	277.0	65.7	281.6	60.5	275.0
I22	23.6	210.9	25.7	217.2	32.2	225.3
rms error			6.8	10.2	30.6	34.9

Table 5.2.2 (continued).

Station No.	$2SM_2$					
	h_o	g_o	h_a	g_a	h_f	g_f
I01	2.4	219.2	3.2	231.1	1.3	224.3
I02	1.3	16.3	0.2	10.4	0.1	313.7
I03	6.7	56.3	7.6	62.5	3.2	150.2
I04	6.4	60.8	8.2	67.1	3.4	152.3
I05	2.3	24.5	2.3	358.3	0.4	331.4
I06	4.4	99.3	2.6	3.5	0.5	335.9
I07	5.6	81.4	8.4	60.2	3.3	144.7
I08	2.0	300.7	2.1	295.9	0.7	325.3
I09	4.2	40.1	5.8	31.7	1.1	38.6
I10	2.4	59.0	2.1	48.9	0.3	307.3
I11	13.1	70.4	9.5	77.0	3.8	158.1
I13	1.0	71.0	1.7	72.6	0.4	307.6
I14	3.4	211.1	2.7	228.2	2.5	199.5
I15	2.5	263.7	3.0	295.4	1.0	327.3
I16	1.3	273.9	1.8	301.9	0.6	332.3
I17	2.2	258.5	3.2	272.4	1.2	298.1
I18	0.7	293.4	0.8	19.3	0.7	18.8
I19	3.4	233.7	4.3	228.2	2.2	210.6
I20	3.0	242.4	3.9	248.3	1.7	237.8
I21	2.1	112.6	2.9	94.6	0.6	4.4
I22	1.2	243.4	1.1	264.9	0.2	282.1
rms error			1.3	31.9	2.8	72.2

Station No.	M_4					
	h_o	g_o	h_a	g_a	h_f	g_f
I01	6.3	200.9	8.5	198.0	6.3	250.4
I02	4.4	218.1	0.6	212.6	0.1	200.0
I03	12.3	13.1	10.8	26.9	20.4	93.9
I04	12.7	32.1	11.9	12.9	26.5	95.2
I05	5.5	314.5	5.7	239.5	3.3	221.0
I06	6.6	239.1	6.0	248.0	4.1	223.9
I07	12.3	344.7	10.4	17.6	22.4	73.3
I08	2.8	89.6	4.1	87.9	3.2	115.5
I09	10.5	350.4	9.0	347.9	16.2	262.8
I10	6.3	305.9	6.5	262.9	6.3	291.5
I11	16.2	355.9	16.6	358.9	39.4	104.2
I12	6.0	29.2	7.0	10.9	25.9	274.3
I13	11.3	19.6	6.0	1.5	3.8	43.7
I14	23.4	202.6	16.7	197.8	23.5	233.6
I15	8.6	90.3	8.6	103.5	9.8	125.0
I16	2.1	65.8	0.4	283.8	1.6	198.5
I18	4.5	180.4	5.0	297.9	5.0	304.6
I19	19.6	244.6	21.8	208.2	21.0	245.8
I20	13.3	251.1	12.1	244.0	9.4	274.6
I21	23.9	62.8	25.0	52.5	13.2	74.9
I22	1.8	93.5	1.5	54.1	0.4	86.4
rms error			2.3	47.4	8.6	69.0

Table 5.2.2 (continued).

Station No.	MS_4					
	h_o	g_o	h_a	g_a	h_f	g_f
I01	3.7	235.3	5.1	238.6	3.4	299.8
I02	2.5	272.5	0.2	255.1	0.0	252.4
I03	6.5	16.2	4.4	29.8	12.1	144.8
I04	4.9	31.4	7.1	19.8	15.7	148.4
I05	2.7	6.6	2.2	295.1	1.6	281.8
I06	1.9	280.3	2.3	305.8	1.9	284.1
I07	8.4	349.7	4.9	13.3	13.8	125.3
I08	0.9	97.8	2.7	114.0	1.6	159.5
I09	5.8	51.0	5.0	54.2	9.4	321.6
I10	3.1	355.7	2.8	295.0	3.6	341.5
I11	14.5	14.1	13.2	21.0	23.4	160.0
I13	5.3	63.2	0.6	129.4	1.6	97.2
I14	14.2	245.4	7.9	247.6	14.5	280.3
I15	8.5	118.4	6.9	141.4	5.5	166.8
I16	1.2	69.2	0.8	17.0	1.1	252.3
I17	0.9	85.5	2.1	350.3	1.8	58.2
I18	3.5	289.5	4.1	340.8	4.2	346.3
I19	11.3	295.1	14.0	248.6	12.8	291.8
I20	6.7	298.6	6.9	286.8	5.2	317.9
I21	12.8	115.2	7.4	112.5	6.2	115.5
I22	0.7	63.7	1.4	238.6	0.2	338.2
rms error			2.6	39.4	4.1	82.7

Station No.	M_6					
	h_o	g_o	h_a	g_a	h_f	g_f
I01	0.6	354.0	1.4	310.9	2.1	316.7
I02	0.4	45.8	0.2	107.3	0.3	36.1
I03	6.4	231.7	5.9	229.2	7.7	70.1
I04	4.1	225.4	6.9	232.8	7.7	74.5
I05	1.1	50.8	1.2	90.3	1.8	53.7
I06	0.6	60.4	1.0	92.5	1.7	61.7
I07	4.7	201.5	7.4	222.3	9.5	69.7
I08	4.0	88.3	2.5	121.9	1.0	205.3
I09	1.9	344.1	2.4	357.3	5.5	230.5
I10	1.4	150.3	1.6	160.3	0.9	342.1
I11	8.2	270.3	7.7	248.6	6.5	86.7
I14	5.5	346.9	2.6	10.2	1.2	7.1
I15	2.5	304.2	1.1	136.5	2.8	182.2
I16	2.6	115.0	2.0	92.3	0.3	30.1
I18	1.3	8.3	1.4	190.9	1.3	205.5
I20	1.4	281.8	1.1	240.3	1.5	343.5
I22	1.8	124.1	1.3	101.4	0.5	327.1
rms error			1.3	65.7	2.3	116.6

Table 5.2.2 (continued).

Station No.	$2MS_6$					
	h_o	g_o	h_a	g_a	h_f	g_f
I01	0.6	27.0	0.9	357.1	2.0	1.1
I02	0.6	89.5	0.2	154.6	0.2	77.1
I03	6.4	270.3	6.0	272.5	6.3	123.5
I04	5.2	266.6	7.2	281.2	6.2	127.2
I05	1.2	73.8	1.0	109.2	1.8	89.0
I06	0.7	96.5	1.0	107.3	1.7	94.4
I07	6.0	252.8	8.2	268.4	7.6	126.0
I08	4.7	142.0	3.0	164.8	0.9	228.9
I09	2.3	49.7	2.4	50.5	4.5	278.9
I10	1.4	202.5	1.7	207.9	0.7	27.5
I11	11.0	319.1	8.4	305.5	4.6	133.1
I14	5.3	28.6	1.9	68.6	1.1	61.0
I15	2.7	350.1	0.6	42.6	2.6	234.7
I16	2.8	159.8	2.4	144.8	0.5	89.1
I18	1.2	42.1	1.5	233.9	1.5	247.2
I20	1.8	324.9	1.3	282.4	1.5	19.5
I21	1.9	137.5	1.9	277.5	8.2	314.6
I22	2.0	166.1	1.8	157.4	0.5	32.3
rms error			1.4	58.7	2.7	115.3

Station No.	$2SM_6$					
	h_o	g_o	h_a	g_a	h_f	g_f
I01	0.3	15.9	0.1	51.1	0.5	39.4
I02	0.2	172.6	0.0	176.4	0.0	107.0
I03	1.4	327.4	1.2	332.4	1.1	192.0
I04	1.2	306.4	1.2	350.0	0.9	193.1
I05	0.4	120.0	0.5	129.5	0.5	123.2
I06	0.2	163.2	0.5	129.8	0.5	127.8
I07	1.4	320.3	1.7	348.4	1.2	205.9
I08	1.2	188.0	0.9	211.8	0.2	235.4
I11	3.7	59.2	0.7	20.3	0.5	152.6
I21	1.3	230.0	1.5	271.6	1.3	341.6
rms error			1.0	30.0	1.1	85.9

Table 5.2.3 Comparison of observed (h_o,g_o), assimilation model (h_a,g_a) and Taguchi (2002; h_T,g_T) amplitudes (cm) and phases (°) of M_2 and M_4 at independent stations.

Station No.	M_2					
	h_o	g_o	h_a	g_a	h_T	g_T
T01	140.4	269.5	131.9	270.2	136.2	267.6
T02	392.0	192.0	389.6	190.0	393.0	189.5
T03	315.0	173.0	314.7	171.6	315.6	174.1
T04	292.0	327.0	295.3	324.3	300.2	326.5
T05	125.0	324.0	125.1	325.6	126.4	322.6
rms error			4.2	1.8	4.2	1.6

Table 5.2.3 (continued).

Station No.	M_4					
	h_o	g_o	h_a	g_a	h_T	g_T
T02	13.0	19.0	10.8	26.9	12.3	13.1
T03	5.0	26.0	7.1	11.1	5.5	27.1
rms error			2.1	11.9	0.6	4.2

Table 5.2.4 Comparison of observed (h_o,g_o), assimilation model (h_a,g_a) and Davies and Hall (2000; h_{DH},g_{DH}) amplitudes (cm) and phases (°) of M_2 and S_2 at independent stations.

Station No.	M_2					
	h_o	g_o	h_a	g_a	h_{DH}	g_{DH}
D01	20.4	31.0	19.8	335.9	12.1	6.0
D02	43.3	309.0	45.6	308.0	45.5	284.0
D03	125.5	324.0	125.1	325.6	117.1	324.0
rms error			1.4	31.8	6.9	20.4

Station No.	S_2					
	h_o	g_o	h_a	g_a	h_{DH}	g_{DH}
D01	10.6	134.0	4.3	131.1	2.9	114.0
D02	4.6	355.0	5.4	352.6	10.6	286.0
D03	33.1	7.0	33.5	9.3	33.3	341.0
rms error			3.7	2.5	5.6	44.1

Table 5.2.5 The rms errors of M_2- and S_2 elevations obtained by the assimilation model with 1 day (h_{1D} (cm), g_{1D} (°)) and 4 days (h_{4D} (cm), g_{4D} (°)) time blocks as compared to observation in independent stations.

	M_2				S_2			
	h_{1D}	g_{1D}	h_{4D}	g_{4D}	h_{1D}	g_{1D}	h_{4D}	g_{4D}
rms error	13.5	18.0	14.4	19.1	6.8	10.2	6.7	11.0

An experiment in the canal model with overlapping interval of 105+40 is appropriate for reducing the overestimation of σ_4 elevation significantly. Based on that experiment, an overlapping interval of 4*720+180 is also applied here (1 day simulation time is equal to 720 time steps), but this overlapping still fails to improve the elevation of $2SM_2$. Further experiments are probably needed to know the appropriate time block should be chosen to obtain the best estimation of this tidal constituent. So far, in view of the evaluations having been done to the assimilation model results, the assimilation model is recognized to have produced an adequate estimation as compared to observations. Furthermore, from the computation point of view (i.e. the need of CPU time and computer memory), this experiment is not too expensive.

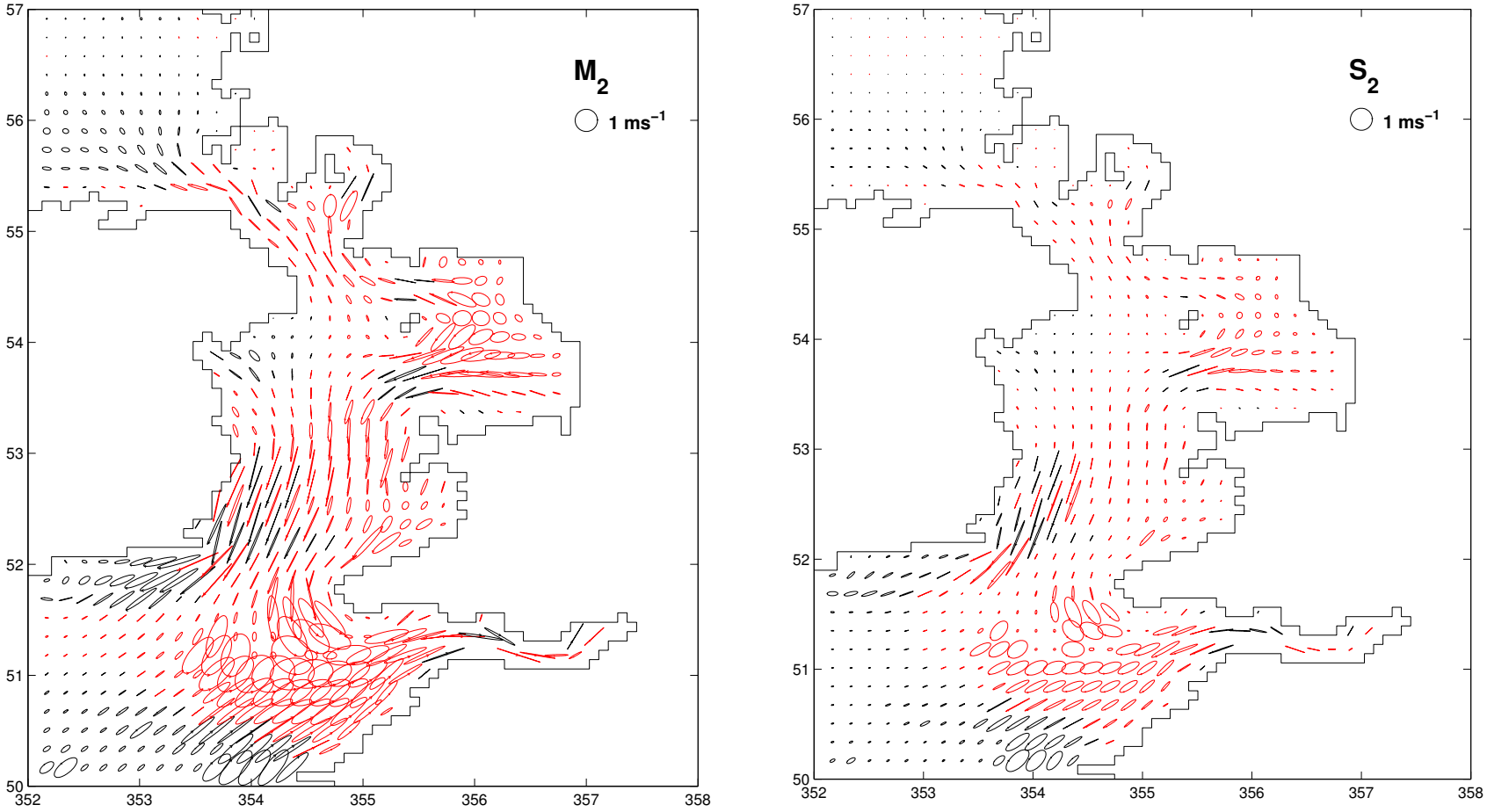

Figure 5.2.14 Current ellipses of M_2 (left panel) and S_2 (right panel) from data assimilation model at every second grid point; black ellipse denotes clockwise rotation and red ellipse denotes anticlockwise rotation.

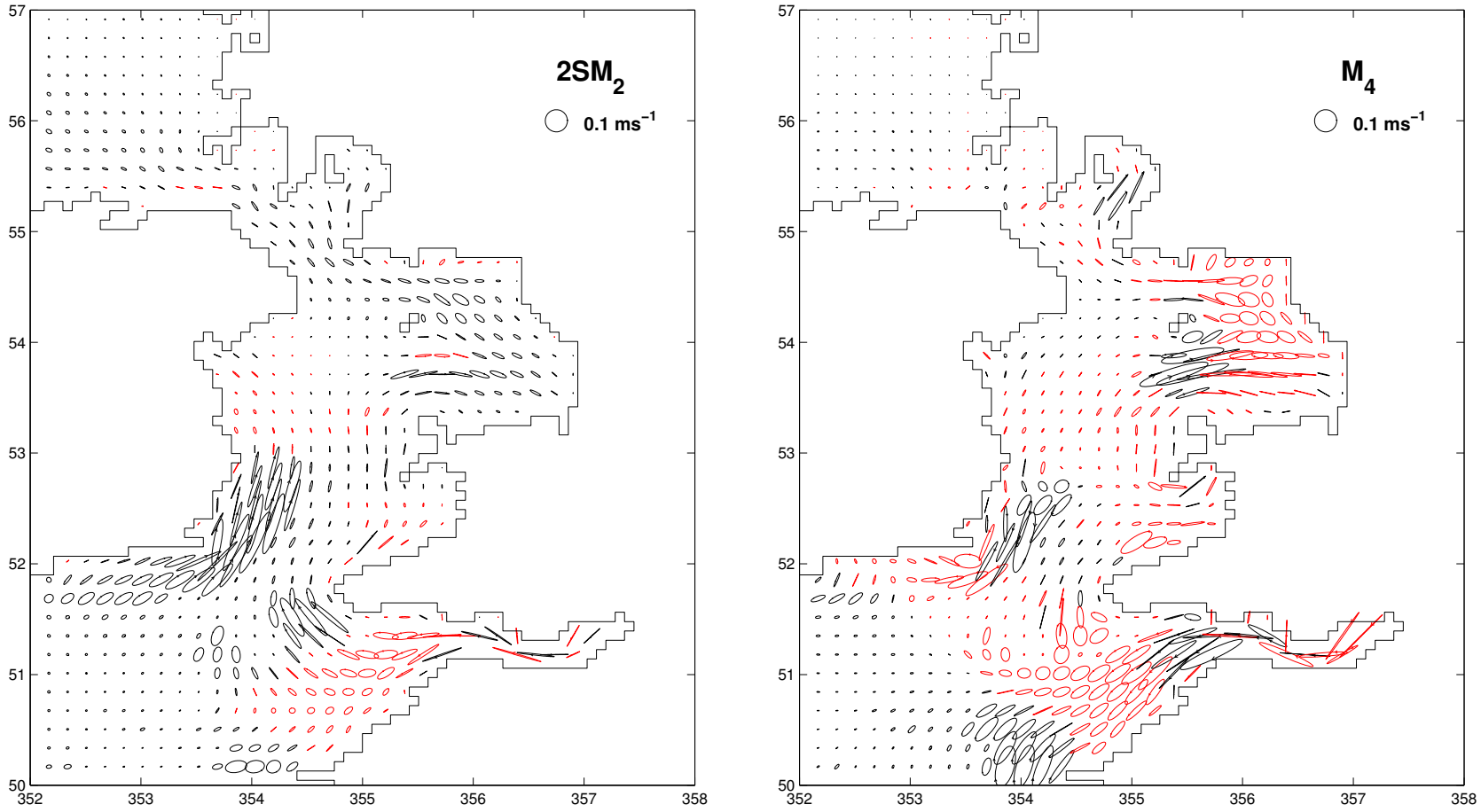

Figure 5.2.15 Current ellipses of $2SM_2$ (left panel) and M_4 (right panel) from data assimilation model at every second grid point; black ellipse denotes clockwise rotation and red ellipse denotes anticlockwise rotation.

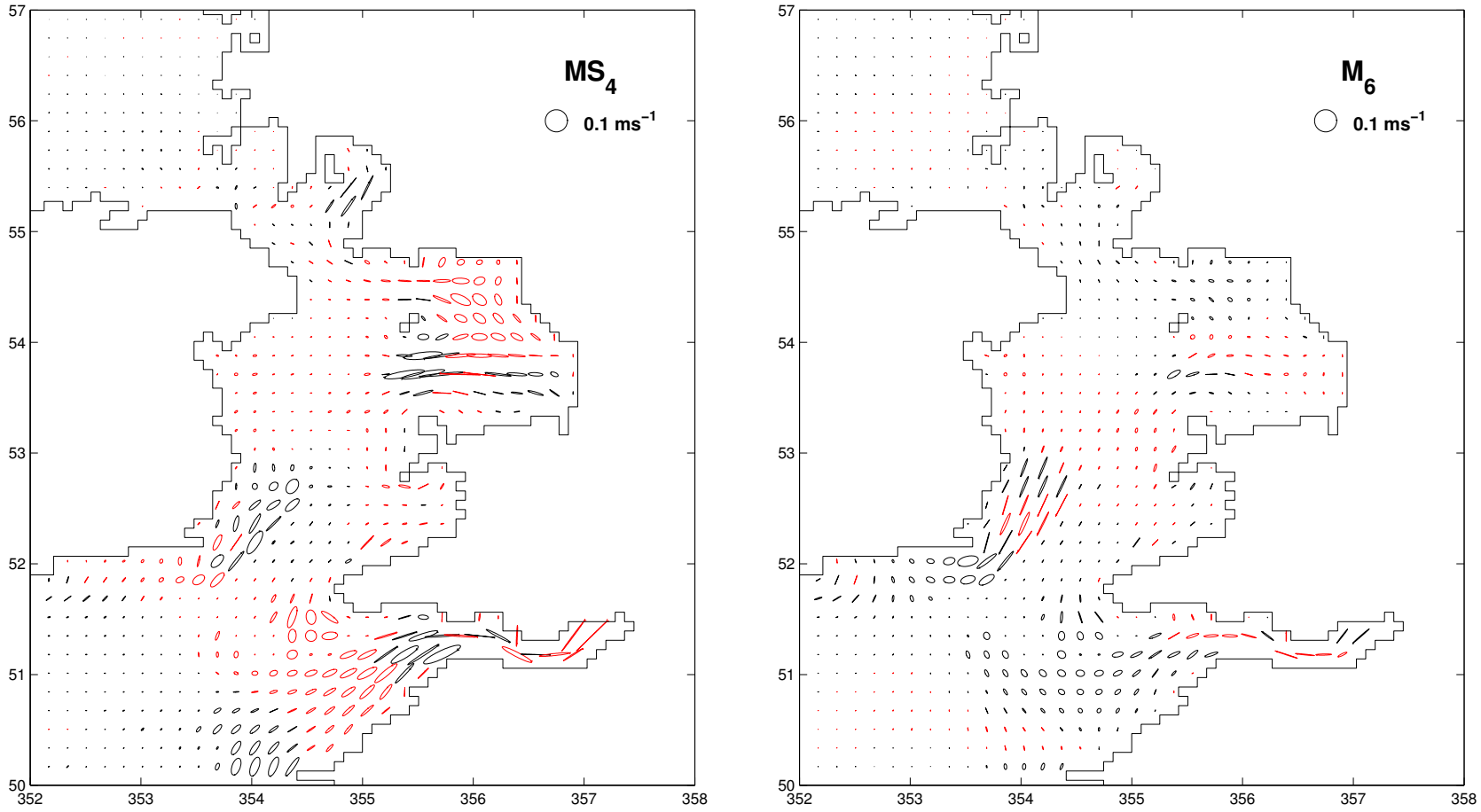

Figure 5.2.16 Current ellipses of MS_4 (left panel) and M_6 (right panel) from data assimilation model at every second grid point; black ellipse denotes clockwise rotation and red ellipse denotes anticlockwise rotation.

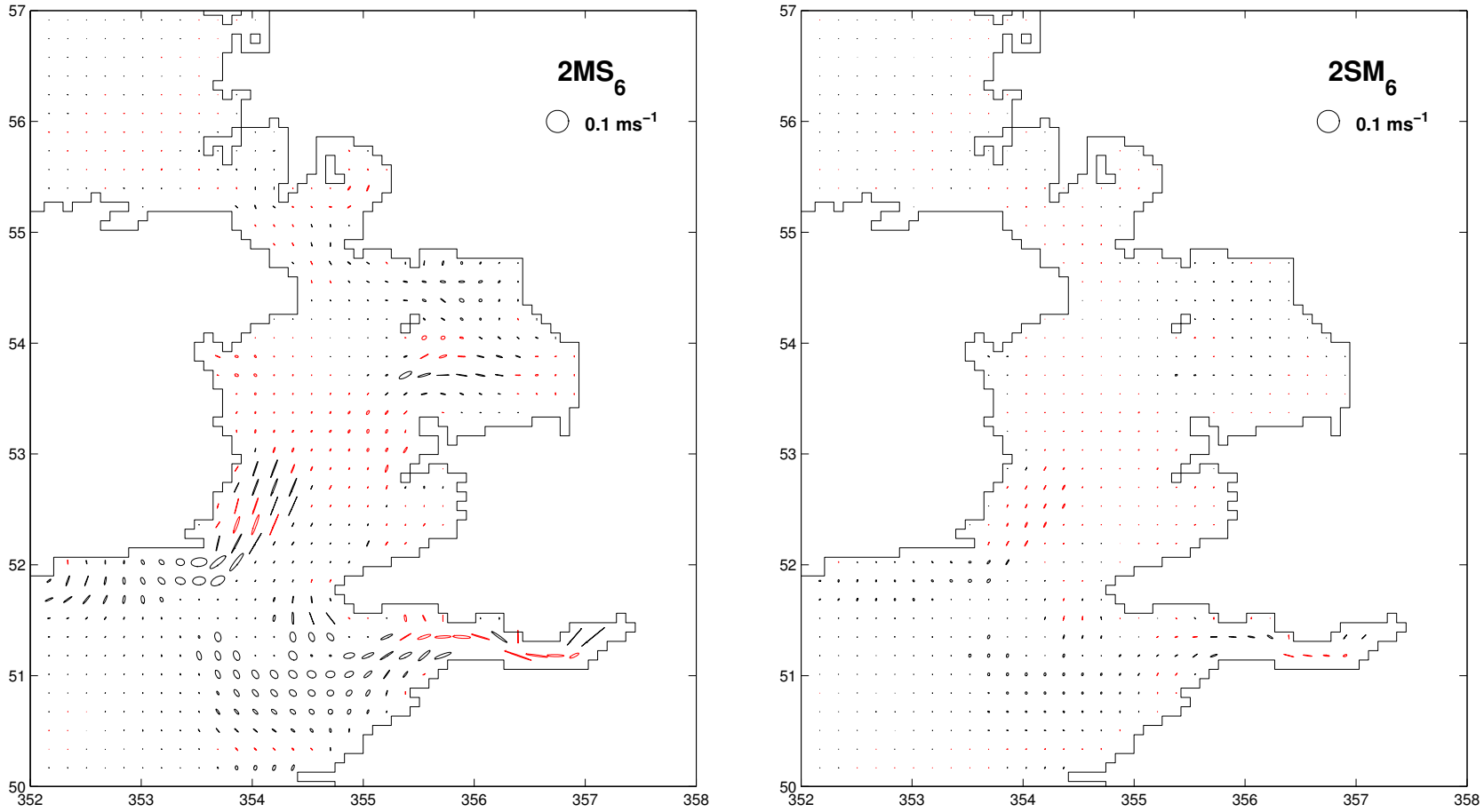

Figure 5.2.17 Current ellipses of $2MS_6$ (left panel) and $2SM_6$ (right panel) from data assimilation model at every second grid point; black ellipse denotes clockwise rotation and red ellipse denotes anticlockwise rotation.

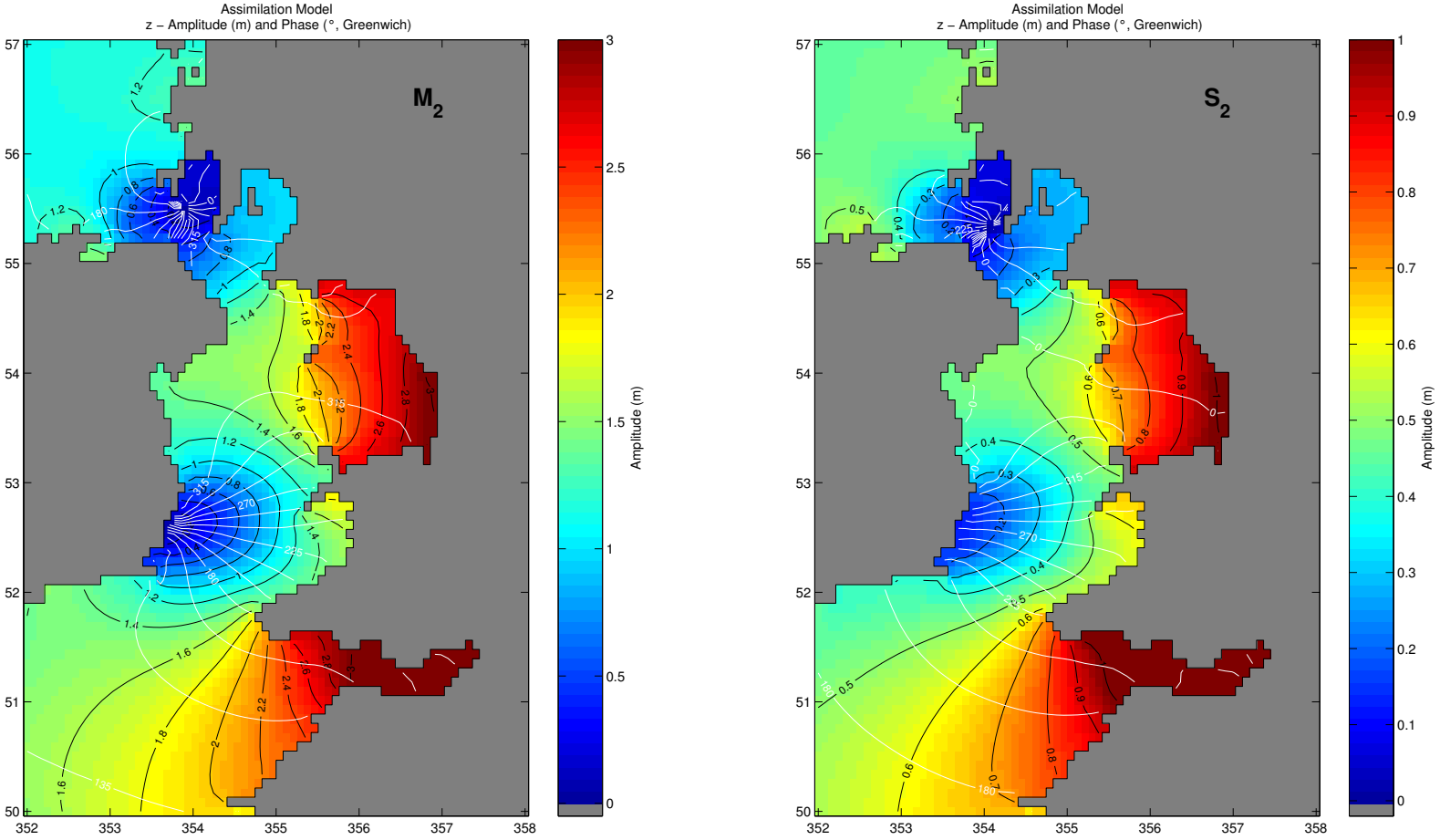

Figure 5.2.18 Tidal elevations of M_2 (left panel) and S_2 (right panel) from the assimilation model with 4 days time block length.

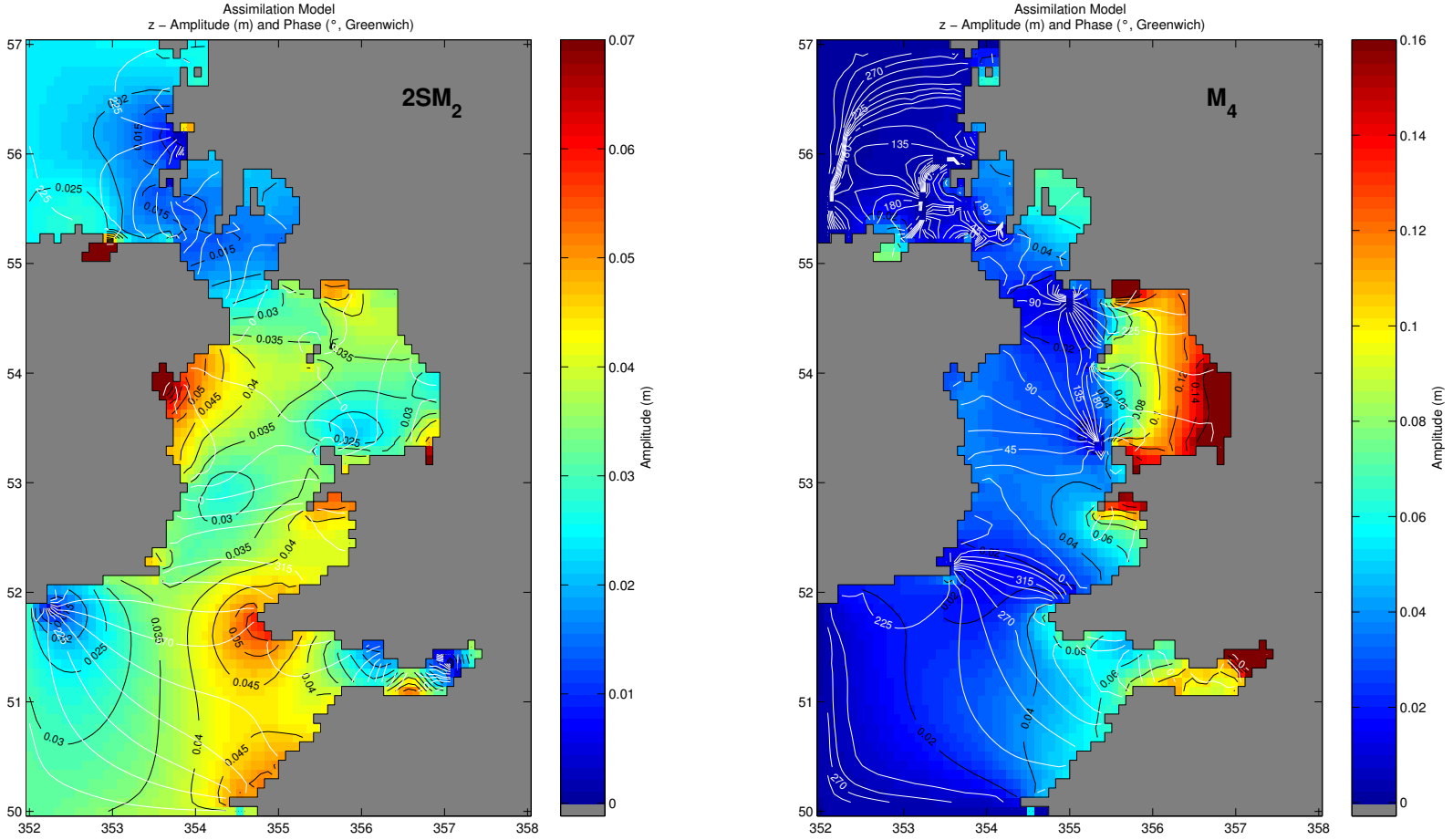

Figure 5.2.19 Tidal elevations of $2SM_2$ (left panel) and M_4 (right panel) from the assimilation model with 4 days time block length.

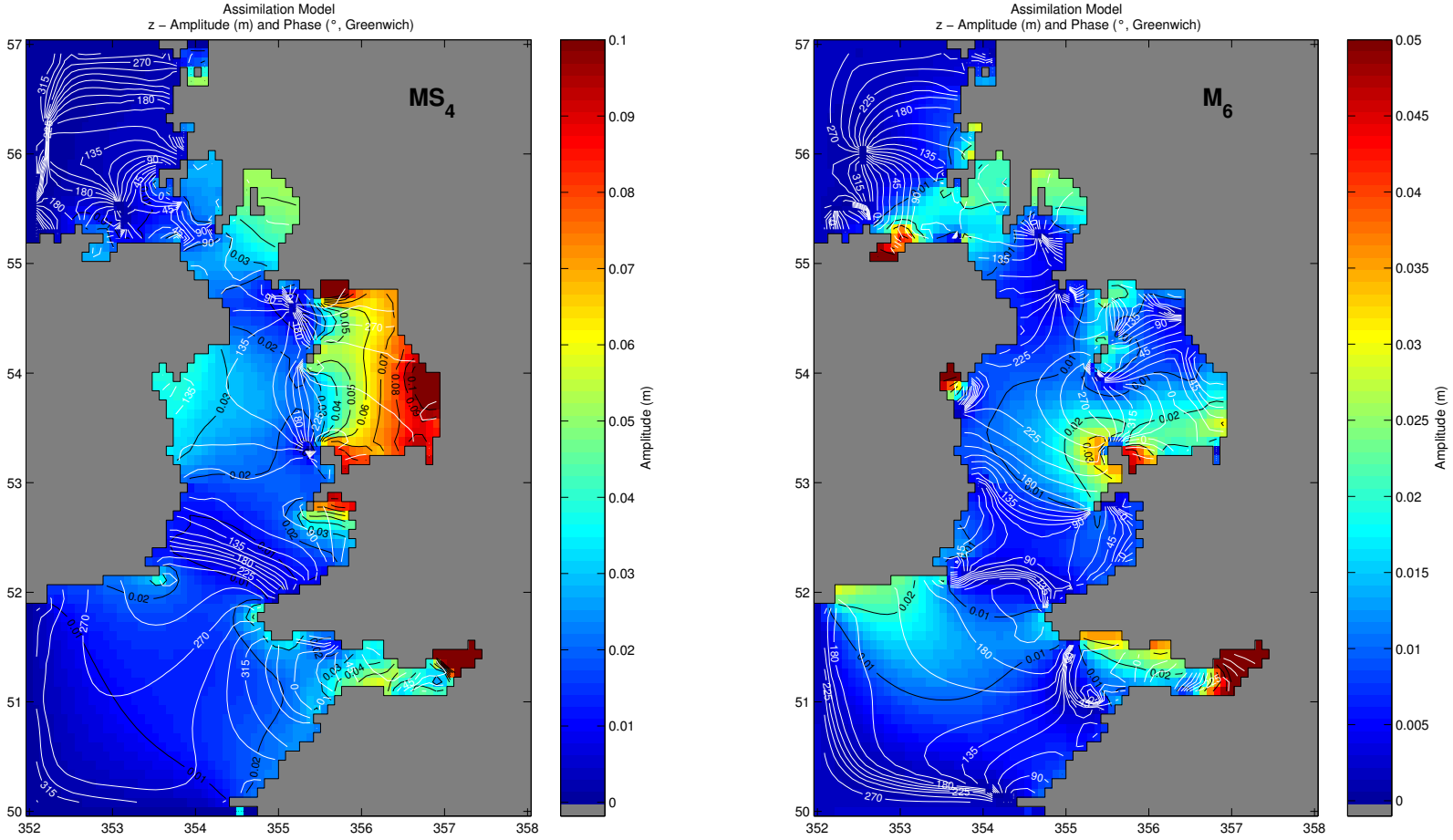

Figure 5.2.20 Tidal elevations of MS_4 (left panel) and M_6 (right panel) from the assimilation model with 4 days time block length.

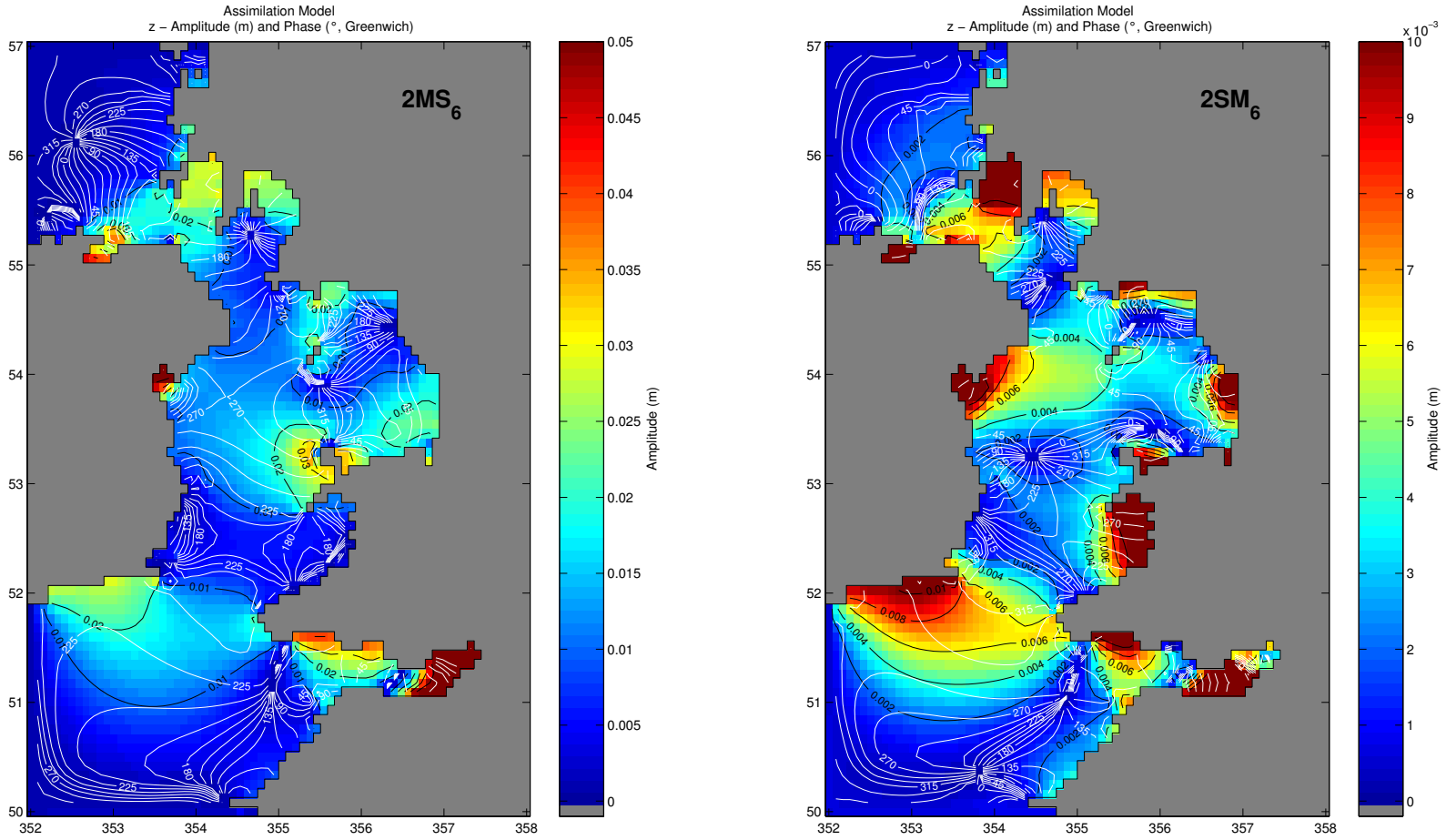

Figure 5.2.21 Tidal elevations of $2MS_6$ (left panel) and $2SM_6$ (right panel) from the assimilation model with 4 days time block length.

Table 5.2.6 The rms errors of over- and compound tides elevations obtained by the assimilation model with 1 day (h_{1D} (cm), g_{1D} (°)) and 4 days (h_{4D} (cm), g_{4D} (°)) time blocks as compared to observations at independent stations.

	$2SM_2$				M_4				MS_4			
	h_{1D}	g_{1D}	h_{4D}	g_{4D}	h_{1D}	g_{1D}	h_{4D}	g_{4D}	h_{1D}	g_{1D}	h_{4D}	g_{4D}
rms error	1.3	31.9	3.7	129.2	2.3	47.4	3.5	48.9	2.6	39.4	2.6	55.1

	M_6				$2MS_6$				$2SM_6$			
	h_{1D}	g_{1D}	H_{4D}	g_{4D}	h_{1D}	g_{1D}	h_{4D}	g_{4D}	h_{1D}	g_{1D}	h_{4D}	g_{4D}
rms error	1.3	66.6	1.4	59.0	1.4	62.6	1.3	58.2	1.0	30.0	1.0	53.2

5.2.2.2. Data assimilation with smoothing of residual

The dynamical residuals obtained by the data assimilation model properly applied (see canal model) reflects the main features of the true residuals, and using this method of data assimilation promises that information on the unknown deficiencies of the classical model can be taken from the dynamical residuals arising. In this experiment, first order differences of the dynamical residuals have been considered in the minimization functional with choosing weighting coefficients such that an appropriate decorrelation length scale of the dynamical errors is introduced.

It is found that considering the first order differences of the dynamical residuals in the model leads to an adequate smoothing of the residuals, primarily. It is evident that without minimizing the differences of the dynamical residuals, highly unrealistic spikes of the dynamical residuals occur at the positions where data are assimilated (see Figures 5.2.22 – 5.2.24 left panels).

Figures 5.2.22 – 5.2.24 (right panels) show the dynamical residuals of M_2 after introducing the first order differences of the dynamical residuals into the minimization functional. From these figures it can clearly be taken that the dynamical residuals become smoother, in particular, in the neighbourhood of the cells where data are assimilated. Interpreting the residuals with respect to which model deficiencies they compensate, is a difficult task, which requires additional investigations and also the use of higher order differences, in particular.

Figures 5.2.25 – 5.2.28 show the elevation cotidal charts of this experiment. Comparing these charts with those obtained by the data assimilation model without smoothing of residual (Figures 5.2.5 – 5.2.12 right panels), it is found that in general the pattern of both results are almost equal. Table 5.2.7 gives the comparison of both results at the independent stations and can be seen clearly that the rms error differences are insignificant. A significant difference is found only for $2SM_6$ phase, where the rms error obtained by the assimilation model with smoothing of residual is larger by 32.6° than without smoothing of residual. This significant difference is mainly caused by the phase underestimation by 145° at station I02 in the Celtic Sea. It means that, in general, introducing the first order

differences of the dynamical residuals into the minimization functional will not affect significantly the solution but mainly will reduce the unrealistic spikes of the dynamical residuals occurring at the positions where data are assimilated, altogether leading to an adequate spatial smoothing of the residuals. The length scale of the residuals then corresponds to the decorrelation lengths assumed for the dynamical errors and hopefully to the scale of the compensated deficiencies, as applying to the canal model results.

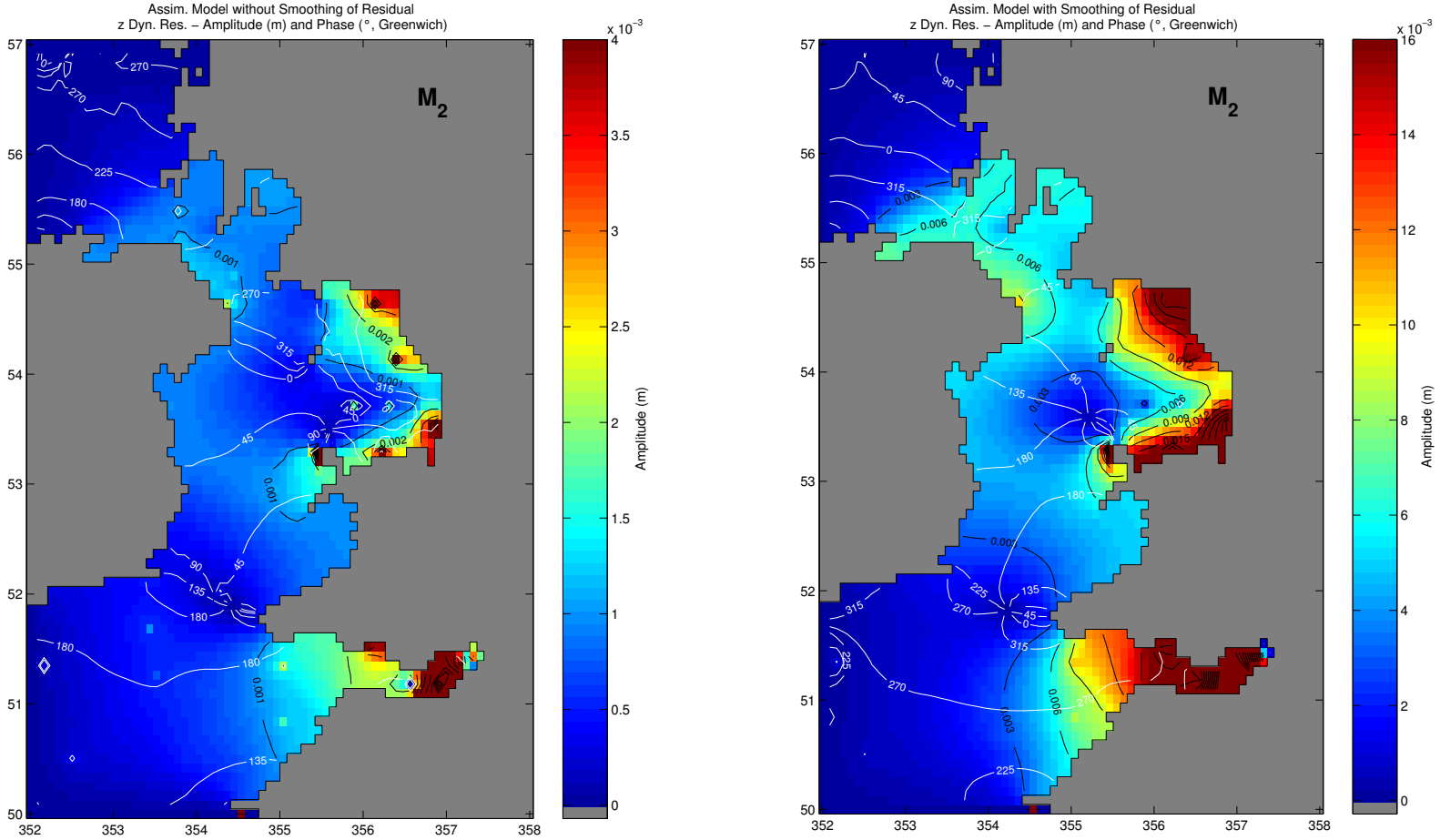

Figure 5.2.22 Dynamical residual of M_2 elevation without smoothing of residual (left panel) and with smoothing of residual (right panel).

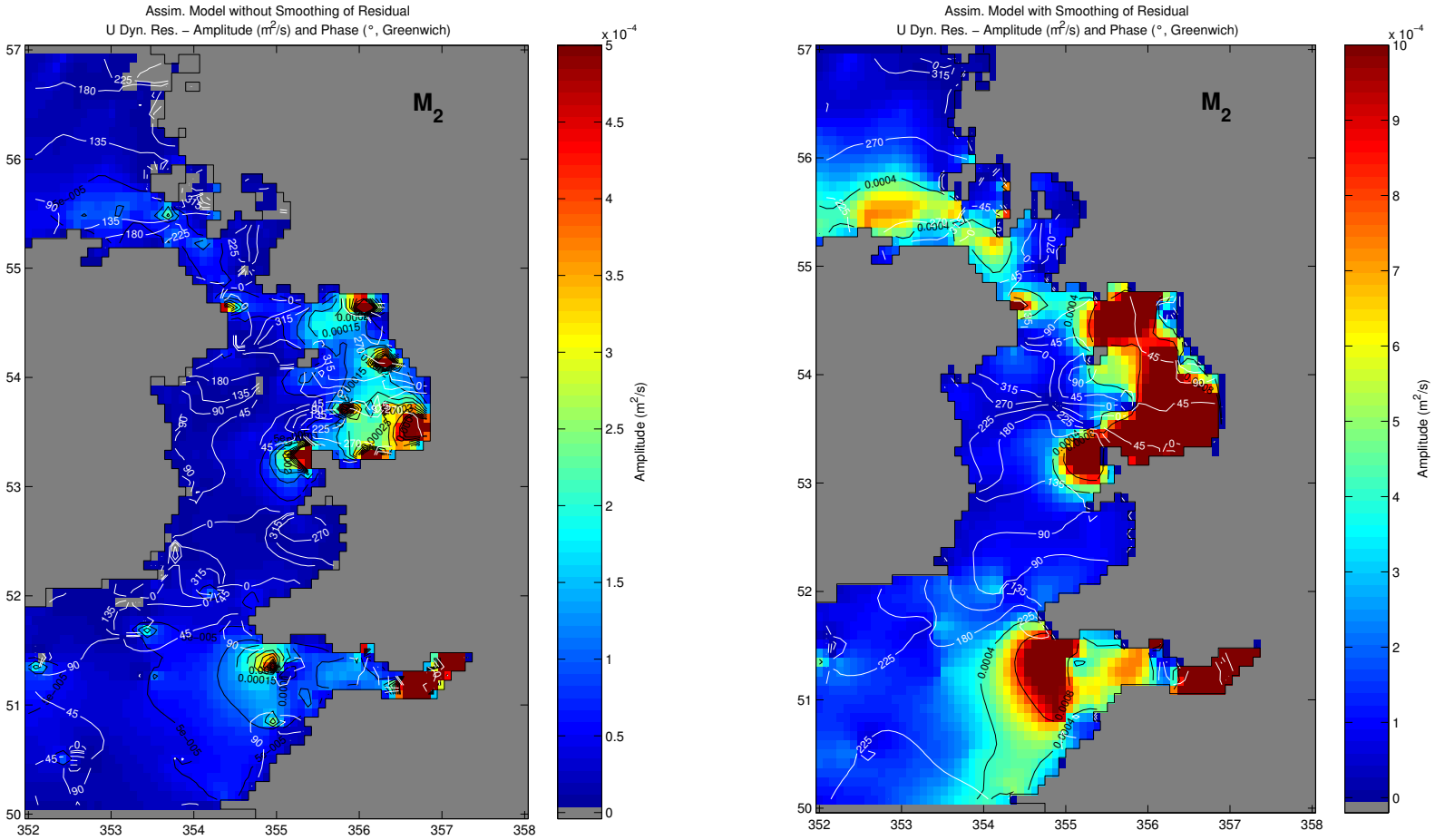

Figure 5.2.23 Dynamical residual of M_2 east-west volume transport without smoothing of residual (left panel) and with smoothing of residual (right panel).

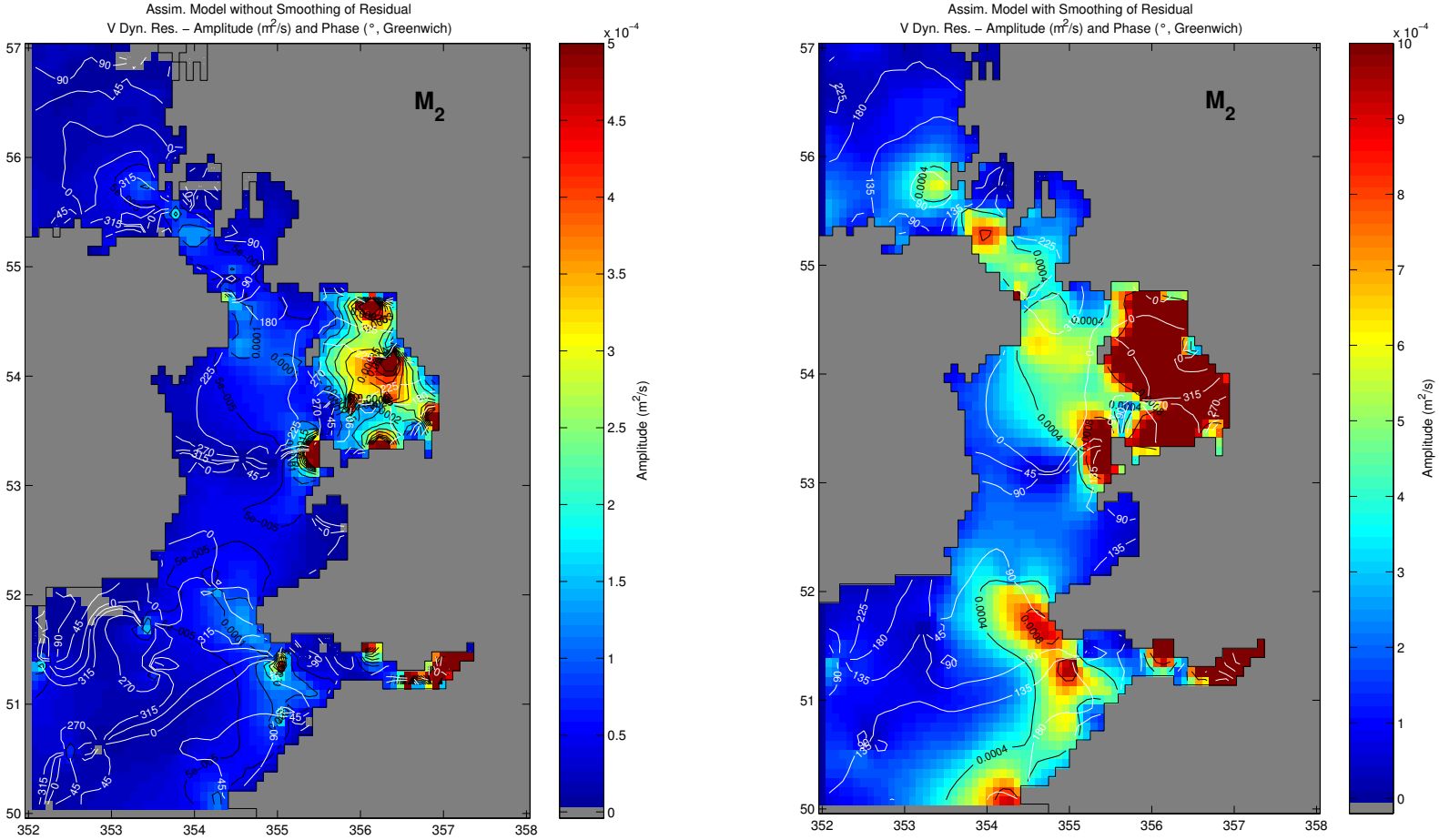

Figure 5.2.24 Dynamical residual of M_2 south-north volume transport without smoothing of residual (left panel) and with smoothing of residual (right panel).

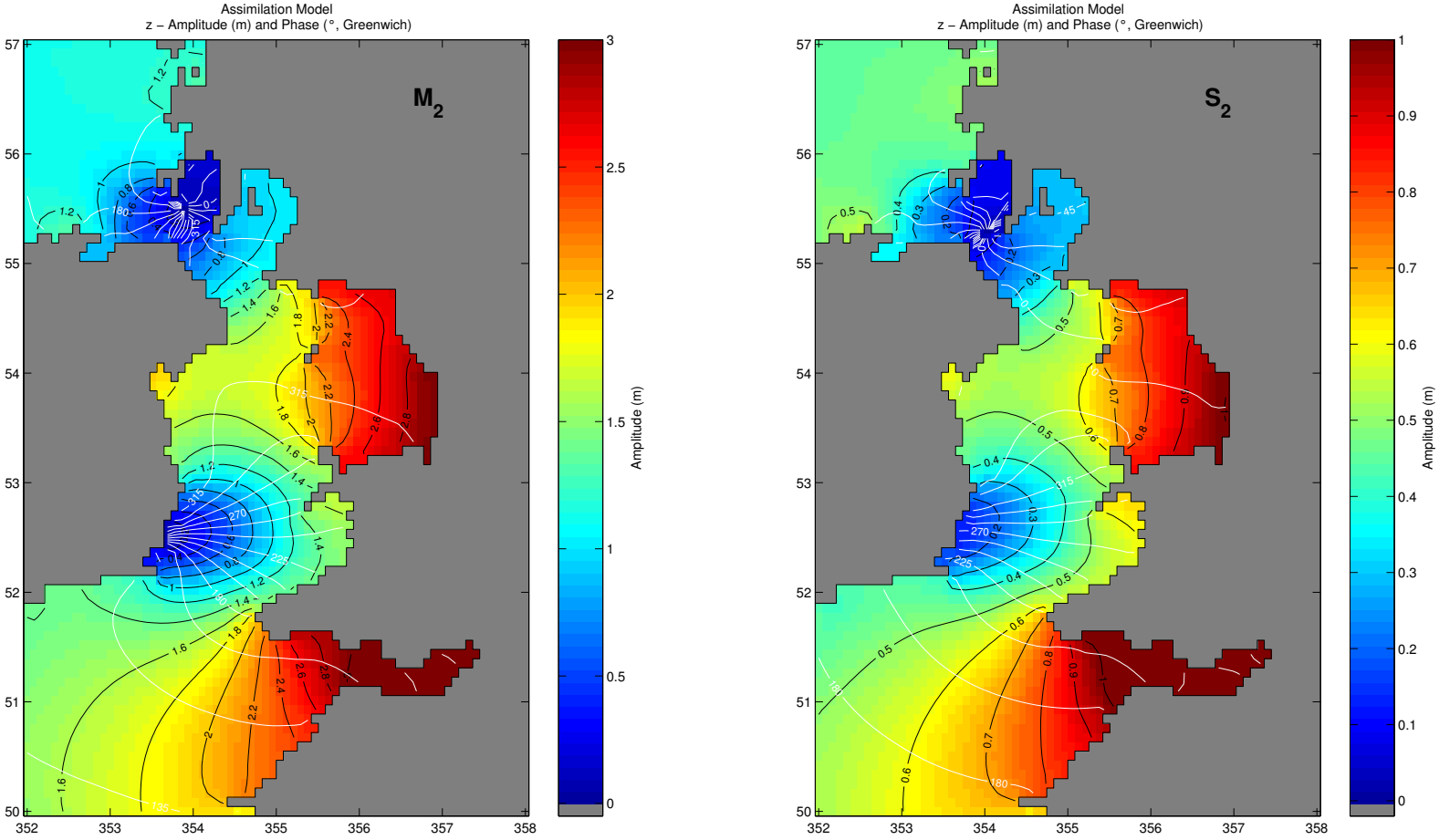

Figure 5.2.25 Tidal elevations of M_2 (left panel) and S_2 (right panel) obtained by the assimilation model with time block length of 1 day where the smoothing of residual is introduced.

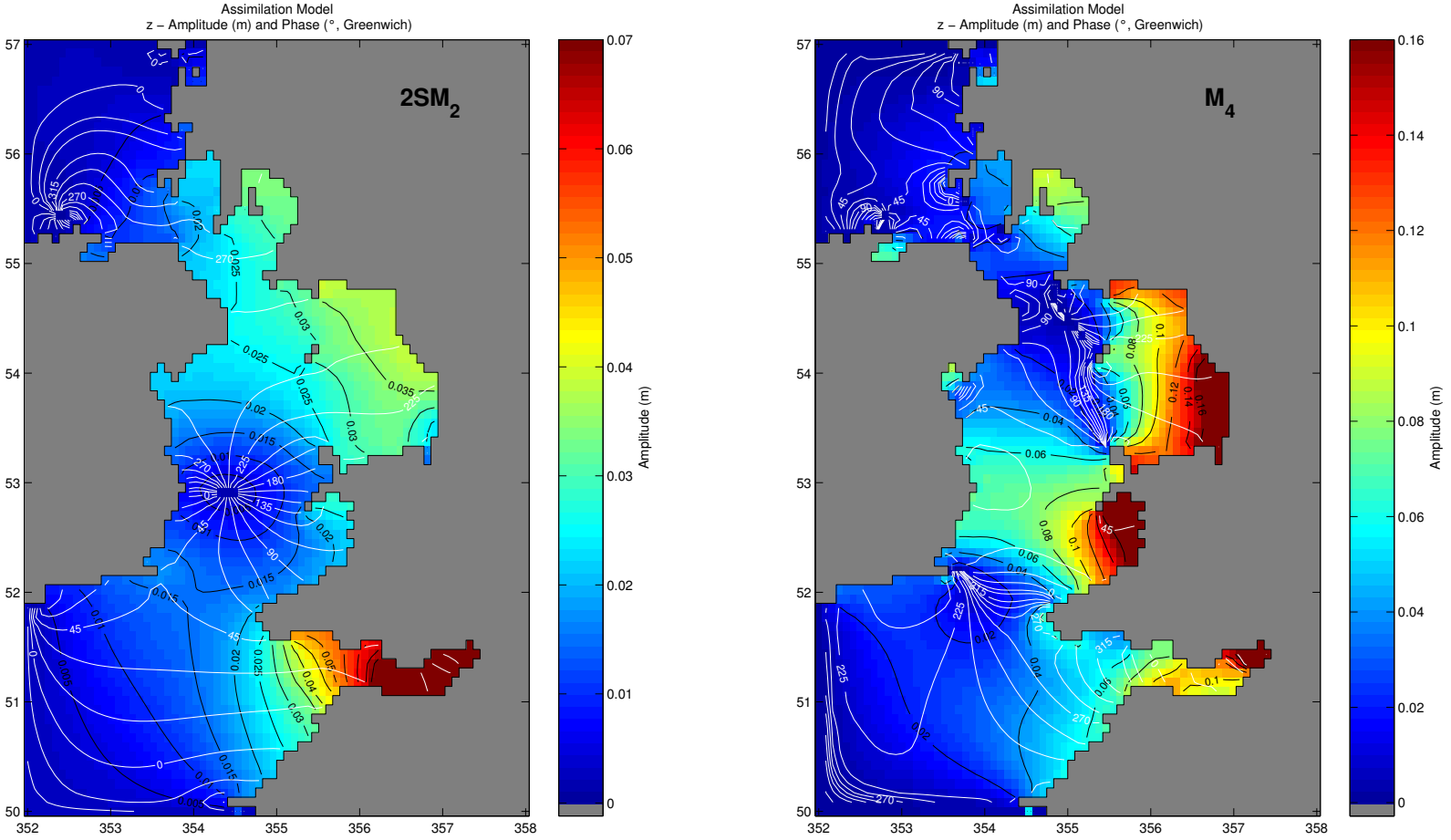

Figure 5.2.26 Tidal elevations of $2SM_2$ (left panel) and M_4 (right panel) obtained by the assimilation model with time block length of 1 day where the smoothing of residual is introduced.

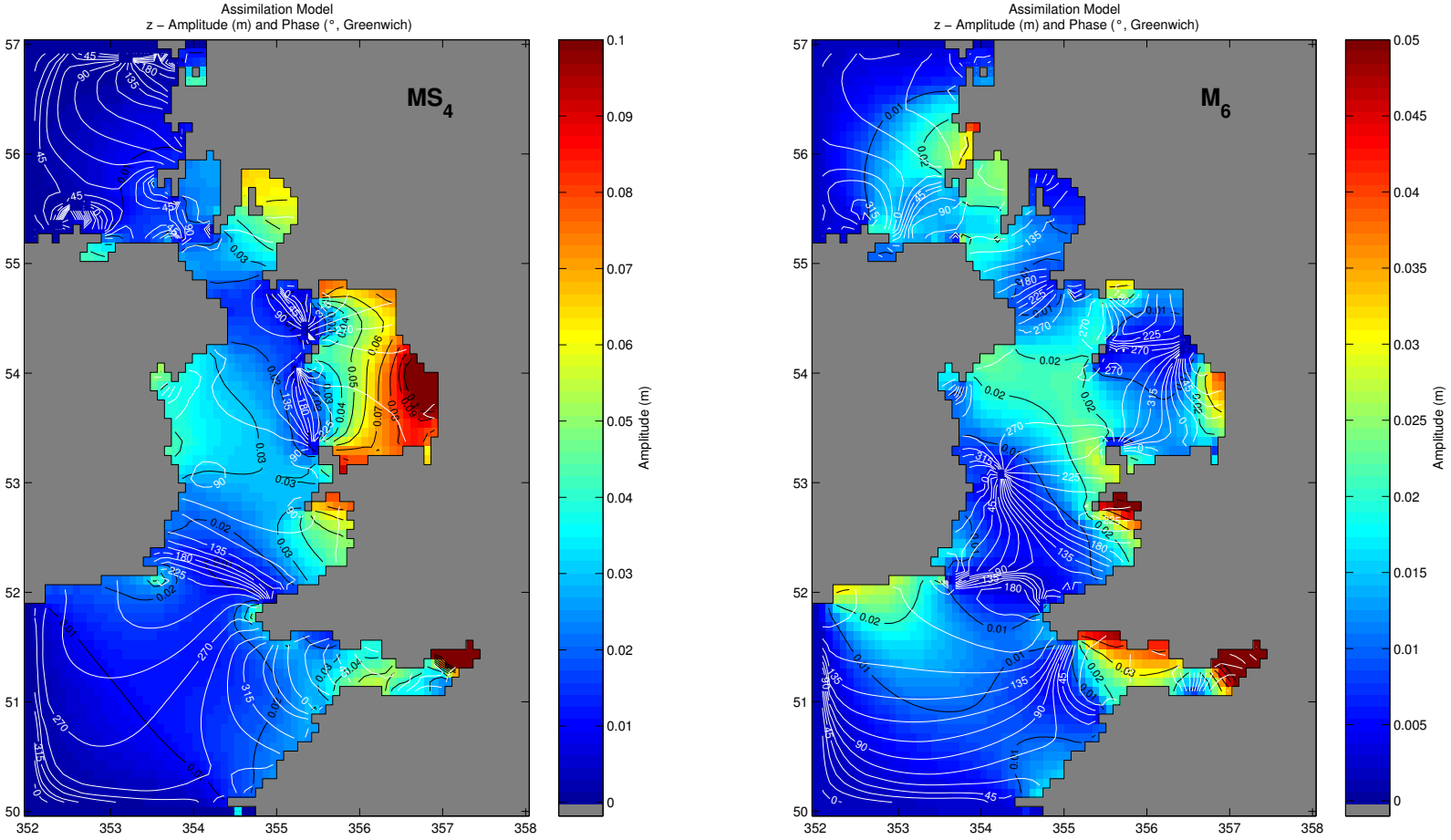

Figure 5.2.27 Tidal elevations of MS_4 (left panel) and M_6 (right panel) obtained by the assimilation model with time block length of 1 day where the smoothing of residual is introduced.

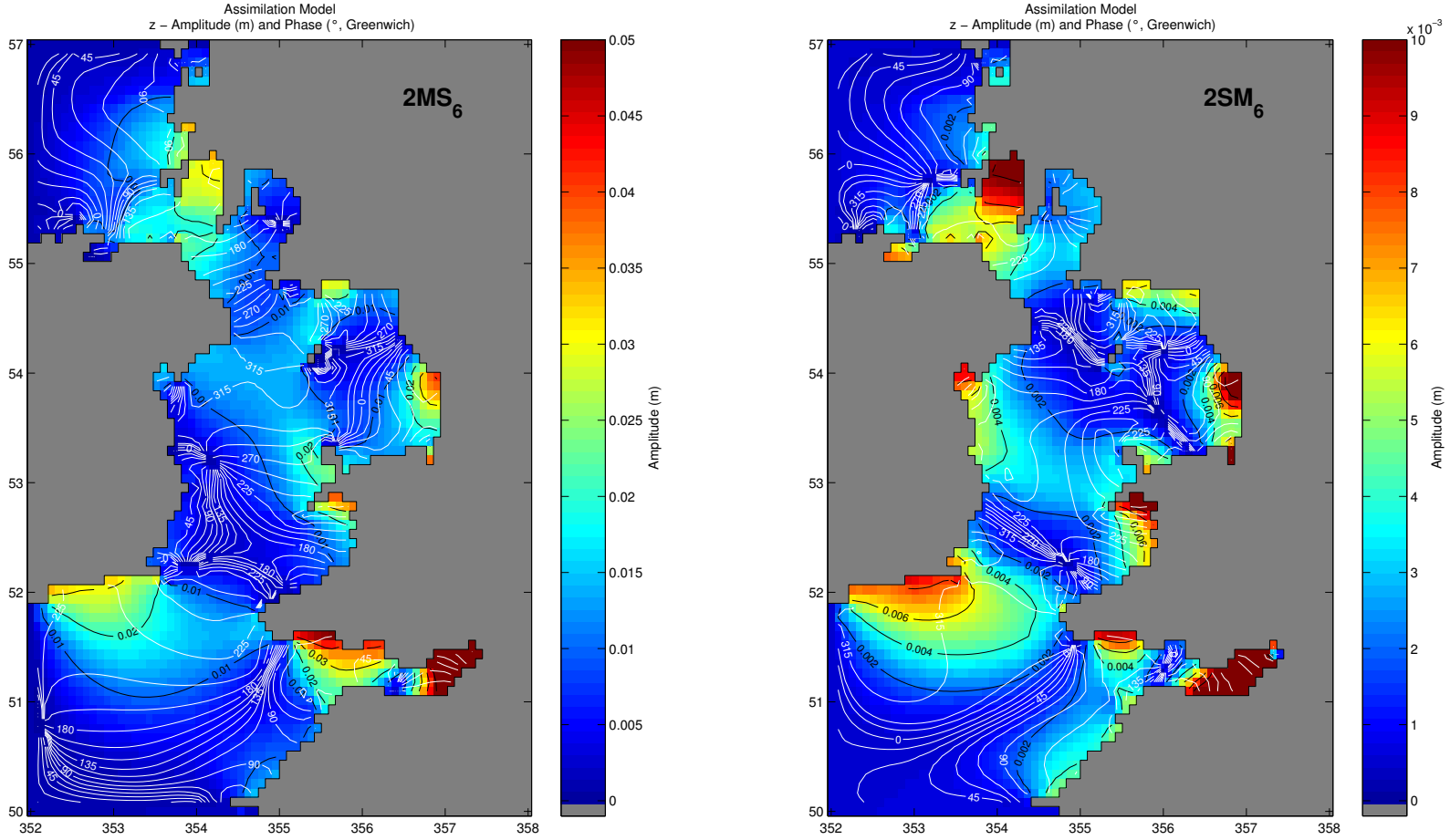

Figure 5.2.28 Tidal elevations of $2MS_6$ (left panel) and $2SM_6$ (right panel) obtained by the assimilation model with time block length of 1 day where the smoothing of residual is introduced.

Table 5.2.7 Comparison of amplitudes h (cm) and phases g (°) of elevations which are observed (h_o,g_o), obtained by assimilation without (h_{an},g_{an}) and with (h_{as},g_{as}) smoothing of residuals, respectively, at independent stations.

Station No.	M_2					
	h_o	g_o	h_{an}	g_{an}	h_{as}	g_{as}
I01	237.4	317.2	240.4	315.1	242.2	315.5
I02	152.9	136.1	158.7	135.3	159.8	135.6
I03	393.1	189.5	389.6	190.0	391.6	190.3
I04	389.3	188.8	392.3	191.3	394.7	191.6
I05	248.0	167.5	230.6	145.0	232.4	145.3
I06	244.4	143.0	236.8	146.6	238.7	146.9
I07	390.1	180.7	395.1	187.7	397.8	188.1
I08	26.5	87.0	15.9	13.1	15.2	13.9
I09	303.8	162.7	307.1	164.5	309.2	164.8
I10	221.0	172.7	220.9	170.0	222.0	170.3
I11	412.9	194.8	399.2	195.7	401.9	196.0
I12	315.0	173.2	313.3	171.8	315.3	172.1
I13	134.7	207.4	143.4	199.8	143.1	200.7
I14	303.1	320.7	294.7	316.4	296.9	316.5
I15	111.7	342.7	101.9	356.6	100.9	356.9
I16	16.0	89.8	11.3	99.9	11.4	103.8
I17	133.7	332.3	179.3	340.1	180.9	340.4
I18	130.4	168.5	127.2	192.6	128.4	192.8
I19	315.7	325.5	295.3	324.3	297.3	324.3
I20	272.9	332.1	264.1	332.7	265.5	332.8
I21	145.1	238.8	164.3	245.8	164.4	247.6
I22	53.7	197.3	58.1	200.2	58.9	200.3
rms error			13.5	18.0	13.5	18.0

Station No.	S_2					
	h_o	g_o	h_{an}	g_{an}	h_{as}	g_{as}
I01	74.5	356.0	80.1	354.6	80.1	354.7
I02	52.0	176.8	54.9	174.6	54.9	174.6
I03	138.8	243.8	140.7	243.3	141.1	242.9
I04	137.2	243.1	140.8	245.3	141.4	244.8
I05	94.0	212.2	84.6	185.9	84.8	185.9
I06	86.3	180.8	87.7	187.7	87.9	187.7
I07	147.6	234.0	142.9	241.0	143.4	240.8
I08	17.6	150.5	8.4	138.6	8.4	140.9
I09	109.4	209.9	115.5	210.7	115.7	210.6
I10	80.1	216.9	82.0	212.2	82.1	212.3
I11	145.8	252.7	142.3	251.2	142.9	250.7
I12	113.0	220.0	115.5	218.3	115.6	218.3
I13	52.6	248.2	56.4	239.9	55.7	240.2
I14	97.2	4.3	99.5	356.7	99.7	356.5
I15	29.3	34.6	30.6	48.5	29.8	48.5
I16	14.2	154.7	12.8	164.3	12.8	165.6
I17	37.3	16.2	56.8	20.7	57.0	21.1
I18	53.0	204.9	51.3	230.5	51.1	230.3
I19	102.2	8.1	99.8	5.7	99.8	5.2
I20	86.8	15.2	89.2	14.7	89.2	14.5
I21	54.2	277.0	65.7	281.6	64.8	284.0
I22	23.6	210.9	25.7	217.2	26.0	217.5
rms error			6.8	10.2	6.2	9.8

Table 5.2.7 (continued).

Station No.	$2SM_2$					
	h_o	g_o	h_{an}	g_{an}	h_{as}	g_{as}
I01	2.4	219.2	3.2	231.1	3.1	227.4
I02	1.3	16.3	0.2	10.4	0.3	350.7
I03	6.7	56.3	7.6	62.5	7.6	61.3
I04	6.4	60.8	8.2	67.1	7.8	66.1
I05	2.3	24.5	2.3	358.3	2.4	356.4
I06	4.4	99.3	2.6	3.5	2.7	0.9
I07	5.6	81.4	8.4	60.2	8.3	59.4
I08	2.0	300.7	2.1	295.9	2.2	290.2
I09	4.2	40.1	5.8	31.7	6.0	29.3
I10	2.4	59.0	2.1	48.9	2.6	46.5
I11	13.1	70.4	9.5	77.0	8.8	76.5
I13	1.0	71.0	1.7	72.6	1.8	76.9
I14	3.4	211.1	2.7	228.2	2.4	222.5
I15	2.5	263.7	3.0	295.4	3.4	283.0
I16	1.3	273.9	1.8	301.9	1.9	302.7
I17	2.2	258.5	3.2	272.4	3.1	263.9
I18	0.7	293.4	0.8	19.3	1.0	40.9
I19	3.4	233.7	4.3	228.2	3.7	227.1
I20	3.0	242.4	3.9	248.3	3.8	245.9
I21	2.1	112.6	2.9	94.6	2.8	117.1
I22	1.2	243.4	1.1	264.9	1.2	271.6
rms error			1.3	31.9	1.4	35.2

Station No.	M_4					
	h_o	g_o	h_{an}	g_{an}	h_{as}	g_{as}
I01	6.3	200.9	8.5	198.0	8.8	197.9
I02	4.4	218.1	0.6	212.6	0.5	232.1
I03	12.3	13.1	10.8	26.9	11.9	26.0
I04	12.7	32.1	11.9	12.9	12.7	13.2
I05	5.5	314.5	5.7	239.5	5.6	244.9
I06	6.6	239.1	6.0	248.0	6.0	253.2
I07	12.3	344.7	10.4	17.6	11.1	18.5
I08	2.8	89.6	4.1	87.9	4.1	85.5
I09	10.5	350.4	9.0	347.9	9.5	349.4
I10	6.3	305.9	6.5	262.9	6.3	265.4
I11	16.2	355.9	16.6	358.9	17.4	358.5
I12	6.0	29.2	7.0	10.9	7.6	12.1
I13	11.3	19.6	6.0	1.5	5.7	1.4
I14	23.4	202.6	16.7	197.8	16.8	197.6
I15	8.6	90.3	8.6	103.5	8.6	101.7
I16	2.1	65.8	0.4	283.8	0.4	299.3
I18	4.5	180.4	5.0	297.9	5.0	302.8
I19	19.6	244.6	21.8	208.2	21.9	208.6
I20	13.3	251.1	12.1	244.0	12.3	244.1
I21	23.9	62.8	25.0	52.5	24.5	54.1
I22	1.8	93.5	1.5	54.1	1.6	47.1
rms error			2.3	47.4	2.4	45.7

Table 5.2.7 (continued).

Station No.	MS_4					
	h_o	g_o	h_{an}	g_{an}	h_{as}	g_{as}
I01	3.7	235.3	5.1	238.6	5.3	235.6
I02	2.5	272.5	0.2	255.1	0.2	279.7
I03	6.5	16.2	4.4	29.8	5.0	29.4
I04	4.9	31.4	7.1	19.8	7.6	19.2
I05	2.7	6.6	2.2	295.1	2.3	298.2
I06	1.9	280.3	2.3	305.8	2.5	308.0
I07	8.4	349.7	4.9	13.3	5.3	15.2
I08	0.9	97.8	2.7	114.0	2.6	111.9
I09	5.8	51.0	5.0	54.2	4.9	50.0
I10	3.1	355.7	2.8	295.0	2.9	295.0
I11	14.5	14.1	13.2	21.0	13.8	18.3
I13	5.3	63.2	0.6	129.4	0.4	136.5
I14	14.2	245.4	7.9	247.6	7.9	245.1
I15	8.5	118.4	6.9	141.4	6.3	142.6
I16	1.2	69.2	0.8	17.0	0.8	11.7
I17	0.9	85.5	2.1	350.3	1.6	338.6
I18	3.5	289.5	4.1	340.8	4.2	342.6
I19	11.3	295.1	14.0	248.6	14.2	248.1
I20	6.7	298.6	6.9	286.8	7.0	284.9
I21	12.8	115.2	7.4	112.5	7.7	104.6
I22	0.7	63.7	1.4	238.6	1.4	53.2
rms error			2.6	39.4	2.5	41.7

Station No.	M_6					
	h_o	g_o	h_{an}	g_{an}	h_{as}	g_{as}
I01	0.6	354.0	1.4	310.9	1.2	305.5
I02	0.4	45.8	0.2	107.3	0.2	58.4
I03	6.4	231.7	5.9	229.2	5.8	239.8
I04	4.1	225.4	6.9	232.8	6.9	242.2
I05	1.1	50.8	1.2	90.3	1.2	75.0
I06	0.6	60.4	1.0	92.5	1.0	73.8
I07	4.7	201.5	7.4	222.3	7.2	228.5
I08	4.0	88.3	2.5	121.9	2.5	123.1
I09	1.9	344.1	2.4	357.3	2.8	354.4
I10	1.4	150.3	1.6	160.3	1.5	152.3
I11	8.2	270.3	7.7	248.6	8.3	257.7
I14	5.5	346.9	2.6	10.2	2.4	18.4
I15	2.5	304.2	1.1	136.5	0.5	128.0
I16	2.6	115.0	2.0	92.3	2.0	94.0
I18	1.3	8.3	1.4	190.9	1.3	192.1
I20	1.4	281.8	1.1	240.3	1.2	229.1
I22	1.8	124.1	1.3	101.4	1.3	107.4
rms error			1.3	65.7	1.4	65.3

Table 5.2.7 (continued).

Station No.	$2MS_6$					
	h_o	g_o	h_{an}	g_{an}	h_{as}	g_{as}
I01	0.6	27.0	0.9	357.1	0.8	356.6
I02	0.6	89.5	0.2	154.6	0.1	107.5
I03	6.4	270.3	6.0	272.5	6.5	281.2
I04	5.2	266.6	7.2	281.2	7.8	288.5
I05	1.2	73.8	1.0	109.2	1.0	95.1
I06	0.7	96.5	1.0	107.3	0.9	91.7
I07	6.0	252.8	8.2	268.4	8.5	273.2
I08	4.7	142.0	3.0	164.8	3.1	165.6
I09	2.3	49.7	2.4	50.5	2.5	43.9
I10	1.4	202.5	1.7	207.9	1.5	205.3
I11	11.0	319.1	8.4	305.5	9.7	310.0
I14	5.3	28.6	1.9	68.6	1.9	77.7
I15	2.7	350.1	0.6	42.6	0.8	22.7
I16	2.8	159.8	2.4	144.8	2.3	146.3
I18	1.2	42.1	1.5	233.9	1.5	234.3
I20	1.8	324.9	1.3	282.4	1.3	276.6
I21	1.9	137.5	1.9	277.5	3.7	271.1
I22	2.0	166.1	1.8	157.4	1.8	161.4
rms error			1.4	58.7	1.4	55.5

Station No.	$2SM_6$					
	h_o	g_o	h_{an}	g_{an}	h_{as}	g_{as}
I01	0.3	15.9	0.1	51.1	0.0	69.1
I02	0.2	172.6	0.0	176.4	0.1	26.7
I03	1.4	327.4	1.2	332.4	1.9	331.5
I04	1.2	306.4	1.2	350.0	2.0	340.6
I05	0.4	120.0	0.5	129.5	0.4	112.5
I06	0.2	163.2	0.5	129.8	0.4	112.1
I07	1.4	320.3	1.7	348.4	2.2	337.3
I08	1.2	188.0	0.9	211.8	1.0	205.8
I11	3.7	59.2	0.7	20.3	1.9	347.3
I21	1.3	230.0	1.5	271.6	1.3	303.8
rms error			1.0	30.0	0.7	62.6

Chapter 6
Conclusion

To make possible improving also the non-linear tides determined by different astronomical constituents by assimilating data in a variational sense, this investigation aims at adequately generalizing the method having successfully been applied by Zahel et al. (2000) to open ocean tides and by Taguchi (2002) to the M_2 and its overtides in an adjacent sea area. This step in modelling tides is required by the need for a tidal model system producing highly reliable tidal fields of the global ocean including the near coastal areas properly.

Preparing the generalization referred to above, a schematic ocean scenario is defined, with a dynamic model yielding results declared as real, and a deficient dynamical model producing results that are to be corrected making use of values taken from the field regarded as real. As schematic sea area a canal of constant depth is chosen. This canal has a closed end and an open end, at which the tidal wave being determined by two astronomical constituents enters the canal. Realistic tidal dynamics define the model. The non-linearity is due to quadratic bottom friction and it is rather weak.

A continuation technique is designed based on the previously applied method. Having performed the minimization of the least squares functional for a specific time block, the continuation is started within the time block towards its end; thus an overlapping area is arising. Assimilating data from only 8% of the canal area, a decisive improvement of the solution to be corrected is obtained. This even applies separately for the strongest non-linear constituents, i.e. overtides as well as compound tides, although they are very small as compared to the two astronomical partial tides. Finally, a satisfactory reproduction of the main features of the well known true dynamical residual is achieved in spite of the few data assimilated.

Extending the data assimilation method, having been tried out and optimized in the fictive data assimilation scenario, is straightforward, in principle. However, the demand for computer facilities is considerable in the case of an extended adjacent sea area. Restricting on two incommensurable astronomical partial tides and on minimizing only first instead of also higher order differences of the dynamical residuals does not impede estimating the potential of the new approach, but clearly reduces the computational expense.

Using a time block length of only one day already yields a significant improvement of the computed tidal elevation field as compared with that one obtained from the classical forward model. The change of the tidal oscillation

system brought about by assimilating a rather small number of irregularly distributed data, leads to eliminating former systematic errors, e.g., the underestimation of tidal elevation amplitudes in shallow water areas in the eastern Irish Sea and in the Bristol Channel, and the positions of M_2 and S_2 amphidromic points not being compatible with observations. A detailed comparison to observed elevations at independent positions and to the elevation fields generated by classical high resolution models (Jones and Davies, 1996; Davies and Hall, 2000) and by the data assimilation model of Taguchi (2002) shows good agreement with realistic elevations. So, also the elevation patterns of the non-linear constituents M_4, M_6 clearly resemble those given by Andersen (1999) who calculates shallow water tides on the European shelf using TOPEX/POSEIDON altimetry data. The elevation patterns of the non-linear constituents M_4 also clearly resembles that given by Andersen et al. (2006) who calculates shallow water tides on the European shelf using hybrid altimetry data assimilation methods.

It is characteristic of the developed method that tidal elevation and current velocity fields are computed simultaneously. Although the latter fields can scarcely be compared with reliable data, it was possible to realize that the computed patterns in general agree with those which are available from classical high resolution models and that the computed patterns are as smooth as is typical of real fields. In view of the experience with the relevant previous models and with the canal model in this work, the appearance of the dynamical residual fields, obtained when including the smoothing process suggests that specific experiments will enable taking information on compensated model deficiencies from the residual fields. So, increasing spatial resolution of the model will also make it worth evaluating energy and angular momentum balances and energy transitions in the tidal spectrum with studying the role of the dynamical residuals in this context. This promises giving valuable information on characteristic properties of the dynamical residuals.

Although first order differences of the dynamical residuals have already successfully been introduced and contribute to obtaining more realistic dynamical residual fields, a special treatment and technique should be implemented in the future studies to make this method more economical and computationally efficient, allowing to also consider higher order differences. Considering differences of dynamical residuals, leads to a multiplication of the original number of equations depending on the orders taken into account. As a consequence, more computer resources (memory and CPU time) are needed to perform the calculation. The need of computer memory is increased as a consequence of more equation being involved, while the CPU time, required for performing the minimization iteratively, becomes longer due to the greater number of iteration steps necessary. In this study, a shared-memory parallelization has been introduced to the matrix-vector multiplications which can be further developed for reducing CPU time significantly.

The model approach having been developed, tested and applied in this work also proves as adequate for being included in a data assimilation model system allowing to compute highly reliable tidal fields in the global ocean, in particular considering near coastal shallow water areas.

There are many possibilities left allowing to considerably increasing the potential of the approach, apart from better making use of computer facilities and introducing higher spatial resolution. To these belong optimizing the assimilation parameters, including the inhomogeneous boundary values in the correction mechanism (Gekeler, 1995) and implementing well known techniques for improving the classical model taken as a basis.

References

Alcock G.A. (1982a). Offshore bottom pressure records, North Channel of Irish Sea. IOS-data report No.**27**, Institute of Oceanographic Sciences.

Alcock G.A. (1982b). Offshore bottom pressure records, Celtic Sea, 1980. IOS-data report No.**28**, Institute of Oceanographic Sciences.

Alcock G.A. and M. Howarth (1978). Offshore tide gauge and moored current meter records from the Irish Sea, 1977. IOS-data report No.**15**, Institute of Oceanographic Sciences.

Alcock G.A., D.C.C. MacDonald and J.M. Vassie (1980). Offshore bottom pressure records from the Celtic Sea and South-West Aproaches to the U.K. IOS-data report No.**22**, Institute of Oceanographic Sciences.

Alcock G.A. and D.T. Pugh (1982). Observation of tides in the Severn Estuary and Bristol Channel. IOS-report No.**112**, Institute of Oceanographic Sciences.

Andersen O.B. (1999). Shallow water tides in the northwest European shelf region from TOPEX/POSEIDON altimetry. *Journal of Geophysical Research*, **104**(C4), 7729-7741.

Andersen O.B., G.D. Egbert, S.Y. Erofeeva, R.D. Ray (2006). Mapping nonlinear shallow-water tides: a look at the past and future. *Ocean Dynamics*, **56**, 416-429.

Anderson D.L.T, J. Sheinbaum, K. Haines (1996). Data assimilation in ocean models. *Reports on Progress in Physics*, **59**, 1209-1266.

Barker D.M., W. Huang, Y.-R. Guo, Q. N. Xiao (2004). A three-dimensional (3DVAR) data assimilation system for use with MM5: implementation and initial results. *Monthly Weather Review*, **132**, 897-914.

Bennett A.F. (2002). Inverse modelling of the ocean and atmosphere. Cambridge University Press.

Björck Å. (1996). Numerical methods for least squares problems. SIAM Philadelphia.

Bouttier F. and P. Courtier (2002). Data assimilation concepts and methods. ECMWF meteorological training course lecture series.

Chandra R., L. Dagum, D. Kohr, D. Maydan, J. McDonald, R. Menon (2001). Parallel programming in OpenMP. Morgan Kaufmann Publishers.

Courtier P. (1997). Variational methods. *Journal of the Meteorological Society of Japan*, **75**(1B), 211-218.

Courtier P., and O. Talagrand (1990). Variational assimilation of meteorological observations with the direct and adjoint shallow-water equations. *Tellus,* **42A,** 531–549.

Davies A.M. and J.E. Jones (1992). A three dimensional model of the M_2, S_2, N_2, K_1 and O_1 tides in the Celtic and Irish Seas. *Progress in Oceanography*, **29**, 197-234.

Davies A.M. and P. Hall (2000). A three-dimensional model of diurnal and semidiurnal tides and tidal mixing in the North Channel of the Irish Sea. *Journal of Geophysical Research*, **105**(C7), 17,079-17,104.

Davies A.M. and C.M. Kwong (2000). Tidal energy fluxes and dissipation on the European continental shelf. *Journal of Geophysical Research*, **105**(C9), 21,969-21,989.

Egbert G.D., A.F. Bennett and G.G. Foreman (1994). TOPEX/POSEIDON tides estimated using a global inverse model. *Journal of Geophysical Research*, **99**(C12), 84 821-84 852.

Egbert G.D. and A.F. Bennett (1996). Data assimilation methods for ocean tides. In: *Modern approaches to data assimilation in ocean modelling*, Malanotte-Rizzoli P. (ed.). Elsevier oceanographic series, **61**, 147-180.

Egbert G.D. and S.Y. Erofeeva (2002). Efficient inverse modelling of barotropic ocean tides. *Journal of Atmospheric and Ocean Technology*, **19**(2), 183-204.

Fukumori I. (2001). Data assimilation by models. In: *Satellite altimetry and earth sciences*, Fu, L.-L. and A. Cazenave (eds.). International geophysics series, **69**, 237-265.

Gekeler J. (1995). Assimilating data into a tidal model of the Irish and Celtic Seas. *Continental Shelf Research*, **15**(11-12),1381-1408.

Grawunder D. (1995). Ocean tidal loading in the Arctic and Antartic from numerical modelling, *Proceedings of the 12th International Symposium on Earth Tides*, Science Press, 585-586.

Jones J.E. and A.M. Davies (1996). A high resolution, three-dimensional model of the M_2, M_4, M_6, S_2, N_2, K_1 and O_1 tides in the eastern Irish Sea. *Estuarine, Coastal & Shelf Science*, **42**(3), 311-346.

Kalnay E. (2003). Atmospheric modelling, data assimilation and predictability. Cambridge University Press.

Kantha L.H. and C.A. Clayson (2000). Numerical models of oceans and oceanic processes. Academic Press.

Lee J.C. and A.M. Davies (2001). Influence of data assimilation upon M_2 tidal elevations and current profiles in the Irish Sea. *Journal of Geophysical Research*, **106**(C12), 30,961-30,968.

Lefèvre F., C. Le Provost, F. Lyard (2000). How to improve a global ocean tide model at a regional scale? A test on the Yellow Sea and East China Sea. *Journal of Geophysical Research*, **105**(C5), 8707-8727.

Malanotte-Rizzoli P. and E. Tziperman (1996). The oceanographic data assimilation problem: overview, motivation and purposes. In: *Modern approaches to data assimilation in ocean modelling*, Malanotte-Rizzoli P. (ed.). Elsevier oceanographic series, **61**, 3-17.

Mihardja D.K. (1991). *Energy and momentum budget of the tides in Indonesian waters*. Bericht aus dem Zentrum für Meeres- und Klimaforschung der Universität Hamburg, **14**.

Miller R.N. (1986). Toward the application of the Kalman Filter to Regional Ocean Modeling. *Journal of Physical Oceanography*, **16**, 72-86.

Munk W.H. and D.E. Cartwright (1966). Tidal spectroscopy and prediction. *Philosophical Transactions of the Royal Society of London, Series A*, **259**, 533-583.

NOAA (1988). *Data Announcement 88-MGG-02, Digital relief of the Surface of the Earth*. National Geophysical Data Center, Boulder, Colorado. `http://www.ngdc.noaa.gov/`.

Paige C.C. and M.A. Saunders (1982). LSQR: an algorithm for sparse linear equations and sparse least squares. *ACM Transactions on Mathematical Software*, **8**(2), 195-209.

Rabier F. and Z. Liu (2004). Variational data assimilation: theori and overview. In: *Recent developments in data assimilation for atmosphere and ocean*. ECMWF proceedings series, 29-44.

Ray R.D. (2001). Inversion of oceanic tidal currents from measured elevations. *Journal of Marine Systems*, **28**, 1-18.

Robinson A.R. and P.F.J. Lermusiaux (2000). Overview of data assimilation. *Harvard Reports in Physical/Interdisciplinary Ocean Science*, **62**.

Sasaki Y. (1970). Some basic formalisms in numerical variational analysis. *Monthly Weather Review*, **98**(12), 875-883.

Shewchuk J.R. (1994). An introduction to the conjugate gradient method without the agonizing pain. Carnegie Mellon University.

Sinha B. and R.D. Pingree (1997). The principal lunar semidiurnal tide and its harmonics: baseline solution for M_2 and M_4 constituents on the North-West European Continental Shelf, *Continental Shelf Research*, **17**(11), 1321-1365.

Simpson J.H. (1998). The Celtic seas coastal segment (19,E). *The Sea*, **11**, 659-698.

Sirkes Z., E. Tziperman, W.C. Thacker (1996). Combining data and a global primitive equation ocean general circulation model using the adjoint method. In: *Modern approaches to data assimilation in ocean modelling*, Malanotte-Rizzoli P. (ed.). Elsevier oceanographic series, **61**, 119-145.

Taguchi E. (2002). *Inverse Modellierung nichtlinearer Flachwassergezeiten und ihre Anwendung auf ein Randmeer*. Dissertation, Universität Hamburg, 191S.

Talagrand O. (1997). Assimilation of observation, an introduction. *Journal of the Meteorological Society of Japan*, **75**(1B), 191-209.

Thacker W.C. (1988). Three lectures on fitting numerical models to observations. GKSS, **87**/E/65.

Weis P. (2006). Ocean tides and the Earth's rotation results of a high-resolving ocean model forced by the lunisolar tidal potensial. *Report on Earth System Science*, **36**.

Wunsch C. (1996). *The ocean circulation inverse problem*. Cambridge University Press.

Zahel W. (1991). Modelling ocean tides with and without assimilating data. *Journal of Geophysical Research*, **96**(B12), 20,379-20,391.

Zahel W. (1995). Assimilating ocean tide determined data into global tidal models. *Journal of Marine Systems*, **6**, 3-13.

Zahel W. (1997). Ocean tides. In: *Tidal phenomena*. H. Wilhelm, W. Zürn, H.-G. Wenzel (eds.), Springer, 113-143.

Zahel W., J.H. Gaviño, U. Seiler (2000). Angular momentum and energy budget of a global ocean tide model with data assimilation. *GEOS*, **20**(4), 400-413.

Acknowledgements

I would like to express profound gratitude to my supervisor, Prof. Dr. Wilfried Zahel, for his invaluable support, encouragement, supervision and useful suggestions throughout this research work. His moral support and continuous guidance enabled me to complete my work successfully. I am also highly thankful to Dr. Peter Damm for his valuable suggestions throughout this study.

I would like to thank staff members of Institute for Oceanography (IfM), especially from the Theoretical Oceanography group, PD Dr. Thomas Pohlmann, D. Hainbucher, Dr. I. Hamann, and many thanks to my colleagues Dr. Eifu Taguchi and Malte Müller for their valuable discussions during my studies and Dr. Jens-Olaf Beismann from DKRZ for his valuable discussions in vectorizing and parallelizing the code. I would like to thank also Prof. Dr. Jens Struckmeier, the scientific coordinator of the Graduate School "Conservation principles in the modelling and simulation of marine, atmospherical and technical systems". I am also highly thankful to Prof. Dr. B. Brümmer and Dr. A. Dehghani, members of doctorate committee.

I am also thankful to the Department of International Affairs, University of Hamburg for giving me a financial assistance during January – June 2006.

I am as ever, especially indebted to my parents Bachroen and Susmiati, my parents-in-law Ari Rachmatarwata and Sinta, my wife Mutiara R. Putri, and my daughter Hasna Nabilah for their love and support throughout my life.

This work has been funded by the *Deutsche Forschungsgemeinschaft* (DFG) under the Graduate School initiative "Conservation principles in the modelling and simulation of marine, atmospherical and technical systems".